NREL
NATIONAL RENEWABLE ENERGY LABORATORY

Advanced Thermal Storage System with Novel Molten Salt

December 8, 2011 — April 30, 2013

Matthieu Jonemann
Halotechnics, Inc.
Emeryville, California

NREL Technical Monitors: Harin Ullal and Craig Turchi

NREL is a national laboratory of the U.S. Department of Energy, Office of Energy Efficiency & Renewable Energy, operated by the Alliance for Sustainable Energy, LLC.

Subcontract Report
NREL/SR-5200-58595
May 2013

Contract No. DE-AC36-08GO28308

NREL
NATIONAL RENEWABLE ENERGY LABORATORY

Advanced Thermal Storage System with Novel Molten Salt

December 8, 2011 — April 30, 2013

Matthieu Jonemann
Halotechnics, Inc.
Emeryville, California

NREL Technical Monitors: Harin Ullal and Craig Turchi
Prepared under Subcontract No. NEU-2-11979-01

National Renewable Energy Laboratory
15013 Denver West Parkway
Golden, Colorado 80401
303-275-3000 • www.nrel.gov

Subcontract Report
NREL/SR-5200-58595
May 2013

Contract No. DE-AC36-08GO28308

Table of Contents

List of Figures

List of Tables

Introduction

Halotechnics has demonstrated an advanced thermal energy storage system with a novel molten salt operating at 700 °C. The molten salt and storage system will enable the use of advanced power cycles such as supercritical steam and supercritical CO_2 in next generation CSP plants. The salt consists of low cost, earth abundant materials.

The R&D activity was an effort over a 15 month period that included building a 30 kW-hr two-tank thermal storage system operating between 700 °C (hot tank) and 300 °C (cold tank). The molten salt was heated to up to 740° in the transfer lines, and stored at temperatures nearing 700°C.

Several key pieces of learning were developed during this program. The internally insulated hot tank design using common ceramic materials eliminates the need for an expensive Nickel alloy to contain the molten salt. Halotechnics has developed critical knowledge of the salt/ceramic interaction at elevated temperatures, and this knowledge is being applied to the design of a commercial size system.

The technical design details and experimental results are presented and discussed. They include the design of the internally insulated 700 °C tank, the thermal-fluid properties of the molten salt, the pump performance, the corrosion testing results, and the lessons learned.

The successful demonstration of the functional system minimizes the engineering risk at the prototype level and justifies taking the next step to pilot scale.

System Overview

The laboratory system is shown in Figures 1 and 2 and consists of approximately 400 kg[1] of salt divided into the five major sub-systems:

1. The Hot Tank portion.
2. The Cold Tank portion.
3. The Heat Exchanger (HX) portion.
4. The Furnace Heat Exchanger (FX) portion, and
5. The Pressure Control portion.

This small scale system is designed to accept, reject, transport, and store energy between the two thermal tanks operating at the temperature extremes of 700°C (hot tank) and 300°C (cold tank).

The liquid salt is heated in the FX portion to simulate the energy transport to the working fluid obtained in a full-scale system by concentrating solar energy from a heliostat field onto a power tower; this can be implemented in the laboratory either by a radiant heat furnace or by a direct contact-type heating element or a combination of both that heats the salt transported through a tube. We choose the direct contact-type heating method due to simplicity and reduced cost.

The HX portion simulates an interchange of energy between the working fluid (salt) and another working fluid (for example, air or water) that would then drive a turbine to generate electricity. In the laboratory, this portion simply removes energy from the flow control loop and can be implemented by using a conventional shell and tube countercurrent flow heat exchanger which rejects the energy to water or by another indirect contact method such as air or cooled water tubing jacketing the molten salt pipe; we have chosen a copper t tubing jacketing the molten salt tube for the HX configuration; the water is supplied by a laboratory chiller system, not shown in the PFD/PID.

The Pressure Control System has only two components, a back-pressure regulator (PR-501) and a pressure transducer (PT-501). The back-pressure regulator controls the upstream or flow control pressure by actively opening and shutting an orifice to accept or restrict flow, and is an off-the-shelf component.

The Cold Tank is a central component of the flow control test loop and is heavily instrumented. It serves as the "cold" repository of the working fluid. When full it contains approximately 400 kg of the working fluid (salt) that includes approximately 100 kg that will remain in the tank above the actively heated portion and pump impeller (HT-200 and PU-200), respectively. There is additional plumbing and instrumentation attached and used to pressurize the system with nitrogen, measure the liquid level, and otherwise instrument the tank.

The Hot Tank is the major piece of innovation of the program and is also heavily instrumented. It serves as the "hot" repository of the working fluid. It is designed to contain approximately 400

[1] The system contains enough salt so that 300 kg can be transported between tanks and a residual (called the heel) of about 100 kg can remain in a tank to cover both the immersion heater and inserted vertical pump.

kg of the working fluid (salt) when full, that includes approximately 100 kg that will remain in the tank above the actively heated portion and pump impeller (HT-100 and PU-100), respectively. The hot tank was designed to a heat flux requirement of 389 W/m^2, which is a good design criterion for a large scale thermal energy storage tank.

Piping and Instrumentation Diagram

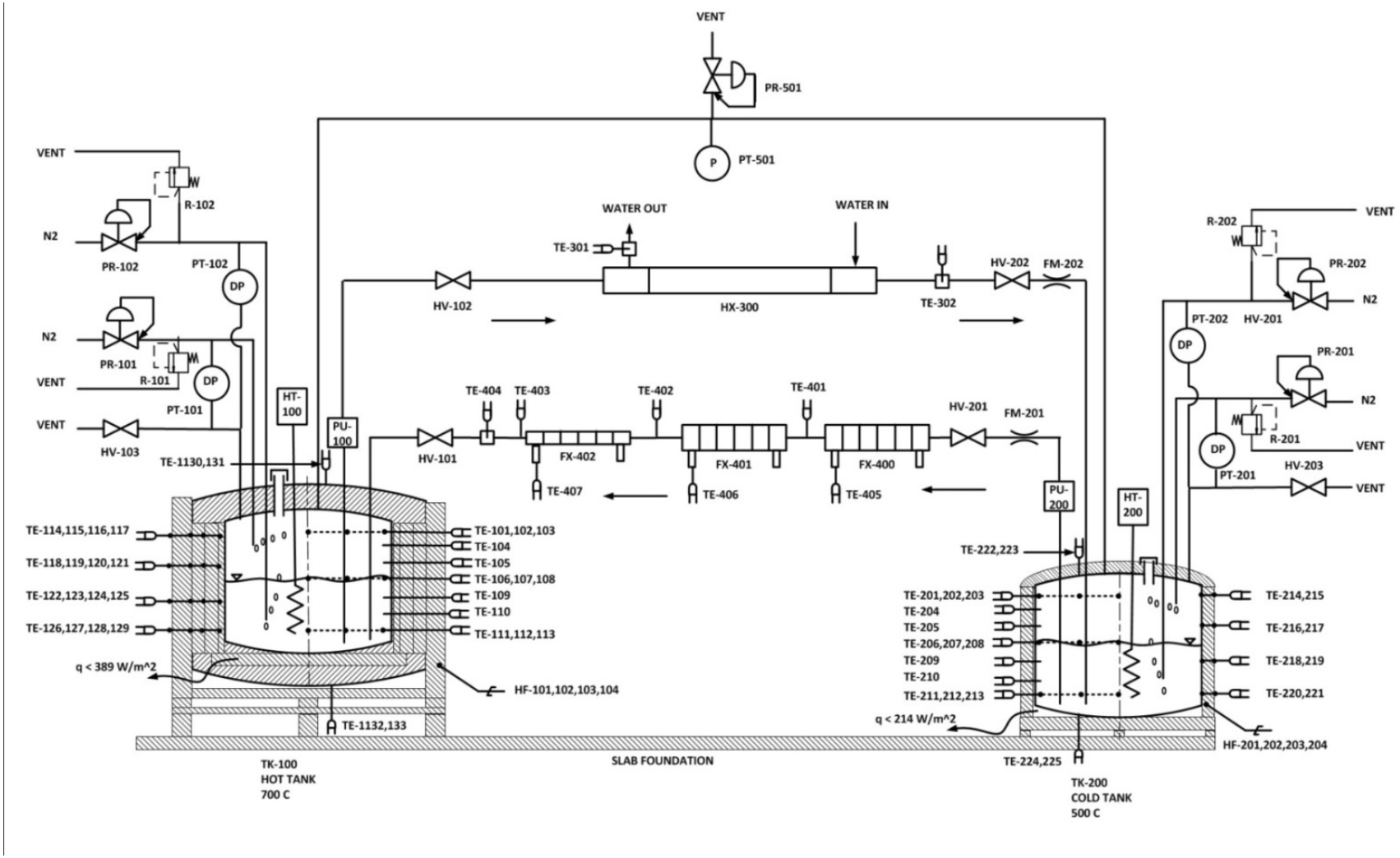

Figure 1. Piping and Instrumentation Diagram (PID) for the NREL Molten Salt Forced Convection Loop.

Process Flow Diagram

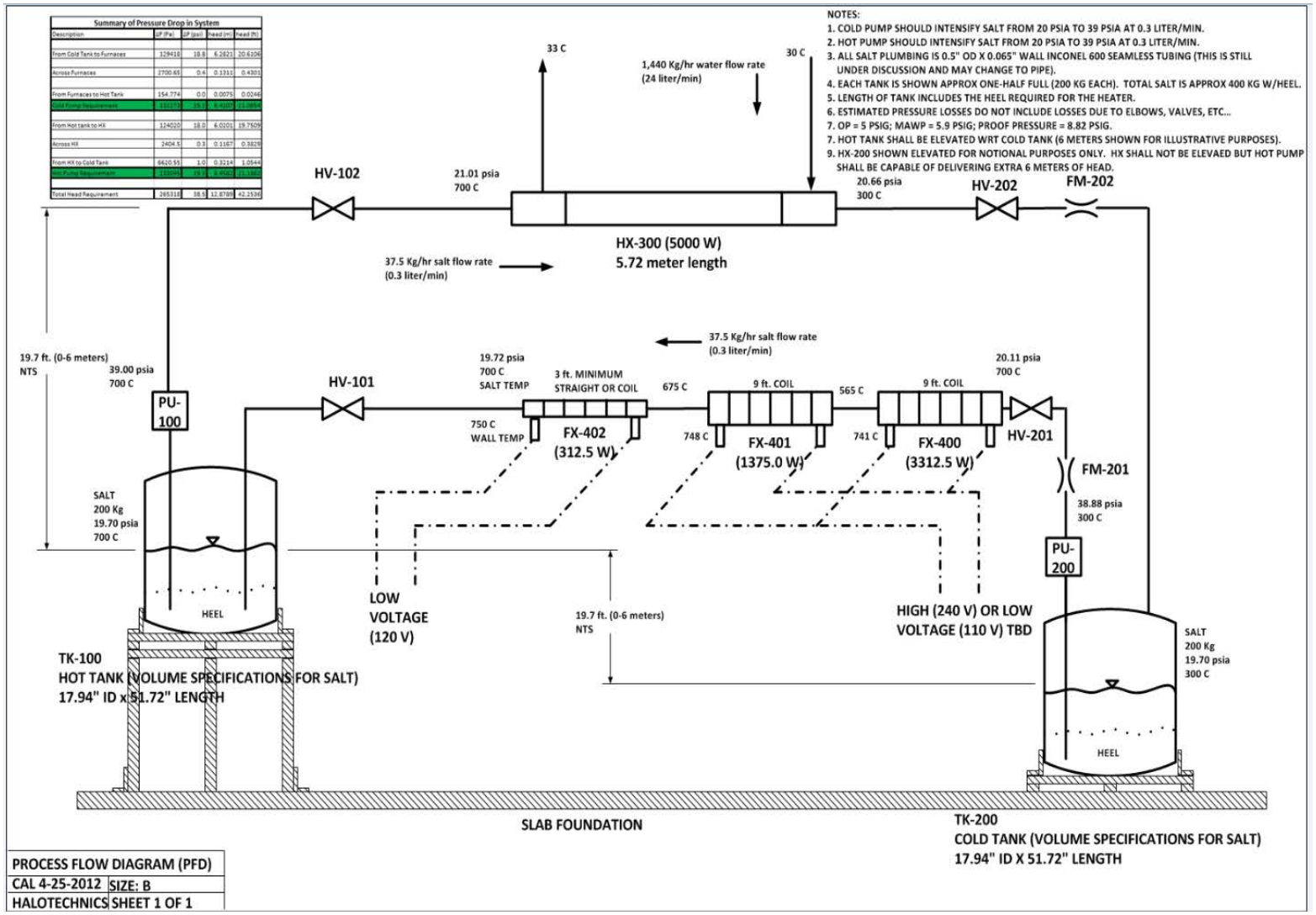

Figure 2. Process Flow Diagram (PFD) for the NREL Molten Salt Forced Convection Loop

The hot tank is similar to the cold tank, however a much more complicated design is necessary to retain salt temperature and meet heat flux requirements: It serves as the "hot" repository of the working fluid; it is conceptually identical in design, form, and function to the cold tank.

The system also contains some other necessary componentry: Heat flux sensors (HF) and two flow rate monitors (FM) are shown on the PID, monitoring heat flux and flow rate, respectively.

In addition to the PID, the requirements and design parameters that help define the system are shown in Table 1. Some of the fluid parameters and material compatibilities are still being determined at this time, and could later impact the system design.

Table 1. Requirements and Parameters for the NREL Flow Control Test Loop.

System Requirements		
Power	5 KW Thermal	
Energy Storage	30 KW-Hours	
Cold Tank Temperature	300 °C	
Hot Tank Temperature	700 °C	
Cold Tank Heat Flux Loss	214 W/m^2	
Hot Tank Heat Flux Loss	389 W/m^2	
System operating Pressure	5 psig	
System Parameters	300°C	700°C
Viscosity [cP]	16.9	1.0
Heat Capacity [kJ/kg.K]	0.79	0.80
Thermal Conductivity [W/m-K]	0.35	0.35
Density [kg/m^3]	2,310	2,100
Thermal Stability [°C]	257° (liquidus)	750° (decomposition)
Fluid Compatibility – plumbing	316 Stainless Steel	Inconel 600
Fluid Compatibility – storage tanks	A516 Grade 70 Carbon Steel	KX-99

Data Acquisition and Instrumentation

Table 2 shows the instrumentation list used to monitor the TES storage loop.

An Agilent data acquisition unit was used with three 20-channel multiplexer cards collecting 4 data points per minute. The instrumentation was displayed on a monitor using a LabView interface.

The instrumentation included:

- 2 pressure transducers to monitor pump pressure generation
- 4 current sensors to monitor storage tank heaters and heat exchangers

- 4 heat flux sensors to measure storage tank heat loss through the sidewalls
- 58 type-K thermocouples for overall system thermal monitoring

Table 2. Instrumentation List

Card #	Description	Card #	Description	Card #	Description
1	Cold Tank	2	FX / HX	3	Hot Tank

Channel	Units	Description	Channel	Units	Description	Channel	Units	Description
101	°C	Salt temp	201	°C	Hot flow control valve	301	°C	Salt temp 1C - 47"
102	°C	Salt temp	202	°C	Hot recirc loop	302	°C	Salt temp 1B - 45"
103	°C	Heater temp	203	°C	Into HX	303	°C	Salt temp 1A - 40"
104	°C	Salt temp	204	°C	HX wall temp	304	°C	Salt temp 2F - 35"
105	°C	Salt temp	205	°C	HX wall temp	305	°C	Salt temp 2E - 30"
106	°C	Salt temp	206	°C	HX wall temp	306	°C	Salt temp 2D - 25"
107	°C	Salt temp	207	°C	Water out	307	°C	Salt temp 3I - 20"
108	°C	Salt temp	208	°C	Hot recirc valve	308	°C	Salt temp 3H - 15"
109	°C	Salt temp	209	°C	Heat trace to HX	309	°C	Salt temp 3G - 10"
110	°C	Tank surface temp	210	°C	Heat trace to Cold Tank	310	°C	Tank surface temp
111	uV DC	Heat Flux	211	°C	Water in	311	uV DC	Heat Flux
112	°C	Tank surface temp	212	°C	HX bucket	312	°C	Tank surface temp
113	uV DC	Heat Flux	213	°C	Heat trace to HX	313	uV DC	Heat Flux
114	V DC	Cold Pump output P	214	°C	HX wall temp	314	°C	FX temp
115	V DC	Hot Pump output P	215	°C	HX wall temp	315	°C	FX temp
116	°C	Cold recirc P1 trace	216	°C	HX wall temp	316	°C	FX temp
117	°C	Cold flow control valve	217	°C	HX wall temp	317	°C	FX temp
118	°C	Cold Tank recirc valve	218	°C	Into FX	318	°C	FX temp
119	°C	Cold recirc P2 trace	219	°C	Out of FX	319	°C	FX temp
120	°C	Out of the HX	220	°C	FX wall temp	320	°C	FX temp
121	A	Heater current [24V]	221	A	Furnace current [240V]	321	A	Heater current [24V]
122			222	A	Heat ex current [240V]	322		

Cold Tank

Cold Tank Design

The tank was modeled and designed by Halotechnics and built by Ajax Electric Company (Philadelphia, PA). It is designed to contain molten salt up to 300°C and hold a nitrogen head pressure of 5 psig. The tank is constructed from carbon steel schedule 80 pipe with a wall thickness of 1". A schematic of the tank design is shown in Figure 3. The bottom of the tank uses structural firebrick for load bearing. The sides of the tank are surrounded by Kaowool insulation for good thermal conductivity. Fibrefrax is added to the top of the tank to reduce heat loss out of the lid; however the protrusions from the lid which include the pump are expected to contribute to significant heat loss. The design of the tank lid can be seen in Figure 4, which shows the layout of the flanges which connect to all the equipment penetrating through the lid into the tank. Three thermocouple trees consisting of three thermocouples clustered together have also been added to the top of the tank. Each thermocouple is spaced 5" down the depth of the tank as shown in Figure 5. More detail on the cold tank design and construction can be found in the D4 deliverable report.

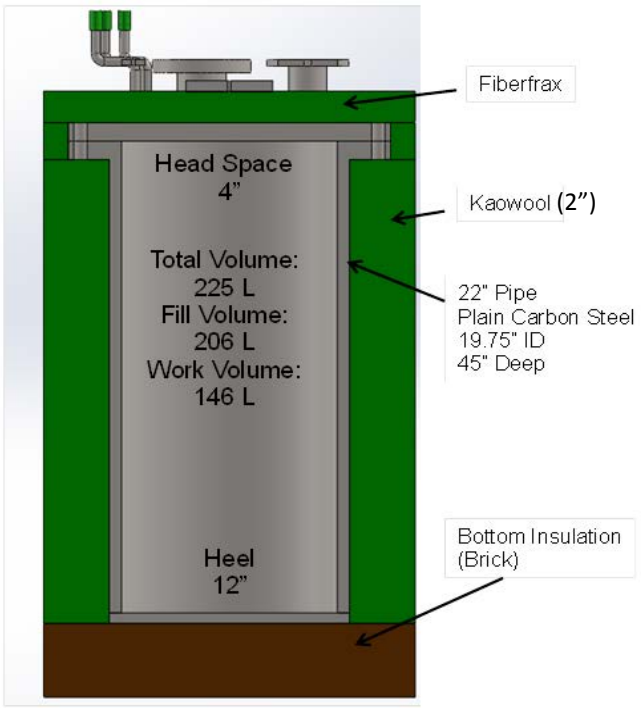

Figure 3. Cold tank schematic

Modeling

Modeling results of the cold tank with a 300°C internal temperature yield a heat flux through the wall of 98 W/m^2 with a 2" thick layer of Kaowool around the sidewall. The project requirement is 214 W/m^2. This result reflects a safety factor of 2 that was applied during the design phase. These results can be seen graphically on Figure 6. The heat transfer coefficient between the external walls of the tank and ambient typically ranges from 5 – 15 W/m^2-K. To obtain more insight into this variable a parameter study was performed with the effect on heat flux and

surface temperature shown in Table 1. From measurements taken directly from the tank it would seem the actual heat transfer coefficient is closer to 15 W/m^2-K.

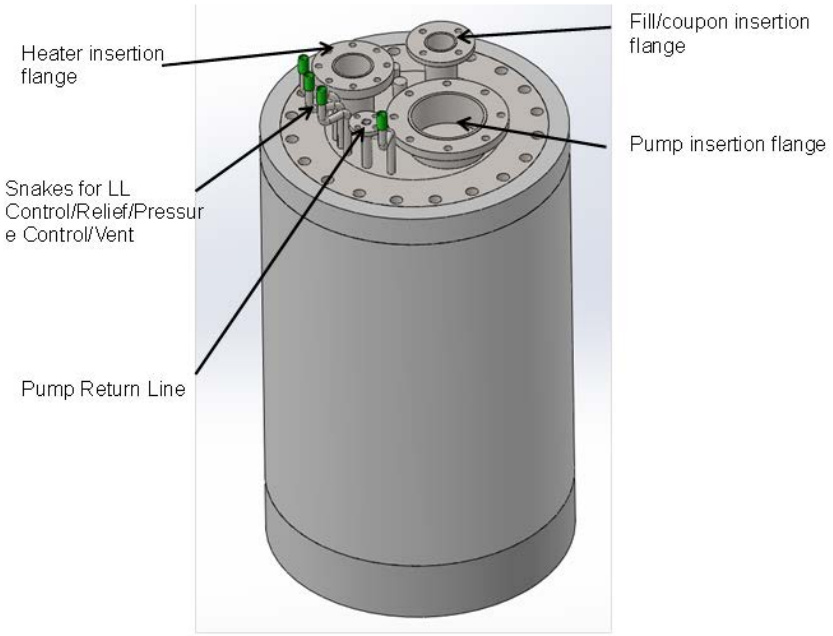

Figure 4. Lid design of the cold tank

Cold Tank

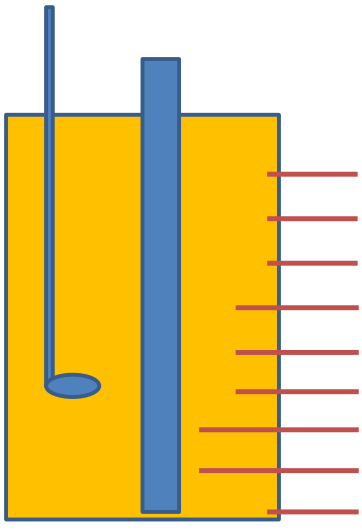

CH	Level
107	38”
108	33”
109	28”
104	23”
105	18”
106	13”
101	8”
102	3”
Ctrl	0”

Hot Tank

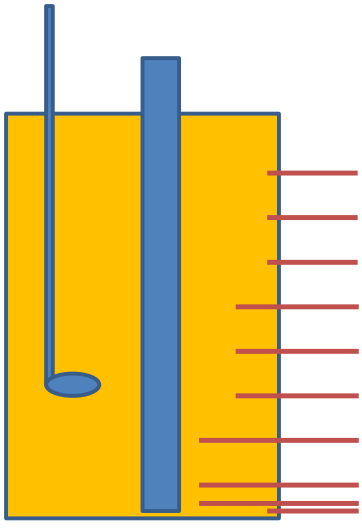

CH	Level
309	40”
308	35”
307	30”
306	25”
305	20”
304	15”
303	10”
302	5”
301	2”
Ctrl	2”

Figure 5. Thermocouple locations in the cold and hot tanks

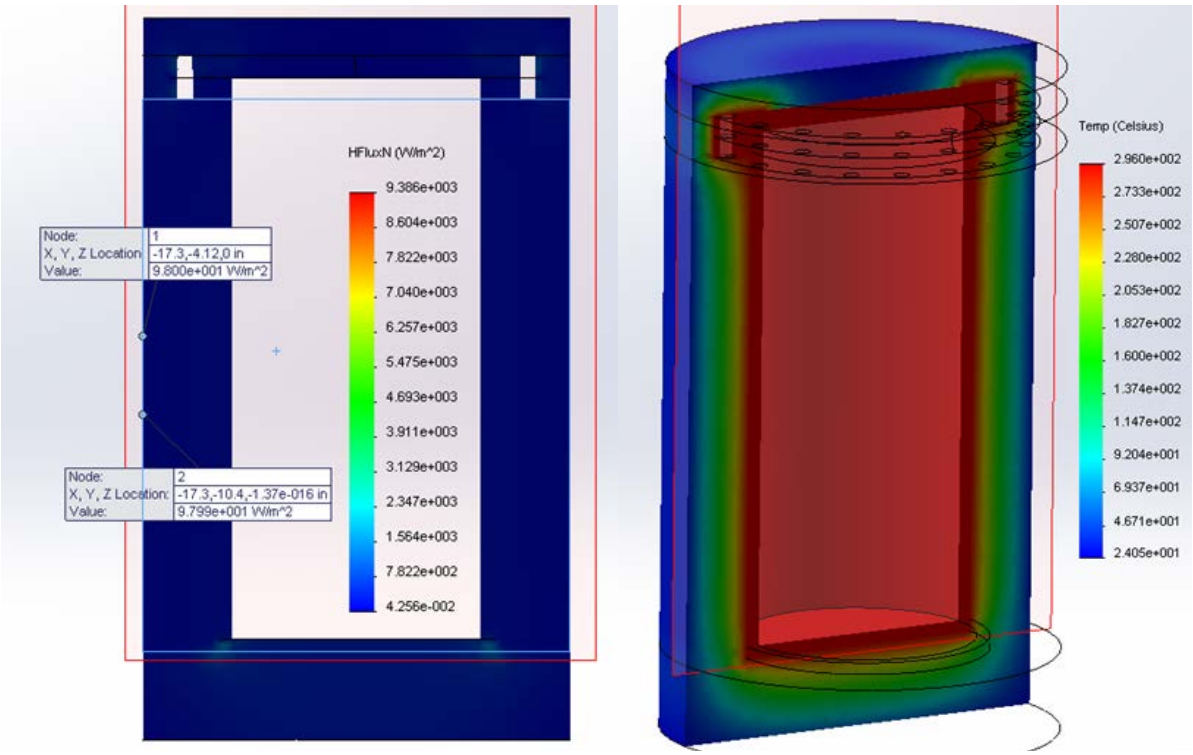

Figure 6. Thermal modeling results of the cold tank

Table 3. Parameter study on the heat transfer coefficient for natural convection along the tank sidewall

H(W/m²-K)	Ts (°C)	q (W/m²)
5	42	95
10	33	98
15	30	99
Measured	30-35	70-110

Cold Tank Performance

Initial data showing the thermal response of the cold tank before and after the final salt fill event can be seen in Figure 7. The fill added 86 kilograms of salt (around hour 25) to bring to a total of 305 kg of salt in the tank (approx. 2/3 full). The thermocouples submerged in the melt are recording 290-300°C, whereas the thermocouples positioned in the head space record significantly lower temperatures. The thermocouples can therefore effectively be used as a low resolution level sensor. The external shell temperature is recording approx. 30°C (diurnal cycles are evident) and the single heat flux sensor in this case fluctuates between 60 – 120 W/m^2. If we zoom into the stable period after the tank fill (60 – 120 hours; Figure 8) then we can see that the average heat flux through the wall of the tank is approx. 85 W/m^2.

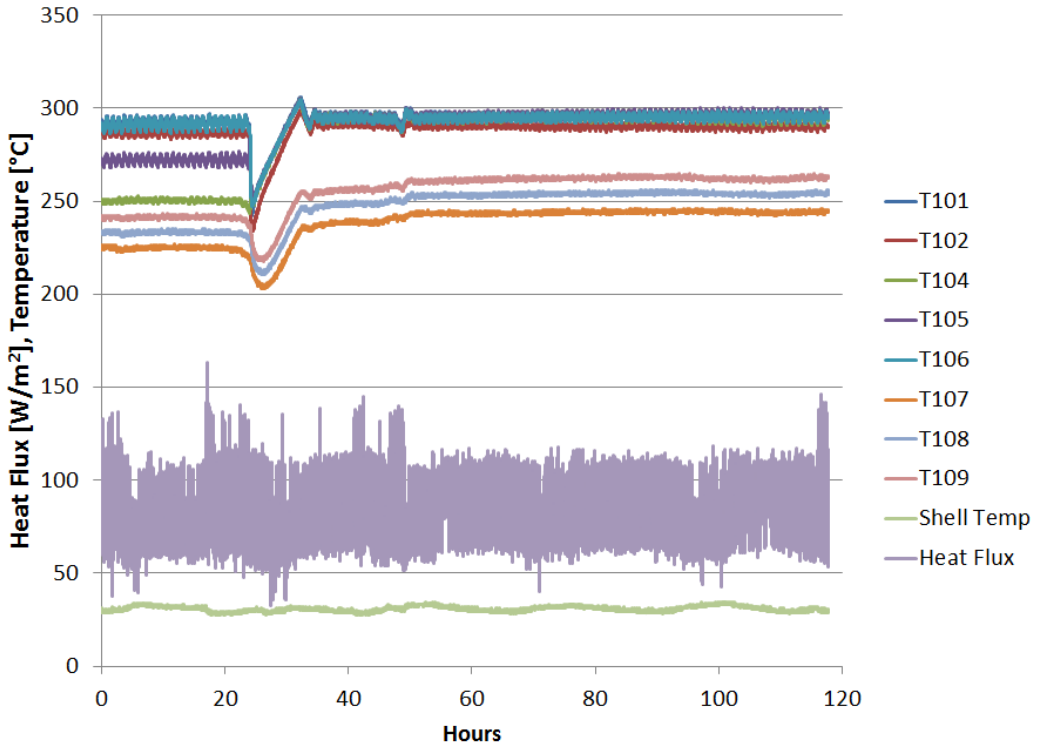

Figure 7. Tank response after a salt fill event. Thermocouple depths are indicated in Figure 5.

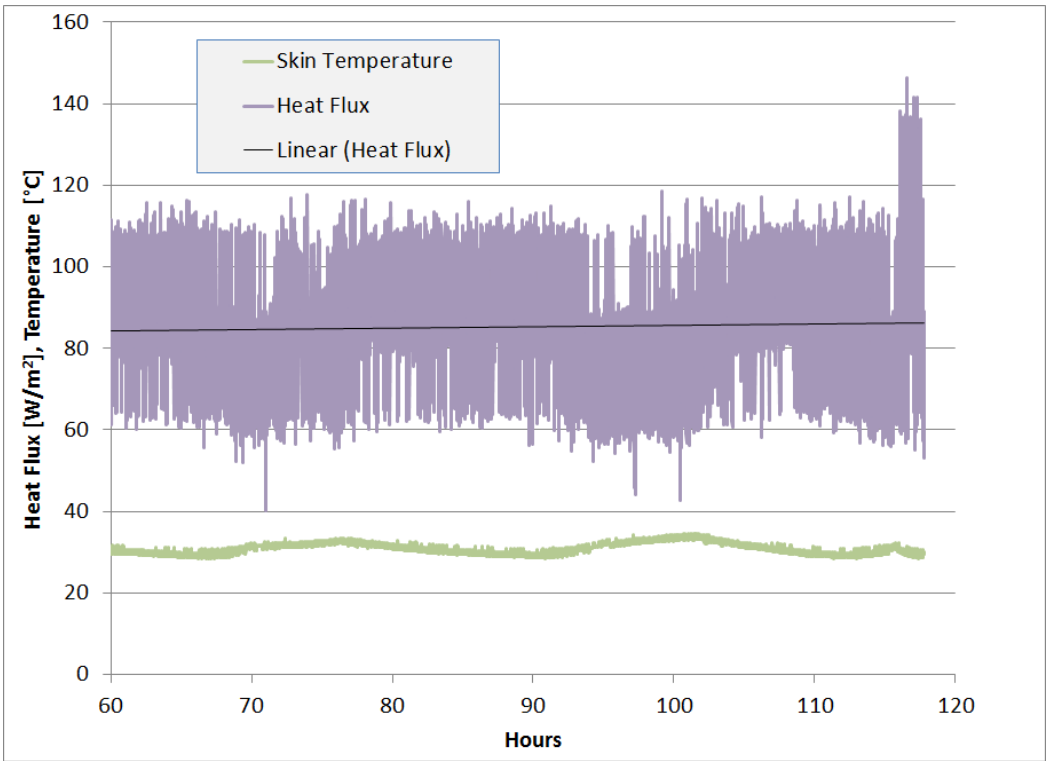

Figure 8. Average heat flux through the cold tank side wall. Thermocouple depths are indicated in Figure 5.

Further data shown in Figure 9 shows a 24 hour period which shows the thermal response to a period after the pump was run for approximately 1 hour at the start of the trace. The pump was recirculating the liquid which promotes mixing thereby creating a more thermally uniform volume of molten salt. The thermocouples submerged in the melt can be seen to approach a uniform value. In this case two heat flux sensors were being recorded, both were at 17" height in the tank, but on opposite sides. The average values are displayed on Figure 9, where heat flux sensor #1 records 81 W/m^2 and #2 records 109 W/m^2. The average of these two values is very close to the calculated value from the modeling results (99 W/m^2).

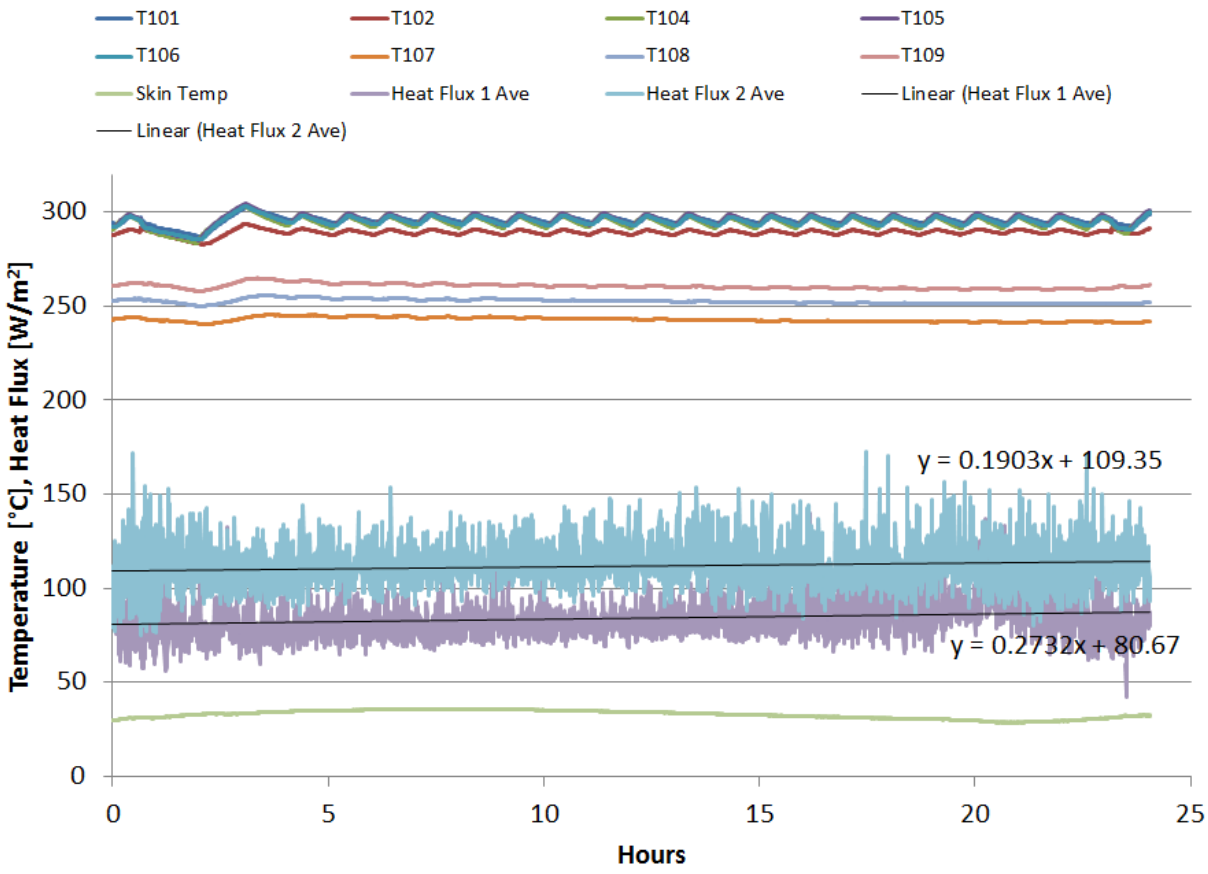

Figure 9. Data after recirculating the molten salt in the cold tank. Thermocouple depths are indicated in Figure 5.

Finally, to look at an alternative method to calculate the overall heat loss, the power supplied by the electrical heater was estimated. The control strategy of the heater is one that turns on and off at a set value, in this case +/- 1°C from the control thermocouple. Therefore by measuring the period the heater was turned on versus turned off, the average power can be calculated. By zooming in of a set of data from a thermocouple close to the heater (T102), we are able to estimate the duty cycle of the heater, see Figure 10. Using a clamp-on current meter we were able to confirm the heater was consuming 125 A at 24 V or 3 kW.

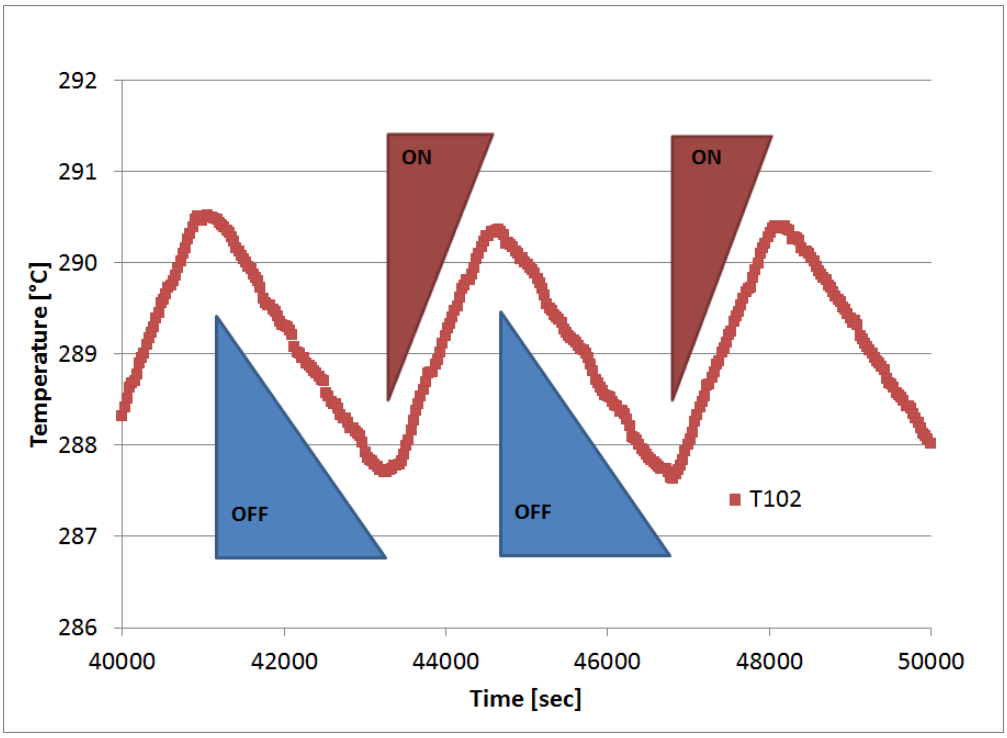

Figure 10. Duty cycle of the heater during steady state operation.

Table 4. Power consumed by the cold tank heater in a steady state mode

Heater	sec	%	Watts
OFF	2325	65.1%	
ON	1245	34.9%	1046

Table 4 shows that the heater was on approx. 1/3 of the time during this period which corresponds to an average power consumption of 1.05 kW over the entire period. The total heat lost according to the original model was 0.65 kW, however that did not include the additional heat lost out through the lid, in particular through the large steel mounting for the pump. It is therefore not unreasonable to expect an additional 400 W of heat lost through the structures and attachments on the lid. See Figure 11 below showing the pump mounted to the top of the tank which is effectively acting as a large cooling fin.

Conclusions

The test data was in excellent agreement with the modeling results in terms of predicting the heat flux through the walls of the tank. Measured average heat flux from the heat flux sensors attached to the side of the tank ranged from 81 W/m^2 to 109 W/m^2 which is well within the allowable 214 W/m^2 prescribed by the Statement of Work.

After 7 months of operation, it can be concluded that the cold tank has performed well. Regular salt samples were collected throughout the duration of the project and analyzed for basic

chemistry analysis (DSC, ferromagnetic content, base content). The test results are reported in Table 5.

Table 5. Cold tank salt sample analysis showing total bases as a fraction of metal oxide

sample	Total Bases as % metal oxide (by weight)
Hot Tank 01/28/2013	0.22
Cold Tank 01/24/2013	0.74
Cold Tank 02/07/2013	0.40
Cold Tank 11/2012	0.53
Cold Tank 08/2012	1.00
Cold Tank 09/2012	0.66

The nitrogen purge was maintained throughout most of the duration of the project, which helped with minimizing the formation of corrosion products. However, due to the large amount of raw salt that had to be added in order to fill the hot tank (described below), we noticed the increased presence of magnetic debris, most likely from the oxidation of the carbon steel. Because of time constraints, we were forced to melt salt from raw constituents directly in the cold tank, which is not the regular salt melting process.

Figure 11. Picture of the Cold Tank including the pump mounted on the lid.

Hot Tank

Hot Tank Design

Thermal Model

Heat transfer in a laboratory scale model is multi-dimensional in nature, i.e. the flow of energy or "heat" from a small laboratory tank to the surroundings is fully 3D due to the dominance of edge effects. In many ways the design of a large tank is a simpler task as it is a much closer approximation to 1D heat flow.

This can be illustrated by considering the diagram in Figure 13. The composite wall thickness Δt, relative to the radius R of a full-scale solar thermal tank, is shown notionally in the figure. Logically, the edge effect region for heat loss is negligible in comparison with the regions or areas afforded by the sides, top, and bottom portions of the tank. When the wall thickness, Δt, is very much smaller in comparison to the tank radius R, or:

$$\frac{\Delta t}{R} \ll 1$$

the flow of heat or thermal current is accurately and easily calculated by the use of 1D-type analytical thermal resistance formulas for the side, top, and bottom of the tank (see for instance, Edwards, Denny, and Mills [1] or Bird, Stewart, and Lightfoot [2]). The schematic for thermal losses to the environment for this situation, to a very good approximation, is shown in Figure 12. The total heat loss Qtotal is estimated by considering the flow of thermal currents individually, first through the side or lateral surface, then the top, and finally the bottom surface and then summed. Additional discussion germane to solar power, is provided in the recent paper by Gabbrielli and Zamparelli entitled "Optimal Design of a Molten Salt Thermal Storage Tank for Parabolic Trough Solar Power Plants," in the Journal of Solar Energy Engineering [3].

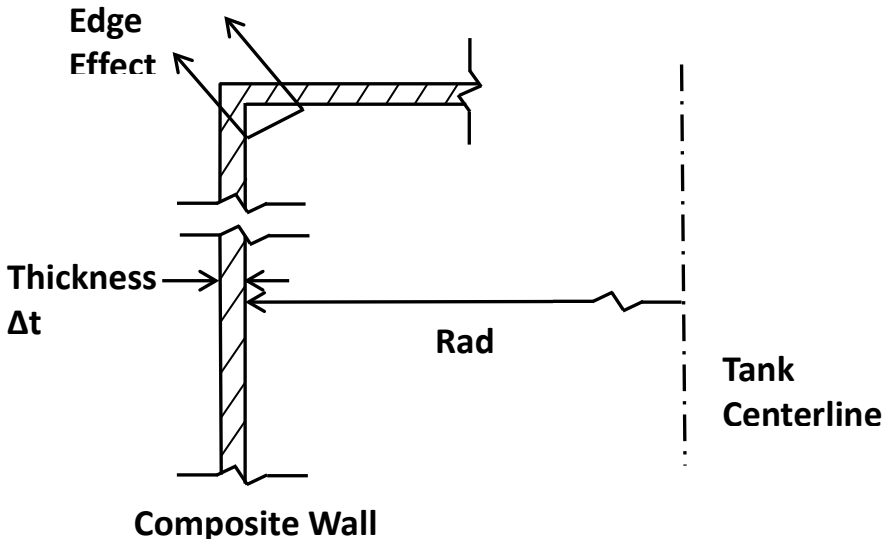

Figure 12. Geometry of a full-scale solar thermal storage tank.

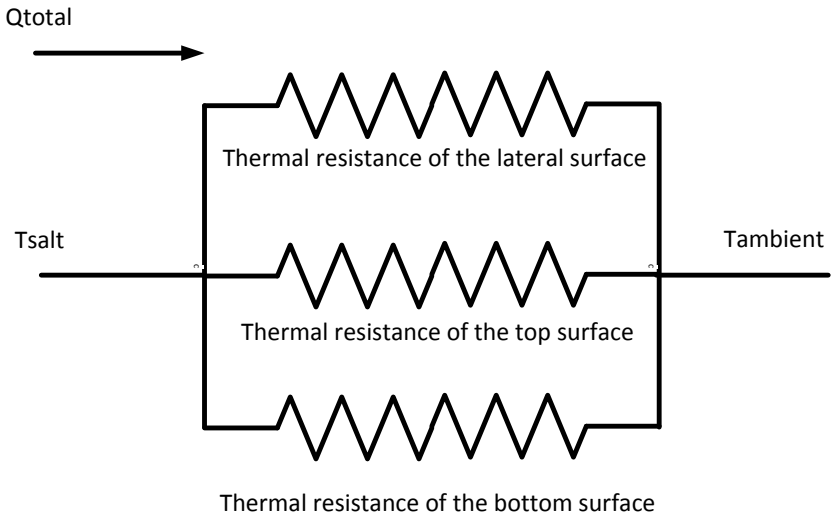

Figure 13. Parallel heat conduction from the salt through the lateral or side, top, and bottom surfaces to the environment [*adapted from Ref. [3]*].

Tank Model

The heat flux [W/m^2] in the normal direction for a representative laboratory scale tank is plotted in Figure 14 (the tank construction is shown in Figure 15); the arrow length represents the relative magnitude of the heat flux vector. The character of heat flow for the central portions adjacent to the top, bottom, and sides, suggest that heat transfer is dominated by a one-dimensional-type-phenomenon at these locations, as in the full-scale condition. However, the figure clearly shows that the overall heat transfer is strongly influenced by edge regions – i.e. the non-uniform and increasing vectors in the edge regions. Such consideration that the character of heat flow of the central portion is primarily of a one-dimensional nature, suggests a conservative approach or rationale for laboratory tank design, as follows:

Thermal current flows out the equatorial region and through the top and bottom most readily because the thermal resistance is geometrically minimized in these directions.

This heat flux must be arrested in these directions to provide a conservative tank design.

This is accomplished by individually adjusting the heat flux laterally, and also through the top, and bottom, for the complex layered system shown in Figure 15 to achieve the requirement of

$$\dot{q}_{limit} \leq 389 \text{ W/m}^2$$

for the prototype tank. This is an important criterion that facilitates the tank design strategy.

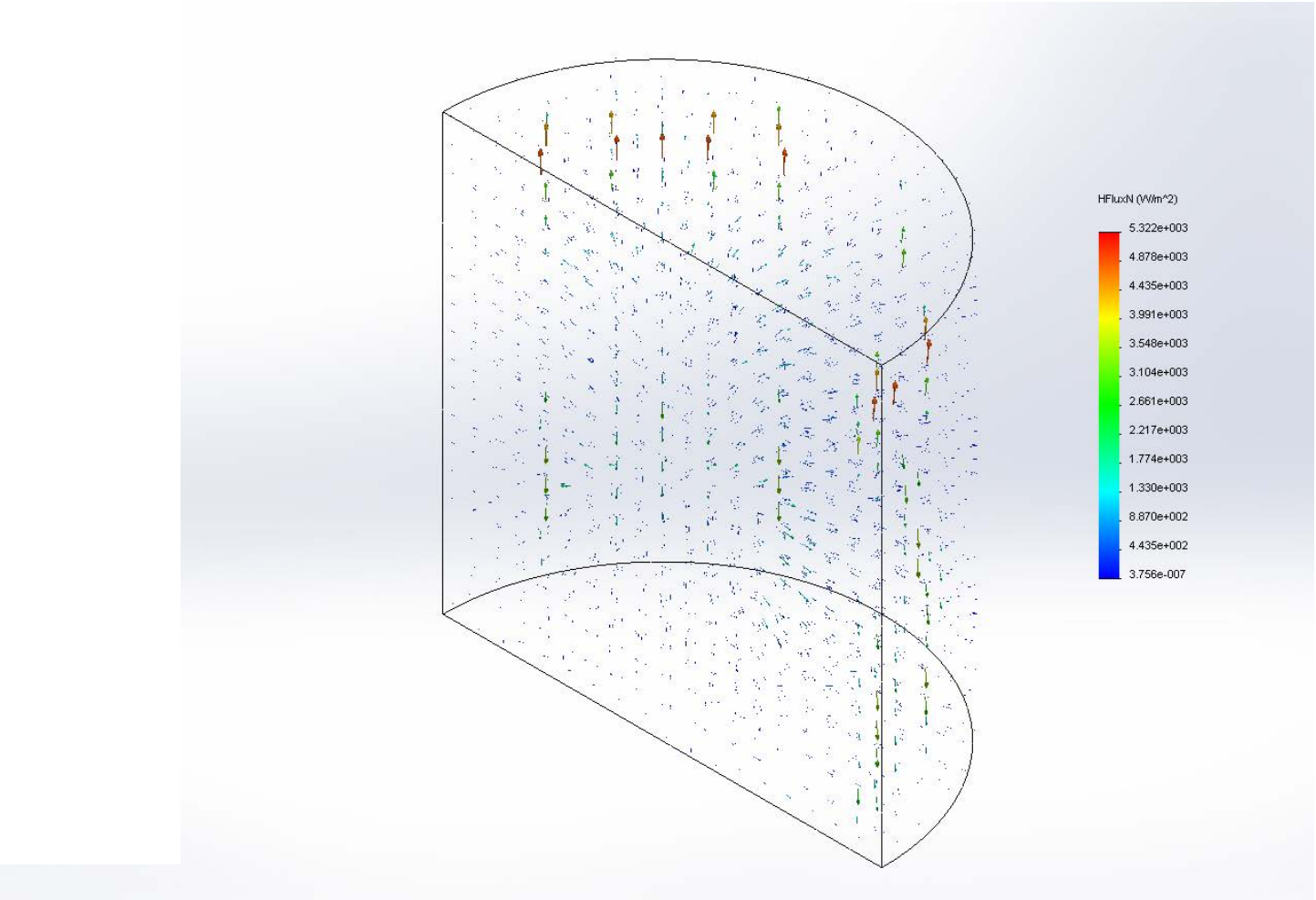

Figure 14. Normal heat flux vector for flow of heat from a laboratory scale thermal storage tank (*prediction using SolidWorks*).

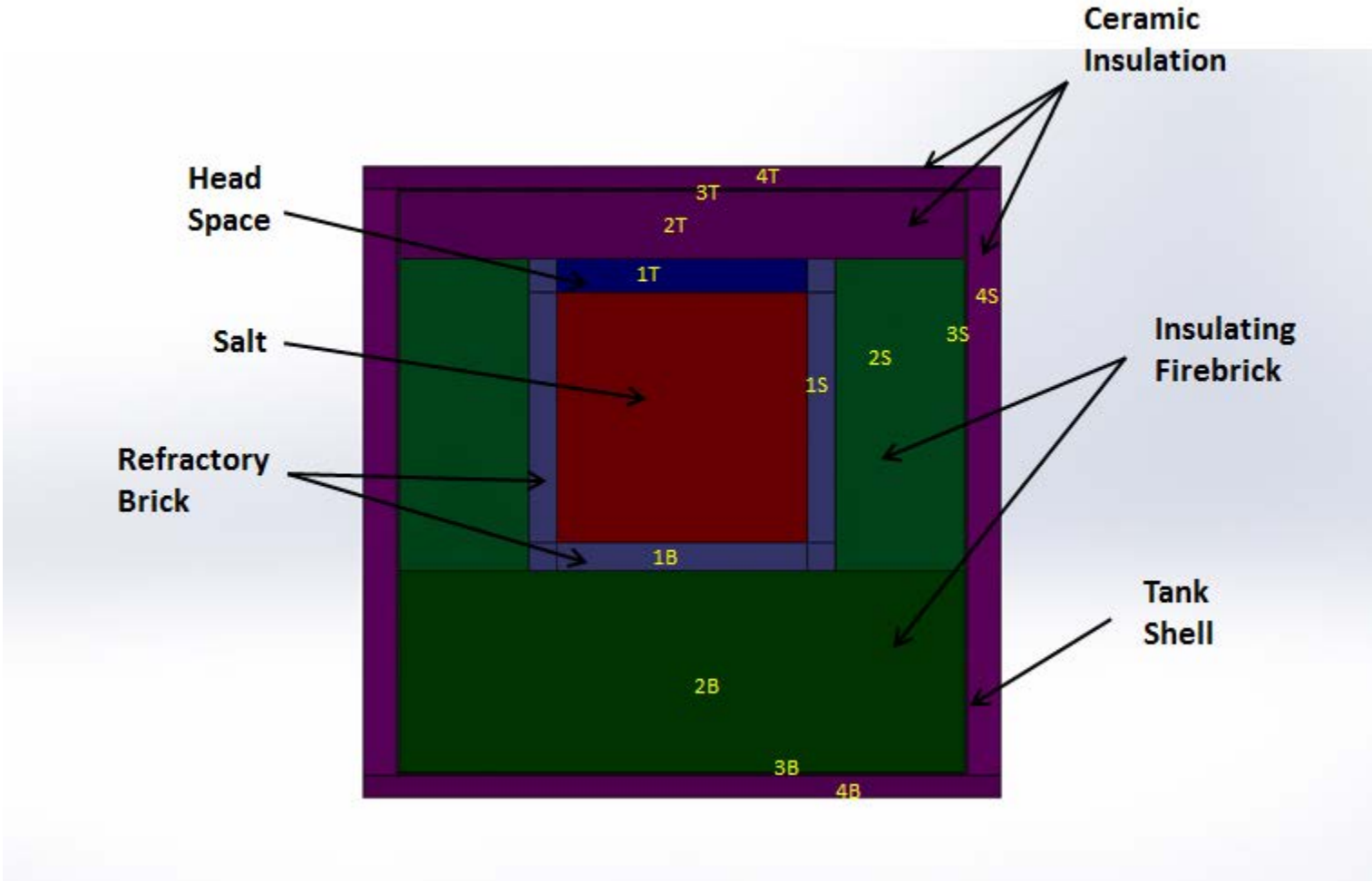

Figure 15. Nomenclature for tank design. Each layer is represented by the primary nomenclature 1, 2, 3, and 4 and the secondary nomenclature S, T, and B to denote the side, top, and bottom regions, respectively. Currently four layers are possible in the Excel Spreadsheet Model (discussed later) but more can be added if necessary.

This situation is described mathematically by the following system of equations:

The lateral or side(s) heat flux is calculated in the following way:

$$\dot{Q}_s = \frac{(T_{salt} - T_{amb})}{\sum R_s + R_e}$$

For each layer, the R_s terms are of the form

$$R_s = \ln(\frac{r_o}{r_i})/(2\pi k_s l_s)$$

The variables r_o and r_i are, respectively, the outer and inner radii for each layer; k_s is the associated layer thermal conductivity; l_s may be taken as a unit length or any other convenient length such as the inner tank length but should be chosen consistently from layer to layer.

The additional resistance for free convection, with associated convection coefficient h_c to the surroundings is given by,

$$R_e = \frac{1}{2\pi h_c r_{o,4} l_s}$$

The overall thermal resistance is given by the sum of all the resistances of the individual layers of insulation and the free convection to the environment:

$$R_{th} = \text{S}Rs + R_e$$

And, finally, the heat flux at the tank surface is denoted as

$$\dot{q}_s = \frac{\dot{Q}s}{2\pi r_{o,4} l_s} = \dot{q}_{limit}$$

In this manner l_s is an arbitrary dimension and does not enter the final equation.

The heat flux through the top is calculated in a similar manner, but is geometrically simpler:

$$\dot{Q}_T = \frac{(T_{salt} - T_{amb})}{\sum R_T}$$

For each layer, the R_T terms are of the form

$$R_T = l_T/k_T \pi r_T^2$$

The nomenclature *S* (side) is replaced by *T* (top); *l* this time denotes a layer thickness.

The additional resistance for free convection to the surroundings is given by,

$$R_e = \frac{1}{h_c \pi r_T^2}$$

The overall thermal resistance is given by the sum of all the resistances of the individual layers of insulation and the free convection to the environment:

$$R_{th} = \text{S}R_T + R_e$$

And, finally, the heat flux is

$$\dot{q_T} = \frac{\dot{Q}s}{\pi r_T^2} = \dot{q}_{limit}$$

In this manner r_T is an arbitrary dimension and does not enter the final equation.

The heat flux through the tank bottom is calculated in an identical manner to that of the top:

$$\dot{Q}_B = \frac{(T_{salt} - T_{amb})}{\sum R_B}$$

For each layer, the RB terms are of the form

$$R_B = l_B / k_B \pi r_B^2$$

The additional resistance for free convection to the surroundings is given by,

$$R_e = \frac{1}{h_c \pi r_B^2}$$

The overall thermal resistance is given by the sum of all the resistances of the individual layers of insulation and the free convection to the environment:

$$R_{th} = \text{S}R_B + R_e$$

And, finally, the heat flux at the surface is

$$\dot{q_B} = \frac{\dot{Q}_B}{\pi r_B^2} = \dot{q}_{limit}$$

In this manner r_B is an arbitrary dimension and does not enter the final equation.

This model was coded in Excel and verified against SolidWorks (SW) simulations prior to developing a 3D model in SolidWorks. Verification was done primarily to increase confidence for both the model coded in Excel and the mesh generated by SolidWorks, particularly since the

SolidWorks simulation was limited to tetrahedral elements.[2] In some sense, both the spreadsheet model and the SolidWorks models can be considered verified.

Comparison with SolidWorks and the Excel Model is shown in Table 6. Temperature distribution for the side as predicted by SolidWorks is shown for illustrative purposes in Figure 16. Note particularly that an attempt was made to arrive at a layered arrangement that reduced steel temperatures to less than 300°C to allow for the use of plain carbon steel. This is a second important criterion that was a driver for the design of the insulating layers. Research indicates that plain carbon steel may be used as a container material below these temperatures and is much less expensive than stainless steel [3, 4].

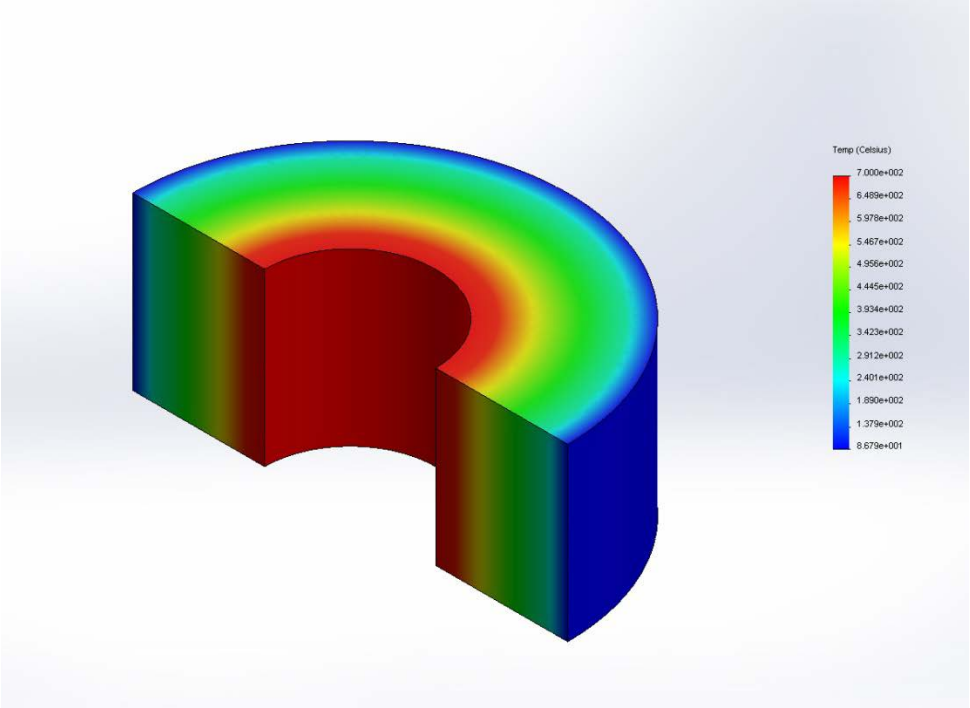

Figure 16:. Example temperature distribution predicted by SolidWorks for the side of a tank when only a one-dimensional simulation is considered.

Table 6. Heat Transfer Assessment: Comparison between Excel Model and SolidWorks (SW) for 1D radial (side), top, and bottom selective temperatures and heat flux. The comparison is excellent.

Direction	Steel Temperature (°C)		Skin Temperature (°C)		Flux @ Skin (w/m^2)	
	Excel	SW	Excel	SW	Excel	SW
Side	294.8	294.8	86.9	86.8	309.7	309.7
Top	247.3	247.3	96.4	96.2	356.7	356.8
Bottom	240.6	240.6	94.2	94.1	345.9	346.0

[2] The shape and type of tetrahedral elements used in Finite Element Analysis (FEA) can influence the accuracy of results.

Excel Design Tool and Design Methodology

Table 6 shows the Excel Model for a design using the properties for thermal conductivity of Monofrax CS-3 Fused Cast Refractory, Greentherm 28 LI Insulating Firebrick, Generic Steel, and Insboard 2300 HD. The model is a steady-state model with approximate values for density or specific heat. However, accurate values for thermal conductivity are used in the spreadsheet. Values of thicknesses for the different layers are iteratively adjusted to produce the results, shown in green, such that:

The tank shell temperature, understood to mean the steel shell temperature, is less than 300°C

The heat flux at the outside surface, denoted as q_s is less than q_{limit} = 389 W/m^2

These criteria are satisfied for each direction, side, top, and bottom. To reiterate, the second criterion of heat flux limit is very important for the success of the design strategy, as is the recognition that heat transfer is primarily 1D at the equatorial region and tank centerline regions.

The values for thermal conductivity are taken from product information sheets; judgment of the engineer is exercised to choose a value that is representative of the temperature of the layer (there is, of course, a temperature gradient across each layer).

The Excel Design Tool is first used to adjust the insulation thicknesses based on heat flux criterion at the surface and temperature targets of the steel tank shell (assumed to be 389 W/m^2 and 300°C, respectively in the spreadsheet shown). These values are then used to create a 3D SW model of the tank (discussed in the next section). The values in green are the Excel Model predictions for temperature and heat flux at various locations; the values in blue are SW's 1D predictions summarized in Table 6; the values in red are SW's 3D predictions discussed in the next section. The technique is conservative but does not take into account the heat loss that will occur due to instrumentation probes and equipment that will access the salt tank through the end-closure, nor heat loss that will occur from strengthening by ribbing that may be necessary to prevent tank warping and increase end-closure strength. The Design Tool also includes a section for estimating cost; the cost numbers are for illustrative purposes only; more research at this time is necessary to determine unit costs and manufacturing/installation costs, which are represented by the Multiplier column.

Note: Temperatures for the 3D model are representative of "hot" areas; there is some gradient predicted by SW at every location.

Definition of terms used to describe the insulating layers:

- Liner: Dense firebrick in contact with the molten material
- Internal Insulation: Either insulating firebrick or a castable material with very low thermal conductivity
- Shell: Carbon Steel, Stainless Steel or high temp alloy
- External Insulation: insulating fiber blanket or board

Three-Dimensional SolidWorks Thermal Model

The success of this modeling strategy is validated[3] or functionally demonstrated by the results for the fully three dimensional FEA performed with SolidWorks 2012 Simulation package. The temperature distribution for the tank, including all layers, is shown in Figure 17 with the temperature distribution for the steel tank alone depicted in Figure 18. The temperature at some locations on the surface is near 30°C while the steel tank temperatures range from 120°C to 246°C. The heat flux distribution was shown previously in Figure 14 and recorded as high as 251 W/m^2 on the side in the Excel Spreadsheet. The geometric configuration was previously depicted in Figure 4.

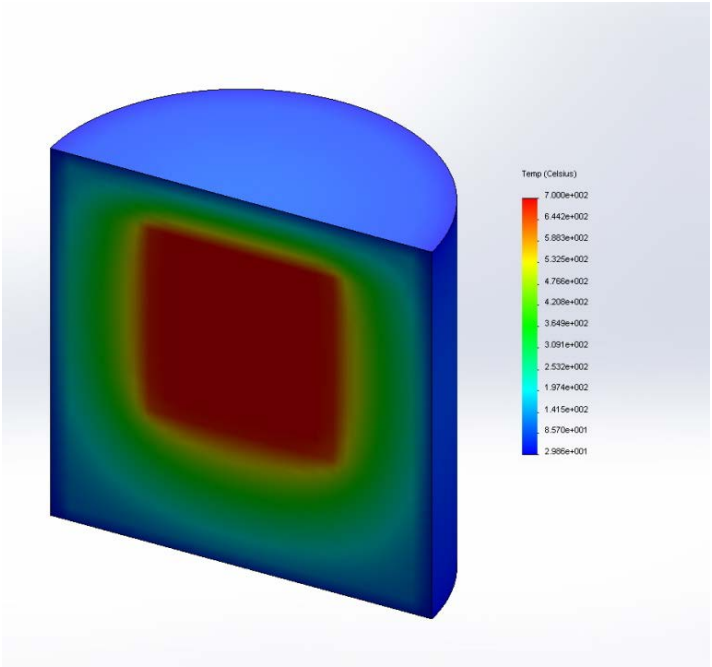

Figure 17. Temperature distribution for the laboratory scale thermal storage tank (salt at 700°C).

Preliminary Mechanical Design and Structural Assessment

A preliminary design and structural assessment was conducted of the tank. The design analyzed is shown in Figure 19, consisting of a stiffened end closure with a rather odd-looking boss for mounting multiple components through the lid. Based on the previous thermal assessment the internal diameter of the vessel is estimated to be about 50 inches. The bottom end closure is assumed to be bolted to a bottom support; hence, no stiffening is required on the bottom. The amount of stiffening required is highly dependent on the amount of internal pressure inside the tank, which is an important point that is discussed further below.

[3] The term "validation" as used in this context should not be confused by the term model validation. It is generally accepted that models are validated only by data and only verified, for example, by analytical results or independent software.

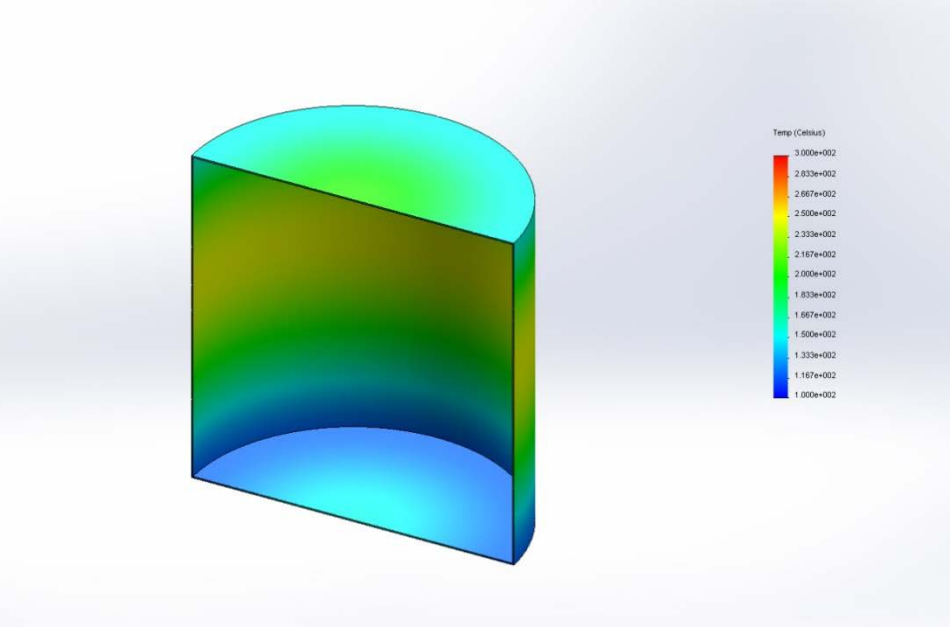

Figure 18. The predicted temperature distribution for the steel shell is between 120°C and 246°C.

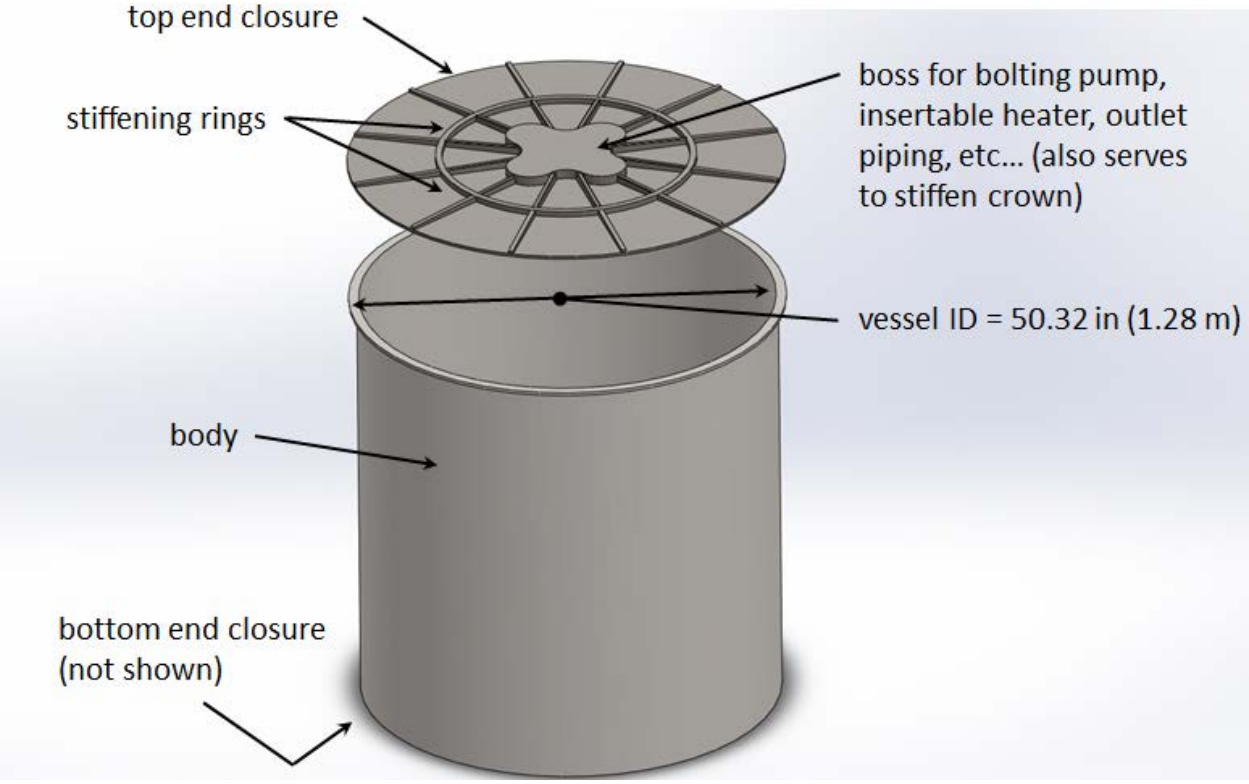

Figure 19. Preliminary design for the tank: Vessel (body) and bottom end closure thickness is 6.35 mm (1/4 inch); top end closure thickness is 9.525 mm (3/8 inch), additional boss thickness is 30 mm (1.2 inch), and rib height is drafted from 30 mm to 9 mm with width at 17.4 mm.

The structure was designed to a requirement of 20 psig applied to the inside. (Note: this was a preliminary pressure specification based on the potential salt vaporization pressure at elevated temperatures. However it is unlikely we will specify internal pressures over 15 psig as this would then be considered a pressure retaining vessel defined by the ASME B&PV Code). For analysis purposes, the 20 psig requirement leads to a loading force on the underside of the lid of,

$$F = P\,x\frac{\pi}{4}ID^2 = 20\,x\,0.785\,x\,(50.32)^2 \sim 40\,Kips$$

Where 1 Kip = 1,000 lbs.

In Figure 20 is shown the Von Mises stress analysis (the deformation of the lid is exaggerated). The Von Mises stress may be compared to the yield stress of the material and indicates one type of factor of safety based on yield of the material (other parameters like creep, vessel burst, and fracture, can be used to define a factor of safety). In general the averages stresses would be quite moderate at room temperature for steels ranging from 2 Ksi in the body to 3-15 Ksi (1 Ksi = 1,000 psi) in the lid.[4] There is a localized region at the top in the body, known as a discontinuity stress[5], that is approaching 20 Ksi; there is also a localized region of very high stress in the lid that is associated with the rib; the rib design needs refinement. However, the magnitude of the average stresses may not be moderate at elevated temperature (approximately 250°C) in the region where the lid and flange are bolted together and some more attention to design is also warranted in these areas.

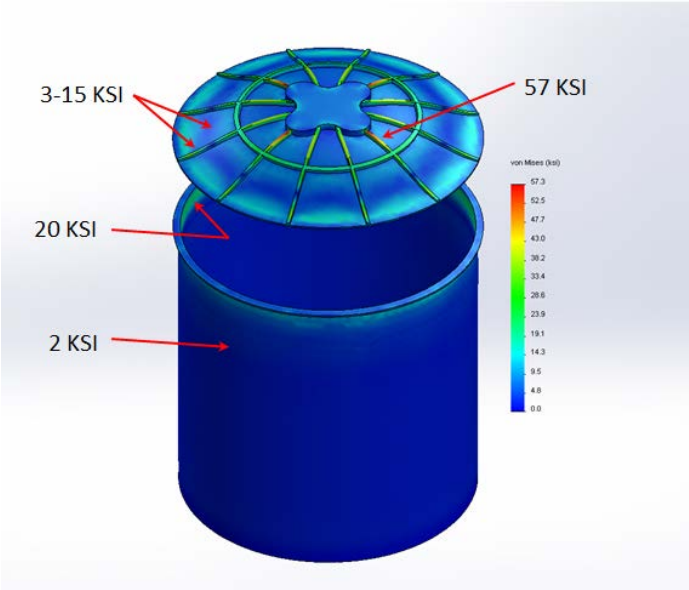

Figure 20. Von Mises stress for the hot tank.

[4] The yield strength of annealed stainless is typically on the order of 30 Ksi; A high strength steel, having a yield strength 40-50 Ksi, can probably be used for this lid application.

[5] A discontinuity stress occurs at regions with discontinuous geometry upon expansion (e.g., due to the pressure loading). In this case, the lid and right circular cylinder, as bolted, exhibit this discontinuous geometric feature. It is often difficult in practice to eliminate this type of stress concentration but it can be minimized by careful design. This phenomenon is absent at the bottom because the bottom closure is prevented from expanding.

Below are some discussion points based on the structural assessment:

The bottom end closure is not necessarily supported by the ground (it is assumed fixed in the analysis). Supporting this tank on the ground would require an assessment of concrete slab temperature stability. Most likely this tank can be supported on top of a relatively thin steel sheet, bolted to this sheet, and then attached on top of some sort of I-beam or unistrut arrangement with an air-gap to be defined. Note the thermal assessment assumes that heat is removed from the bottom by convection.

Any vessel of this type operating above 15 psig will need to be ASME certified; it is therefore paramount to determine the operating pressure requirement of this tank. An ASME stamp will add time and expense to the design, fabrication, and procurement, although we do have expertise for this in house. If the vapor pressure is only 20 psia (5 psig) then the vessel will likely not fall into the ASME cert category. A spring loaded relief device could be attached through the top end-closure set at 5 psig (a separate rupture type disc relief device must be installed for personnel safety set at a higher value but less than 15 psig). Then gaseous vapor that is generated would displace the head space gap at the top and the vessel would be pressured to only about 5 psig.

The lid weighs 332 lbs and the body weighs 740 lbs.

Hot Tank Construction

The assembly drawing for the hot tank and dimensions are shown in Figure 21 and Figure 22, respectively: The tank is constructed from approximately 4.5 inches KX-99 Tile that forms the inner liner, which is in intimate contact with the salt; it is then backed with 13.5 inches of G-23 Insulating Brick that forms a secondary liner; this composite forms the inner container. The inner container is framed by ¾ inch single seam 304L stainless steel sheet rolled into a cylindrical shell; approximately 1-½ inch Kaowool #6 bat insulation is then placed between the inner 304L shell and the 3/16 inch carbon steel casing that forms the outer secondary shell or container. In the final configuration, an additional 8.5 inches of insulation (Morgan Superwool Plus Blanket, 8#/sq. ft.) is added to the outer container to reduce heat loss.

The overall tank dimension is 61-¾ inch diameter by 80 inches high, as shown in Figure 22, and does not include the final 8.5 inches of insulation; also shown in this figure is the salt cavity dimension—20 inches in diameter by 45 inches in height. Approximately 4 inches in height was deleted in the final design iteration by adding a "plug" of insulating material and forming it to the lid—this is not reflected in the drawing. This plug was added to prevent heating the lid to high temperature (by direct radiation from the salt); without the plug the temperature of the lid could approach 700°C and reduce the material strength of the lid as well as increase heat loss from the top of the thermal storage vessel.

The lid has the same ports for instrumentation as the cold tank. This lid detail is repeated as Figure 23. The lid design is a critical feature for data acquisition, form, and function: It consists of multiple ports for temperature and pressure acquisition, pump and heater integration, and an additional port labeled as a 3" fill port where instrumentation can be placed and/or salt can be added after the lid is bolted to the flange.

The construction of the inner "pot" with refractory brick lining (KX-99) is shown in Figure 24; the tank is constructed from the bottom up with layers being progressively added; the trapezoidal design shown in the figure is necessary to conform to cylindrical geometry but added to the cost of the tank. The plastic liner or bag that is shown is only to provide a barrier for leak testing of the lid enclosure; it is later removed.

After adding the layers from the bottom-up, the lid is assembled to the tank to perform the leak test, as shown below in Figure 25. Note that channel steel is used to stiffen and flatten the outer portion of the lid; after machining the outer portion is uneven prior to stiffening with the channel steel. These ribs also support the lid for the low internal pressure that tends to deform the lid in a convex manner (even low pressure is a design concern due to the large area of the lid and the operating temperature—stiffening with ribs in this manner is standard design practice).

Table 7. Insulation layers in the hot tank

Insulation Name		**KX-99**	**G-23**	**Kaowool**	**Superwool Plus 128**	**BTU-Block**
Type		Refractory Brick	Insulating Brick	Ceramic blanket	Ceramic blanket	Ceramic board
Manufacturer		RHI	RHI	Morgan	Morgan	Morgan
Thickness	inch	4.5	13.5	2	8	2
Location		Liner direct salt contact	Liner	Interior	Exterior Sidewall	Exterior Bottom
Temperature Use Limit	°C	1,753	1,427	1,260	1,200	982
(Normal oxidizing atmosphere)						
Thermal conductivity	W/m.K	1.41	0.33	0.12	0.12	0.03
at 500°C						
Density, Avg.	kg/m3	2,290	769	128	128	288

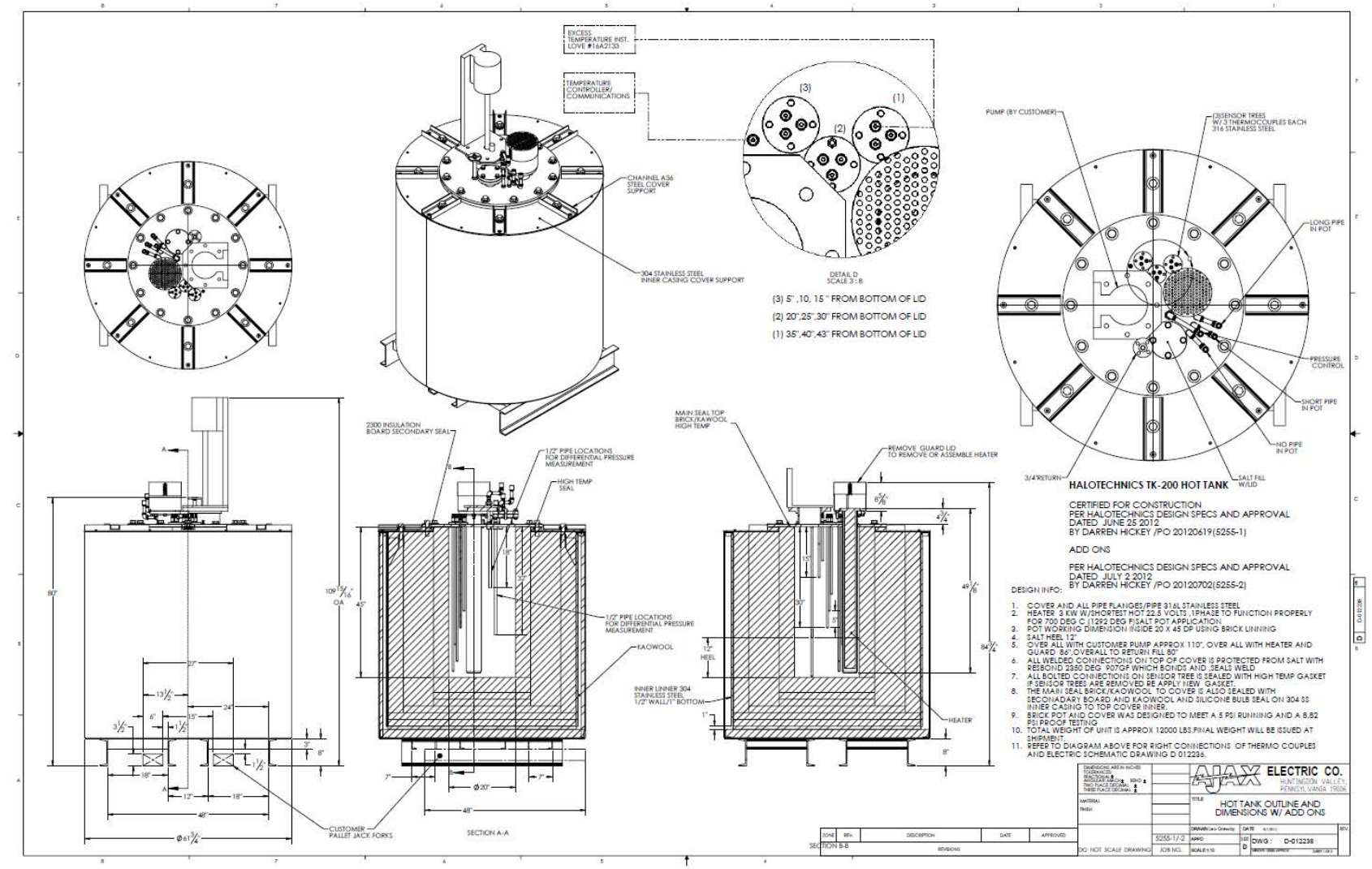

Figure 21. Hot tank definition.

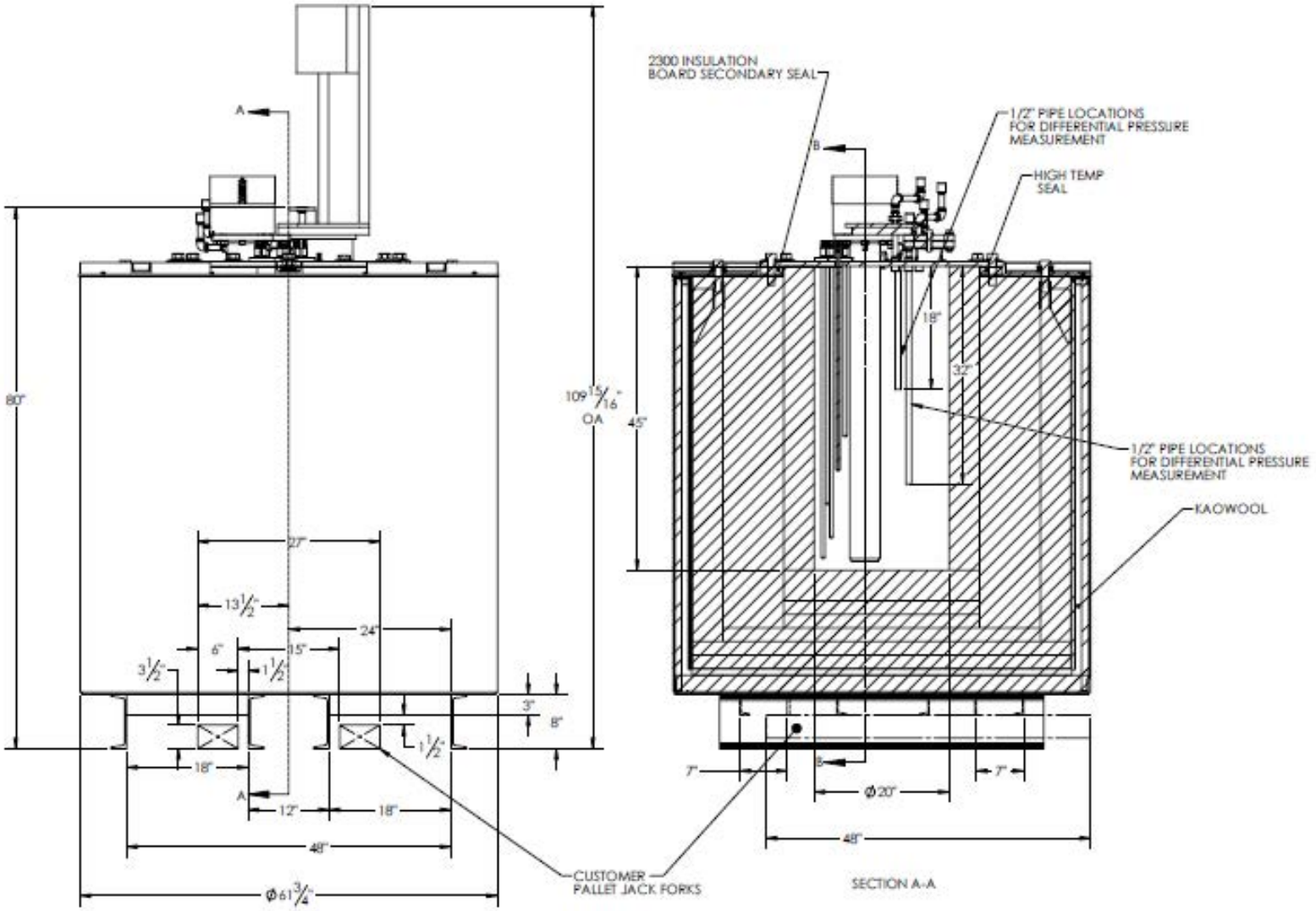

Figure 22. Hot tank dimensions.

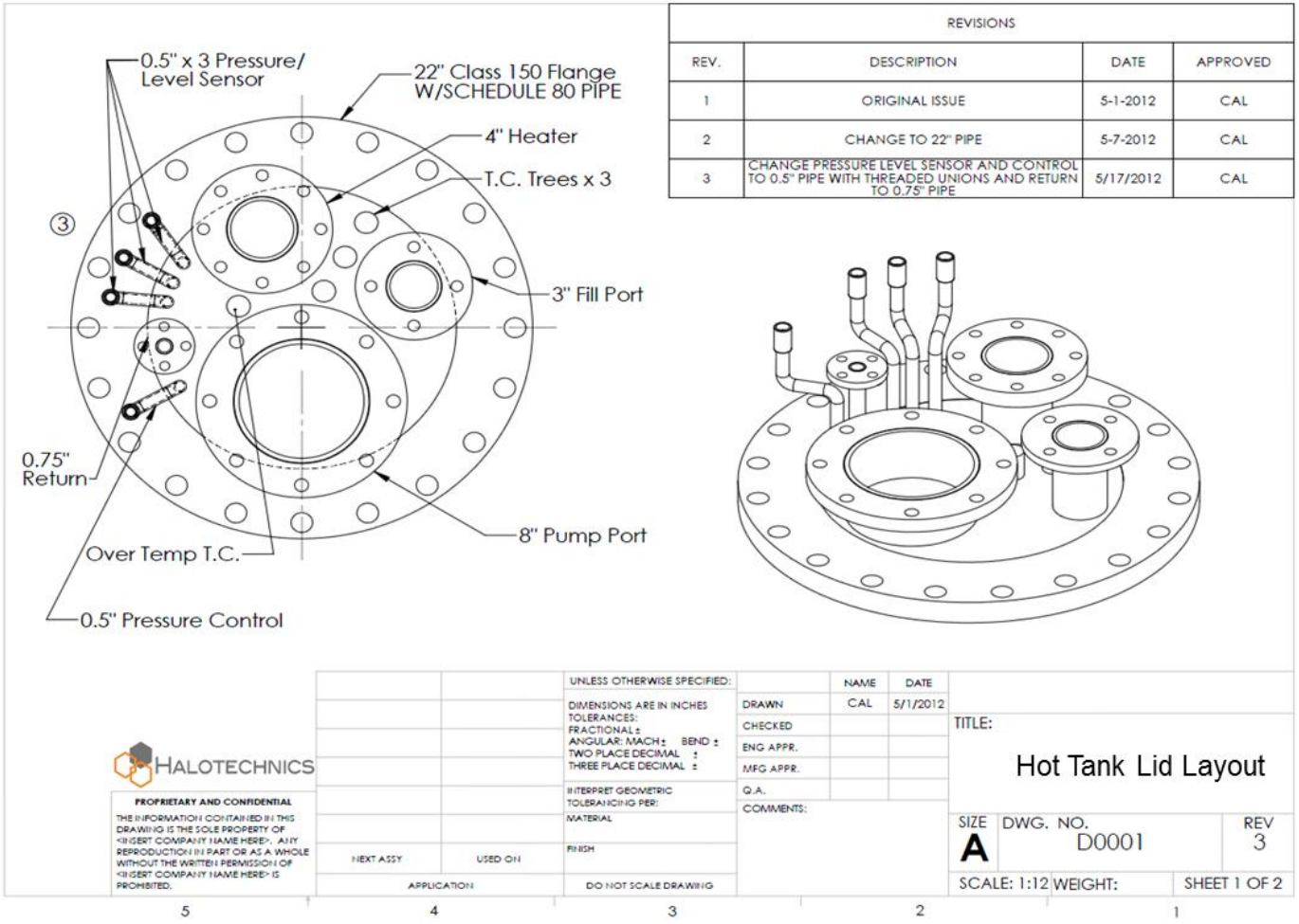

Figure 23. Lid detail; the hot tank lid detail is identical to the cold tank but all flange and piping is 316 SS.

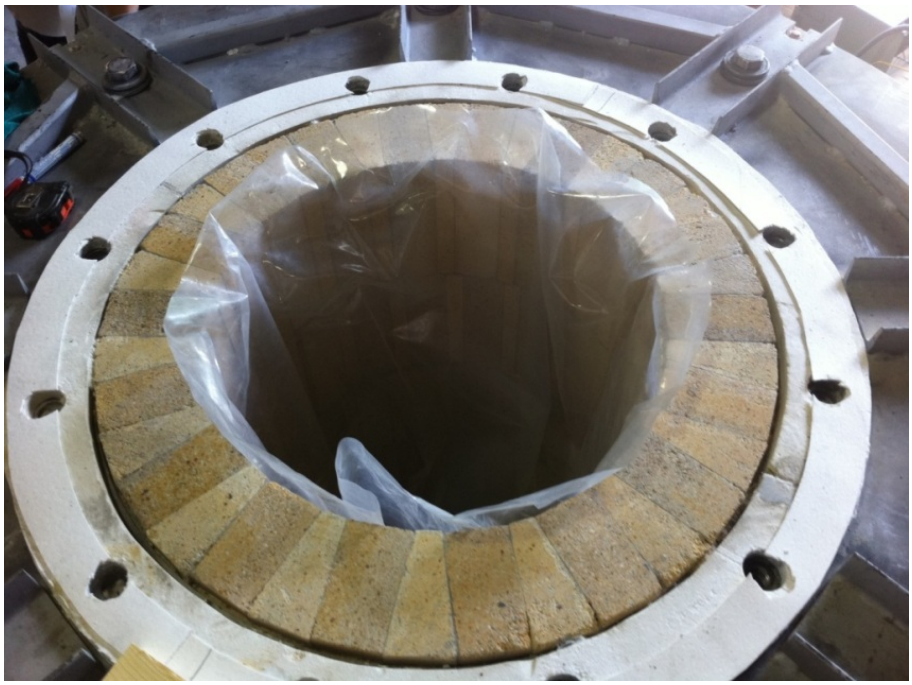

Figure 24. Refractory brick lining on the hot tank. Note: The bag is installed for leak testing purposes.

Figure 25. The lid is assembled for leak testing.

Hot Tank Performance

Thermal History

The hot tank temperature for the duration of operation is shown in Figure 26; it was operated from early November, 2012 to late February, 2013 for 95 days (2280 hours). As described later in this report, the tank was operated at a nominal temperature of 500°C for a long period due to conditioning of the firebrick and then increased to nominally 700°C for the final test. The thermocouple locations are indicated on Figure 5. Looking at Figure 26, it is interesting to note that the salt in the deeper part of the tank is initially at a hotter temperature than the top. Towards the end of December, there is a significant drop in the bottom temperatures A301 and A302 compared to the rest of the tank. This is believed to be due to salt infiltrating into the firebrick causing a deterioration of the brick's insulating properties. A post mortem inspection needs to take place to determine the condition of the bottom layer of insulating firebrick.

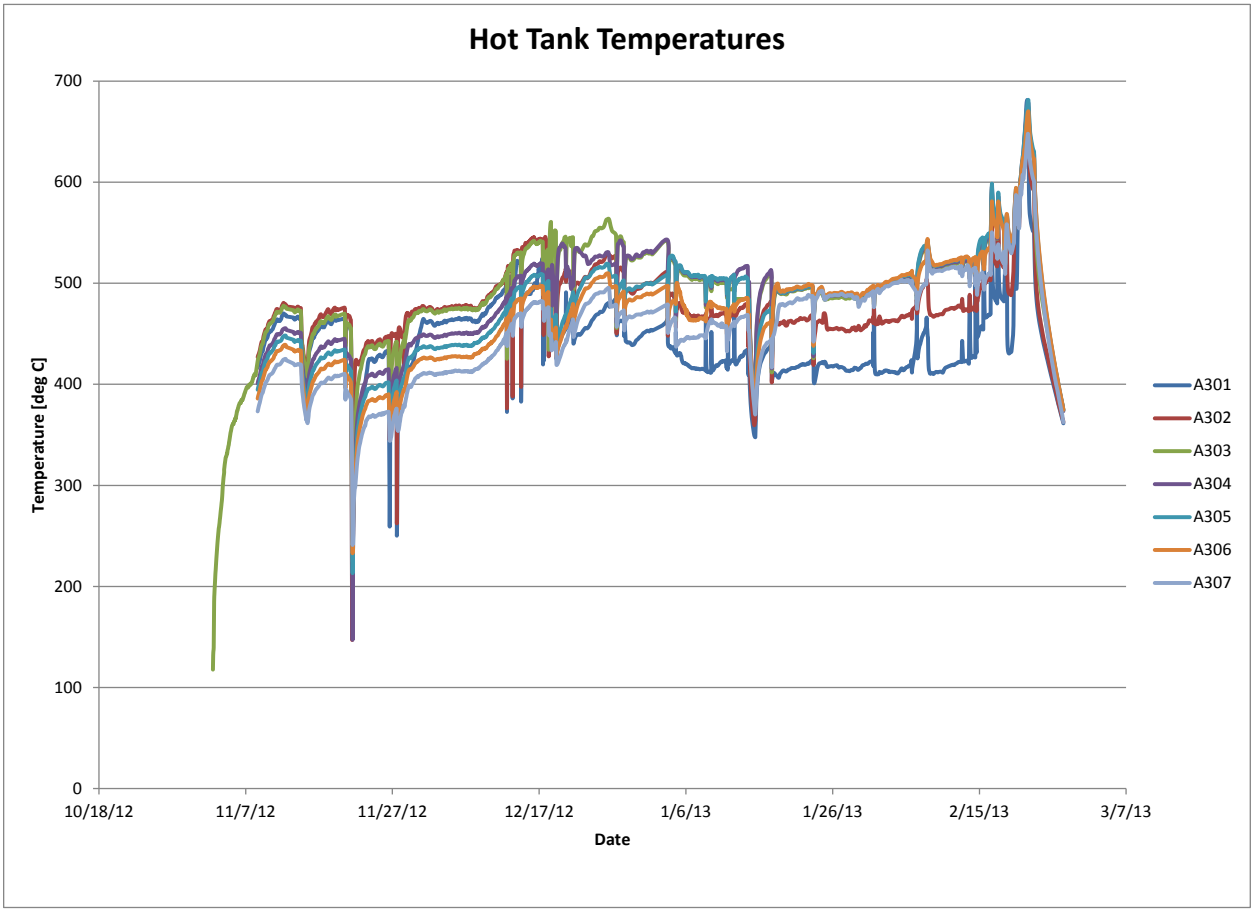

Figure 26. Hot Tank Temperatures. Thermocouple locations described in Figure 5. Spikes are due pulling the pump or heater for repair.

The initial fill of the hot tank was November 6, 2012. This inventory was heated to 400°C and began permeating into the brick. All salt additions are recorded in Figure 27. Initially, no

external insulation was added; the temperature increase stalled at about 425°C and insulation was progressively added; the insulation additions are also recorded in Figure 27.

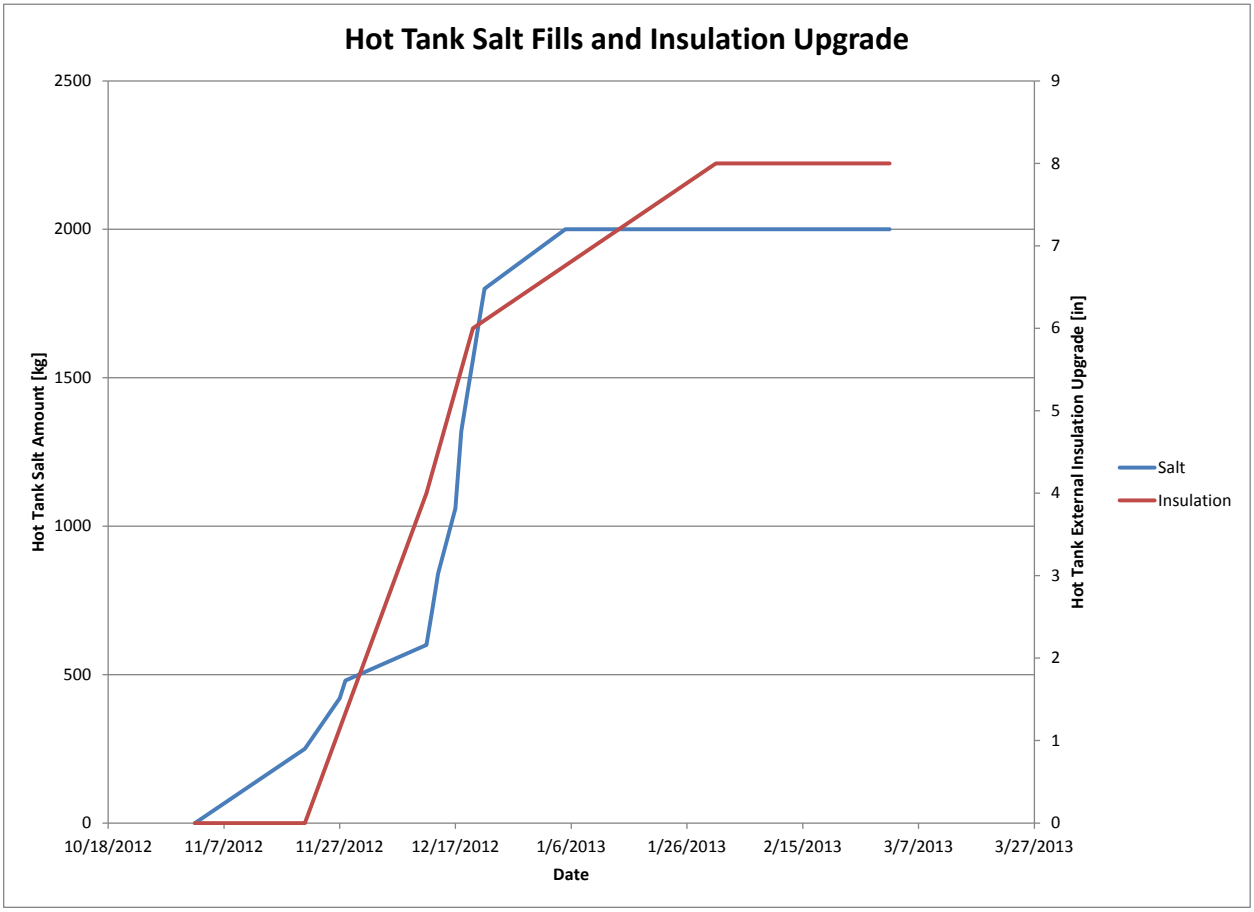

Figure 27. Hot tank timeline showing salt additions and external insulation upgrades.

The heat flux history for the hot tank is shown in Figure 28. In general the heat flux varied from about 70 W/m^2 to 170 W/m^2 for the duration of the program; this is discussed further in the next section.

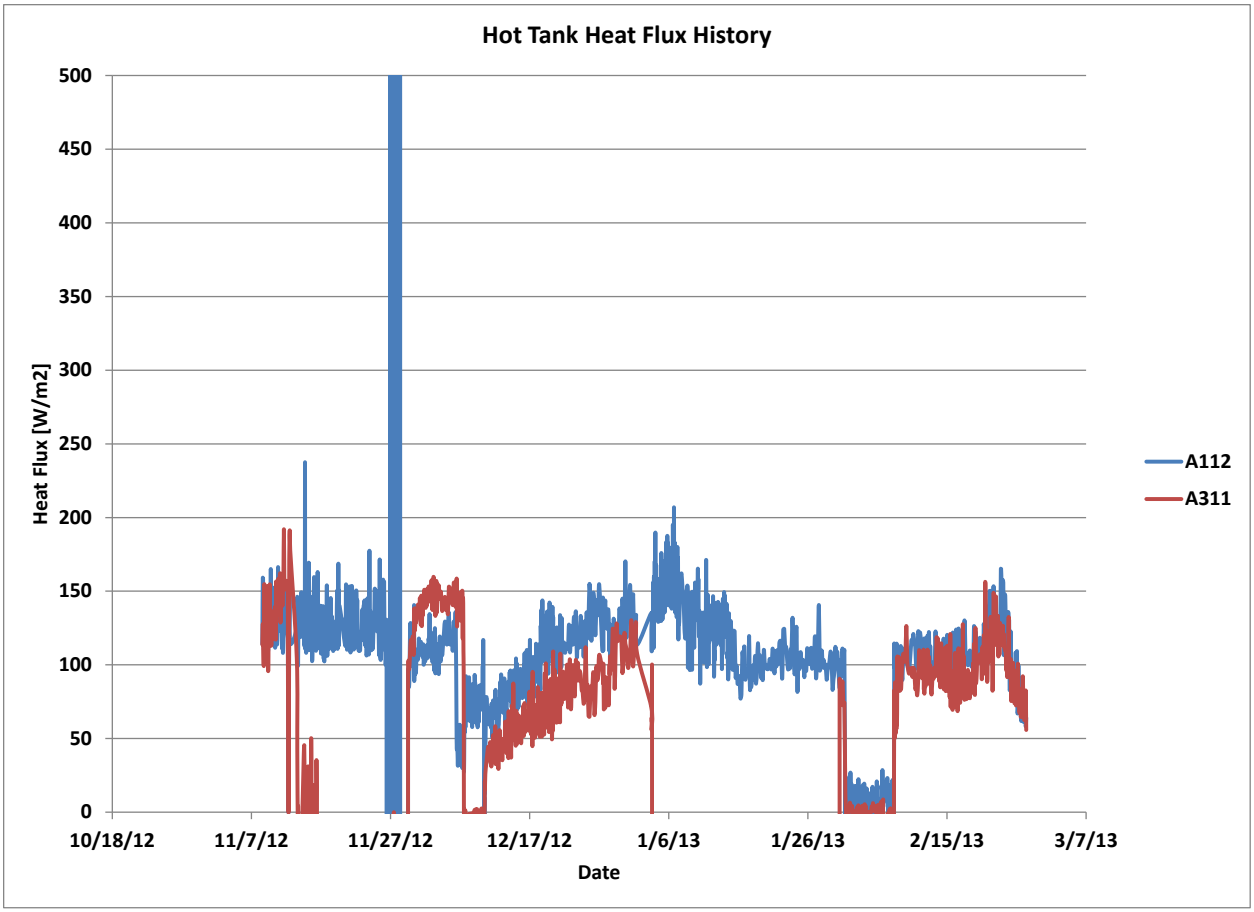

Figure 28. Hot tank heat flux history. Heat flux sensors installed on the hot tank exterior sidewall.

Thermal Performance

In order to increase the temperature in the Hot Tank to 700°C the FX was plumbed in a direct recirculation loop to provide an additional 7 kW of heat to the tank. A picture of the system connected in this way is shown in Figure 29. In this configuration, additional energy is added to the salt through the FX and the heated salt is then delivered back to the hot tank without first entering the cold tank. This energy added to the flowing salt is in addition to the energy added directly to the salt in the hot tank from the 3 KW insertable heater.

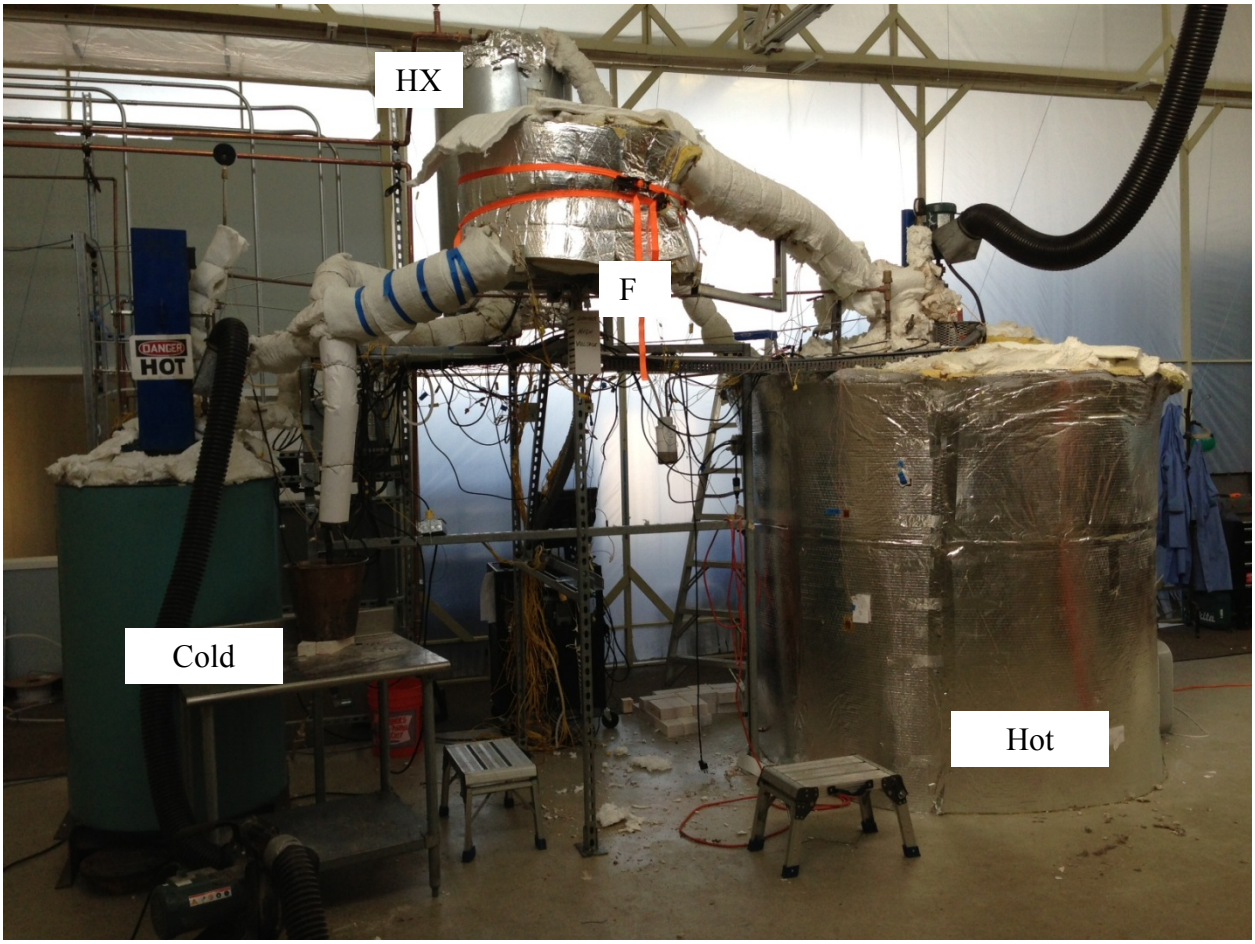

Figure 29. Complete system with the hot tank connected to the FX in a circulating loop.

The system was then run continuously for three days with round the clock supervision. The temperature increased from 550°C to 689°C before a ruptured tube forced the system to shut down. The temperature trace for this time duration is shown as : Approximately at midnight on 2/20 (2/20/12 0:00) the main heater in the hot tank failed and was replaced; during the replacement time the temperature dropped to approximately 575°C as shown. The other non-linear sections of the curve are due to increasing the flow rate or pump speed at various places during the operation. The final pump RPM was 1600 when the tube ruptured. The temperature of the salt being pumped into the tank was between 730°C and 740°C for the duration of the three day test.

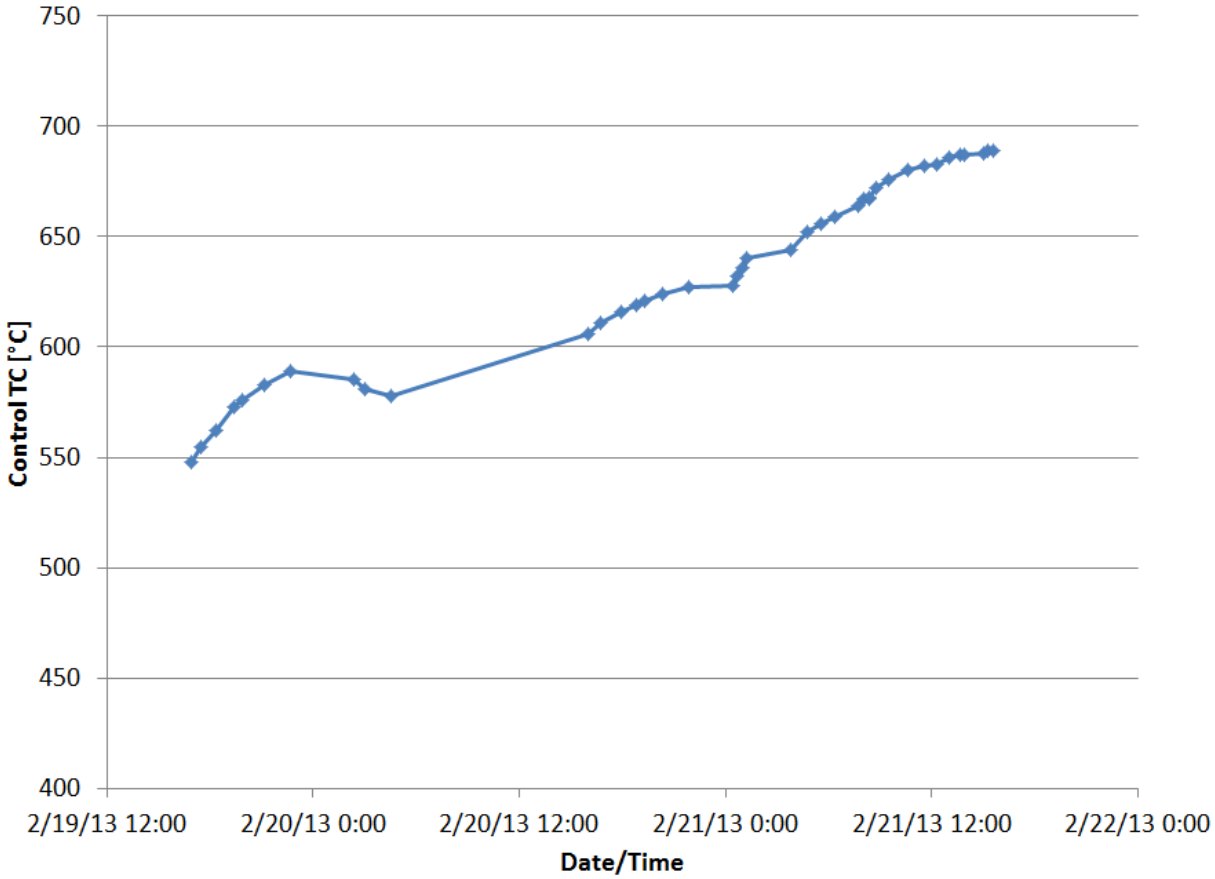

Figure 30. Temperature history of the hot tank when connected in the recirculation mode.

The recorded side heat flux is shown in Figure 31; nominally it is 150 W/m^2 although it does increase to a value of approximately 170 W/m^2 near the duration of the test; regardless, this is a lower heat flux than what was expected at the high temperatures (see previous quarterly reports) and is probably due to additional exterior insulation added for the final laboratory test.[6]

The hot tank insulation consisted of the following layers:

- Dense ceramic brick (4.5”) in direct contact with the salt
- Insulating firebrick (13.5”) immediately surrounding the dense brick
- Kaowool ceramic insulating blanket (2”) located around the inner stainless steel pot

[6] An assessment of heat loss from the hot tank suggests large heat loss through the lid via the pump integration at the flange and through the bottom of the tank. The 3 kW insertable heater could not raise the tank above about 500◦C despite the modest heat loss through the side. An additional 7 KW was then added to the salt stream by the FX in the closed recirculation loop described in this section to compensate for this situation.

- Superwool ceramic insulating blanket (8”) located around the carbon steel outer casing

The virgin thermal conductivity of the fire brick is also believed affected by infiltration of the salt; the affect is estimated in the following way:

Energy (Watts) transferred radially through the side, from classical heat transfer theory is given by

$$Q = 2\pi k\mathrm{L}\,(T_a - T_b)/\ln(\frac{R_b}{R_a})$$

where Q is the energy transferred through a homogeneous medium between locations a and b; R is the radial location and T is temperature.

All temperature locations throughout the assembly could be sampled except at the stainless steel shell (pot). Also, the thermal conductivity of the Kaowool and exterior insulation is not compromised by the salt. Conserving energy, this equation can be used to develop two equations in two unknowns to determine the effective thermal conductivity of the ceramic and pot temperature. The results are given below in Table 8. Also shown in Table 8 is the required insulation thickness for a commercial tank with an allowable heat flux of 300 W/m^2, which is 0.37 m. The heat flux of the pilot plant can also be estimated in this manner. The results shown that the pot temperature at elevated temperature (686°C) was 531°C; the effective thermal conductivity of the salt permeated ceramic was 0.73 W/m-K. As a comparison, the virgin material from published data is about 0.34 W/m-K. Table 1 shows the experimentally measured heat flux calculated from this data set as 114 W/m^2.

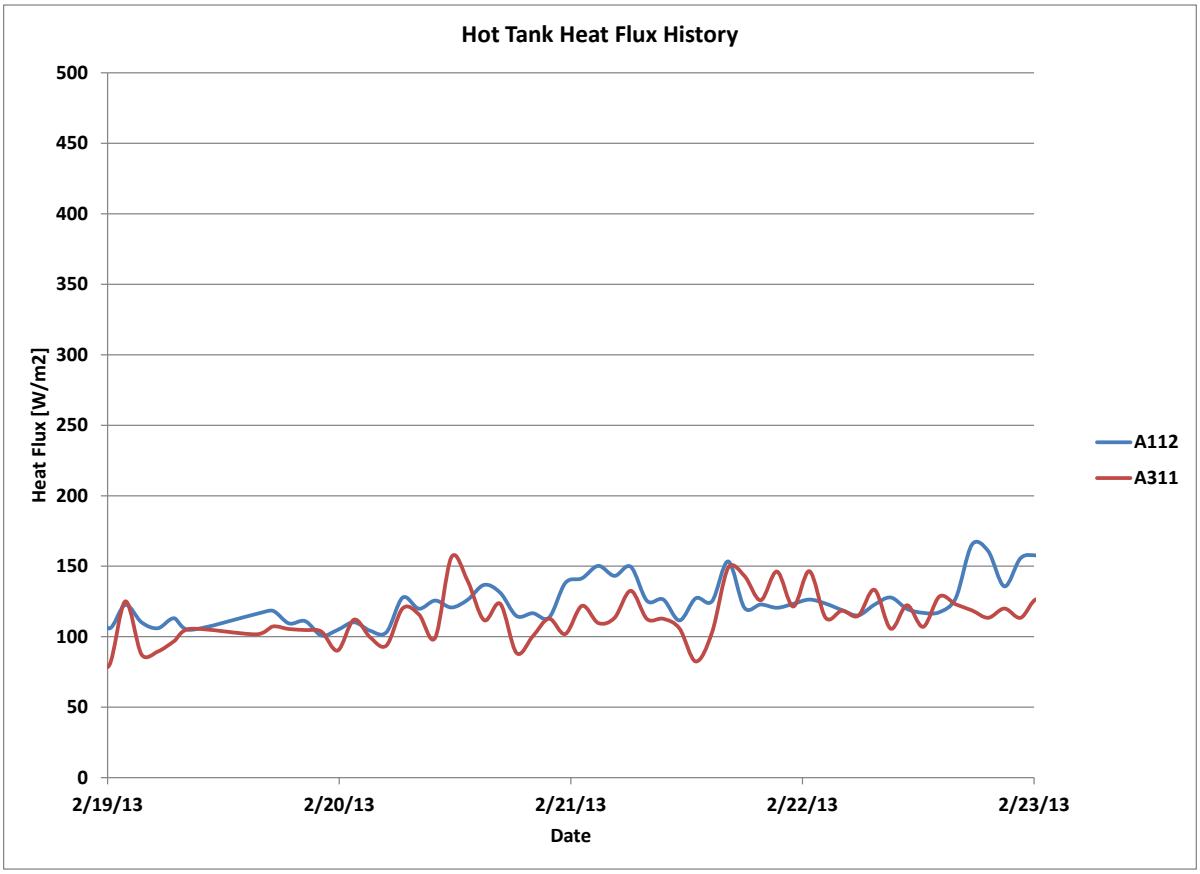

Figure 31. Raw recorded heat flux on the hot tank during the duration of the test. Heat flux sensors located on the external sidewall of the tank.

Table 8. Effective thermal conductivity of salt permeated ceramic and pot temperature.

Laboratory Tank		2/19/2013	2/20/2013	
Salt temperature	T1	574	686	C
Pot temperature (304L)	T2	**450**	**531**	C
Shell temperature (Casing)	T3	400	473	C
Skin temperature	T4	37	40	C
Salt radius	r1	10	10	in
Pot radius	r2	28	28	in
Shell radius	r3	30	30	in
Skin radius	r4	38	38	in
Effective conductivity of salt permeated ceramic	kc	**0.77**	**0.73**	W/m-K
Cond. Kaowool	kw	0.127	0.131	W/m-K
Cond. Insulation	ki	0.06	0.06	W/m-K
Heat Flux	q4	95.46	113.87	W/m^2
Max heat flux	300	W/m^2		
Conductivity of ceramic	0.73	W/m-K		
Salt temperature	700	C		
Desired pot temperature	550	C		
Required thickness	**0.37**	m		

Simulated Solar Receiver (FX)

FX Design

The furnace is divided into three portions to preclude the interfacial salt temperature (the temperature of the salt at the interior wall of the salt tube) from exceeding 740°C; physically, the furnace is a coiled tube similar to the HX but having three heater zones (FX-400,- 401, and -402).

The interfacial temperature (between the inner surface of the salt tube and the salt) can be found by application of heat transport analysis to the salt stream. The resulting equations are relatively simple although the mathematics is involved.

However, this is a classical problem; the detailed treatment can be found in some books on transport or transfer processes, for example, see Edwards, Denny and Mills, pg. 106-111, "Transfer Processes, 2nd edition. The treatment from Edwards, Denny, and Mills is summarized and applied as follows:

In a section of pipe l the energy $\dot{Q}$ in Watts transferred to the salt stream flowing at $\dot{m}_s$ kg/s is:

$$\dot{Q} = \dot{m}_s C_p \Delta T = \dot{m}_s C_p (T_f - T_i) \qquad (1)$$

In this equation T_f is the bulk temperature of the salt stream at the end of the section of length l while T_i is the salt (bulk) temperature at the beginning of the section. It is important to appreciate that the bulk temperature is not the actual temperature of the flowing salt but the temperature that would result should the salt stream be diverted into an adiabatic container and allowed to equilibrate.

Note that $\dot{Q}$ can also be represented as

$$\dot{q} = \frac{\dot{Q}}{\pi D_i l} \qquad (2)$$

where D_i is the internal pipe diameter and $\dot{q}$ is the radial (wall) heat flux at the interface between the salt and pipe. It is this heat flux through the length of pipe section l, as shown below, that must be limited so that the salt temperature at the interface does not exceed the temperature that the salt locally decomposes.

It is easy to show that the flow is laminar for the laboratory scale system; then for laminar flow the radial temperature of the salt can be predicted analytically: For each furnace section the wall temperature T_w at the exit of the section is given by (see the previously mentioned reference):

$$T_w = T_c + \frac{3}{4}\dot{q} D_i/(2k) \qquad (3)$$

where

$$T_c = T_f - \frac{7}{24}\dot{q} D_i/(2k) \qquad (4)$$

In these equations k is the salt conductivity and T_c is the centerline temperature of the salt at the end of the pipe of length l. T_w (theoretically equal to the salt temperature at the interface) should not exceed the salt decomposition temperature. Eqs. (3) and (4), if combined with Eq. (2), show that the wall temperature depends only on l, which is not intuitive.

The furnace (FX) domain can be divided into any number of individual sections l_i; the total length of the FX will decrease proportionally as the number of sections increase. As a matter of practicality three sections were chosen. Then, Eqs. 1-4 were applied to arrive at the design shown in Table 9.

Table 9. FX Requirements and Parameters for the NREL Flow Control Test Loop. Thermal conductivity used for calculation purposes was 0.35 W/m-K.

FX-XXX	l (ft)	T_i (°C)	T_f(°C)	T_w(°C)	$\dot{Q}$
FX-400	13	300	565	739	3312
FX-401	14.4	565	675	740	1375
FX-402	5.8	675	700	737	313
Total	33.2	N/A	700	N/A	5,000

FX Construction

The FX was constructed out of coiled 304 stainless steel tubing, ½" OD and 0.035" wall thickness, 36' in length, as seen in Figure 32. The electric heaters were wrapped directly around the stainless steel tubing according to the design which delivers 5kW of heat to the salt. The tubing and heater assembly was then insulated with 4" of fiberfrax on the inside and 4" on the outside. The FX was then encased both on the inside and outside with two sheets of aluminum to contain the insulation, as seen in Figure 33. The FX was instrumented with 12 thermocouples placed at regular intervals down the length of the tube. Three of these thermocouples are used for controlling the three separate heating zones, and the others are used for temperature monitoring across the various stages of the furnace.

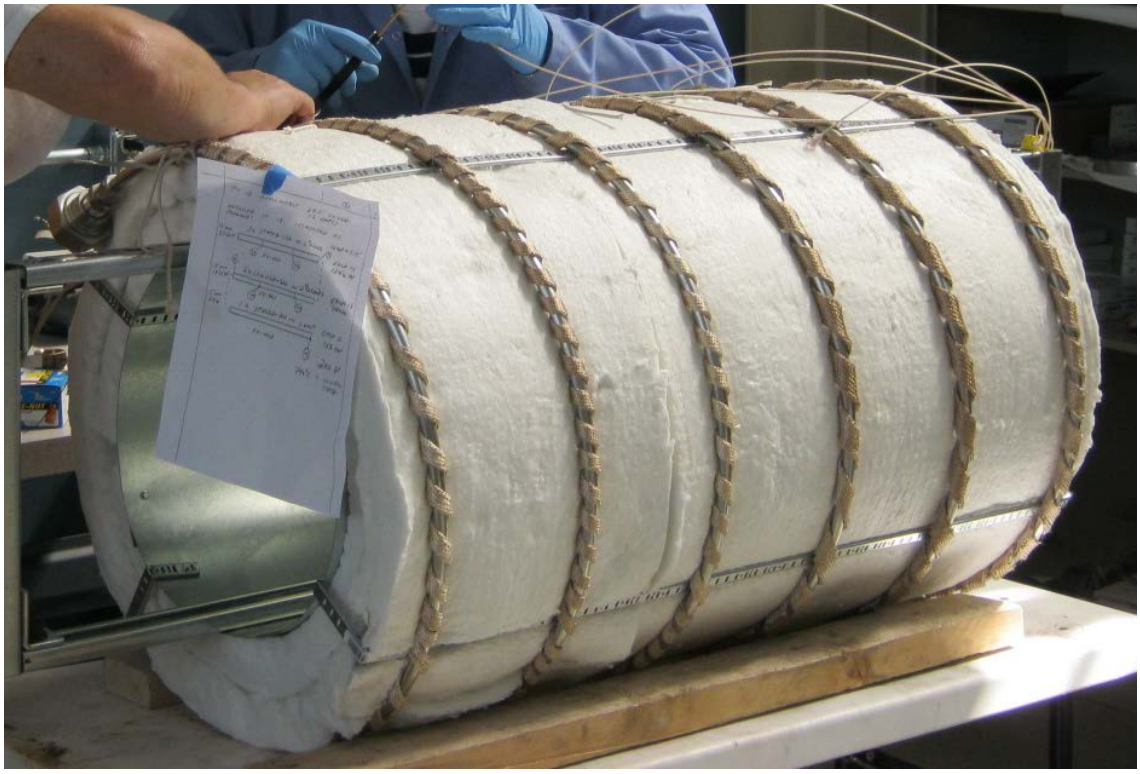

Figure 32. Construction of the FX. Heating tape is wrapped around stainless steel coiled tubing. The coil is encased in Fiberfrax insulation.

After plumbing the FX into the system and turning on the heaters, the circuit breaker tripped within three seconds of the initial power-on. After opening up the furnace for inspection, it was revealed that one of the heaters, possibly deficient in construction, shorted to the stainless steel tube and caused damage to the unit which was irreparable. The FX was rebuilt using a spare stainless steel tubing coil.

The second version of the FX was identical to the first one with the addition of a high temperature electrical insulator between the stainless steel tube and the electric heaters. This insulator will prevent the arcing of a potentially defective heater.

Figure 33. FX encased in a stainless steel jacket, being installed in the system.

Figure 34. Insulation tape is wrapped around the tubing prior to wrapping the electrical heating tape for the second version.

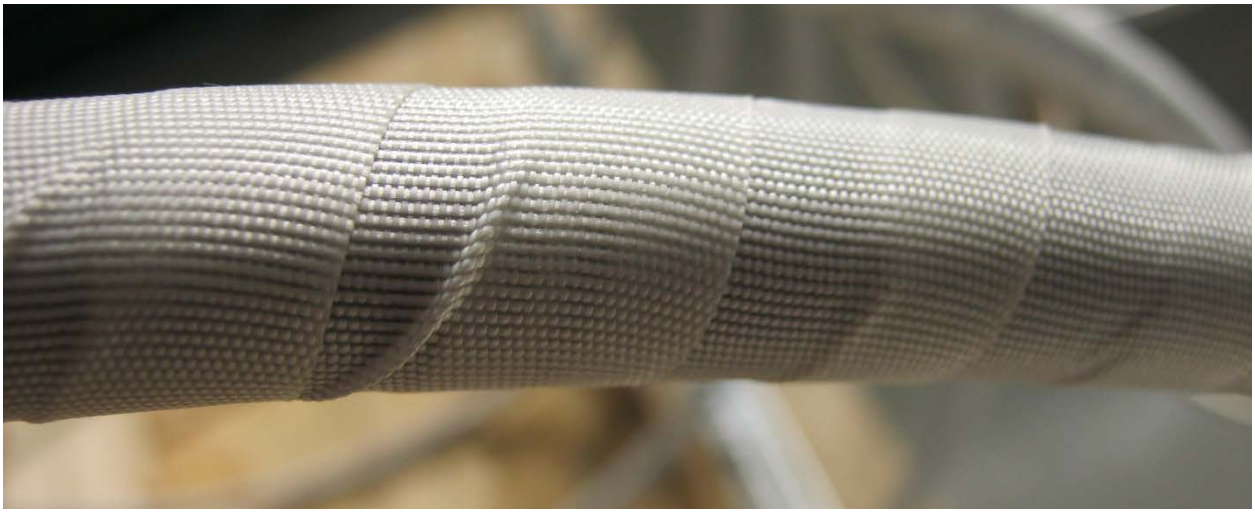

Figure 35. Close up of the high temperature fiberglass insulation tape.

FX Performance

The results demonstrating that 6.5 kW of heat can flow into the salt through the furnace (FX) are presented in Figure 36. Because the electronic scale has a limited range, the longest period of flow measurement is approx. two minutes. The mass is recorded on Figure 36 over the measurement period with a linear approximation indicating a mass flow rate of 19 g/sec. The inlet and outlet temperatures are displayed (approx. 277°C – 702°C). Previous measurements of the heat capacity reveal a value of 0.8 J/g-K. Using these values, the power going into the salt can be calculated using equation (1), which is also plotted in Figure 36 as the Power.

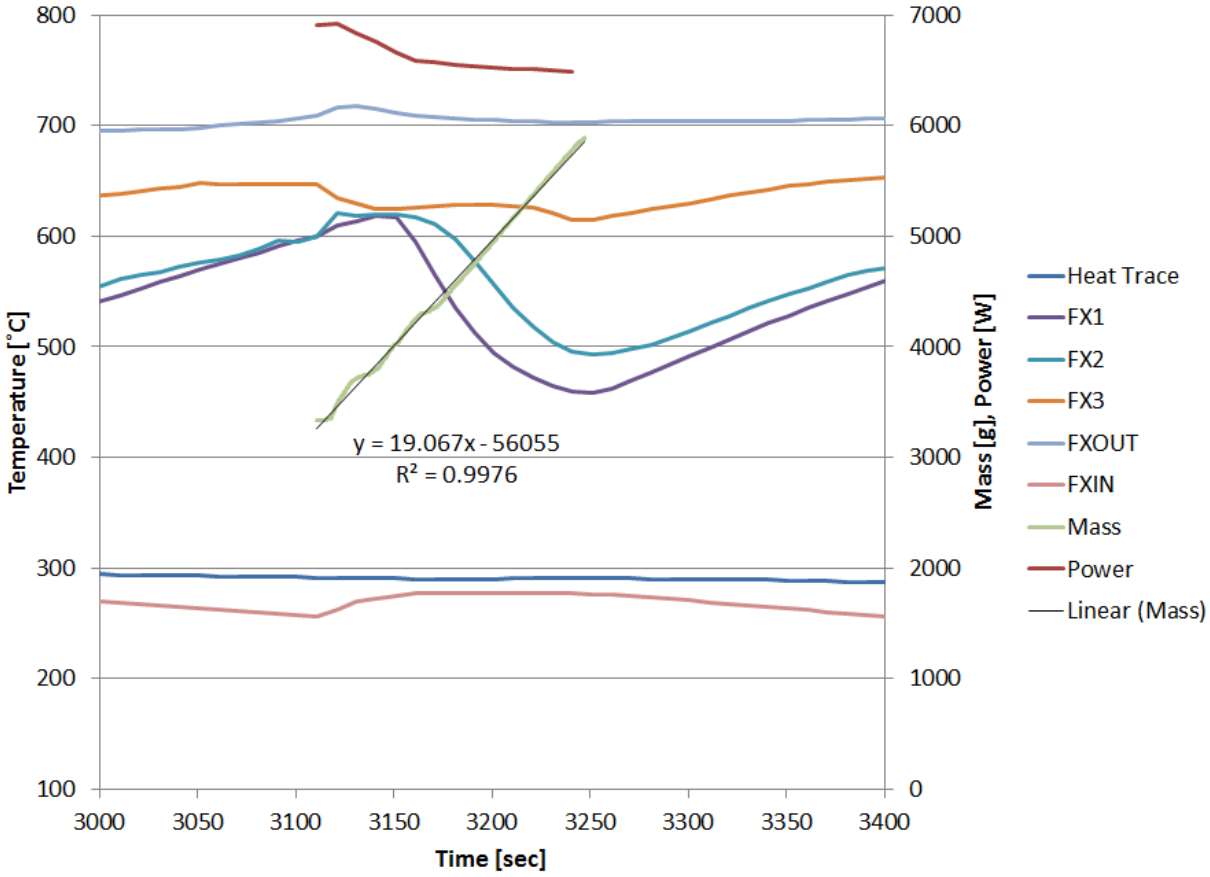

Figure 36. Data chart from the FX indicating 6.5 kW of thermal power

FX1, FX2 and FX3 indicate the salt temperatures in the three zones. FX1 and FX2 temperatures drop as the cold salt flows through the coil. Clearly the FX was not operated long enough to generate steady state data due to the limitation of the scale. However the results are very encouraging in demonstrating the FX and the cold pump can deliver the specified 5 kW of thermal power into the salt at a stable flow rate.

Simulated Steam Generator (HX)

HX Design And Construction

The construction of the HX is shown by Figure 37, Figure 38, and Figure 39; Figure 40 also shows the HX installed into the flow control loop.

The construction of the HX was as follows:

1. The stainless salt tube (304L) is coiled to produce a compact HX. The salt tube is ½" tubing by 0.020" wall.
2. Next, ¼" thin wall copper tubing is wound around the salt tube; the copper tubing carries the chilled water.
3. Copper foil (not shown) is then wound around the assembly to improve heat transport between the salt tubing and the copper tubing.
4. Then, heaters are wrapped around the foil, copper tubing, and salt tube. This construction allows the assembly (salt, salt tubing, copper, and water) to be heated as well as cooled. The copper tubing ends are manifolded together with ½ inch copper tubing to distribute the water; the ends of the manifolds are shown in Figure 38. Finally, insulation and sheet metal are wrapped around the entire heat exchanger, inside and out; the inside of the HX fully assembled with sheet metal and insulation is also shown in Figure 38. Figure 39 shows the exterior of the exchanger being completed. Enough wattage is introduced into the assembly so that both heat losses from the assembly and 5 kW of energy is being removed by flowing the water through the HX prior to salt introduction; prior to salt introduction the salt tubing is heated to 300°C; then the heater is throttled back as the salt starts to flow and the salt energy is then transferred to the water.

The final assembly is shown installed into the flow control loop in Figure 40.

It was not possible to estimate the interfacial heat transfer resistance between the copper tubing and stainless salt pipe; hence, a simple countercurrent flow model was developed that shows in the absence of this interfacial resistance 26 feet was necessary to dump 5 kW into the water heat sink: this length was doubled noting that if the interfacial resistance reduced the effective conductivity of the steel by a factor of 10 for the countercurrent model, then the length of tubing necessary to "dump" 5 kW of energy increased to 50 ft.

Figure 37. The copper tubing is wound around the salt coiled (steel) tubing. The ends of the copper tubing are visible and then fit into the ½ inch copper manifolds.

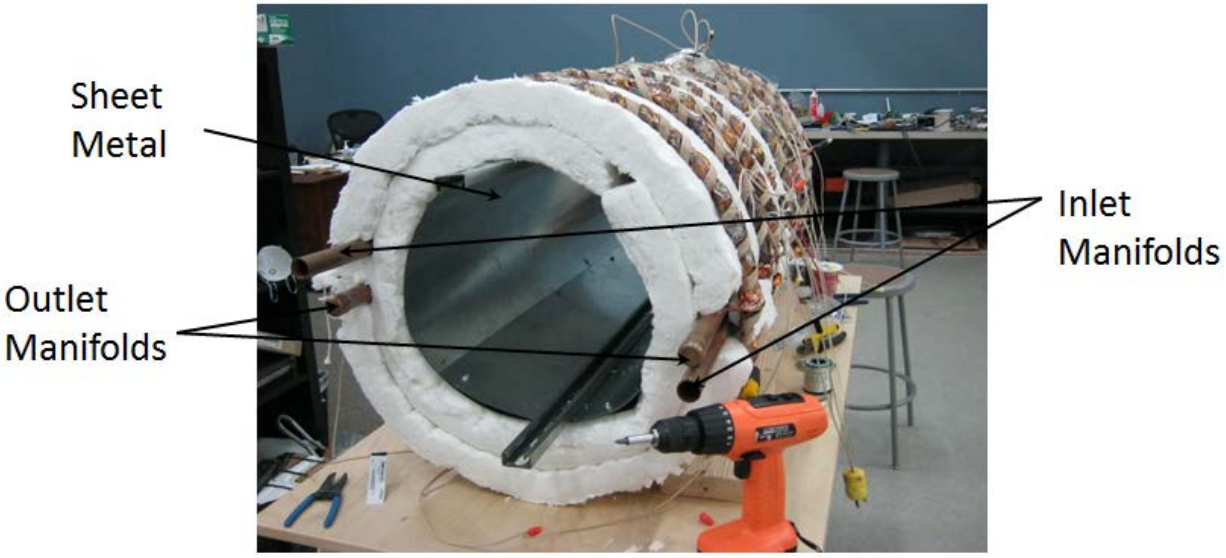

Figure 38. The manifolds are attached, insulation is added, and sheet metal completes the interior assembly of the HX.

Figure 39. Insulation is then added to the exterior followed by a sheet metal casing, as was shown for the interior in Figure 11 (exterior sheet metal is not shown).

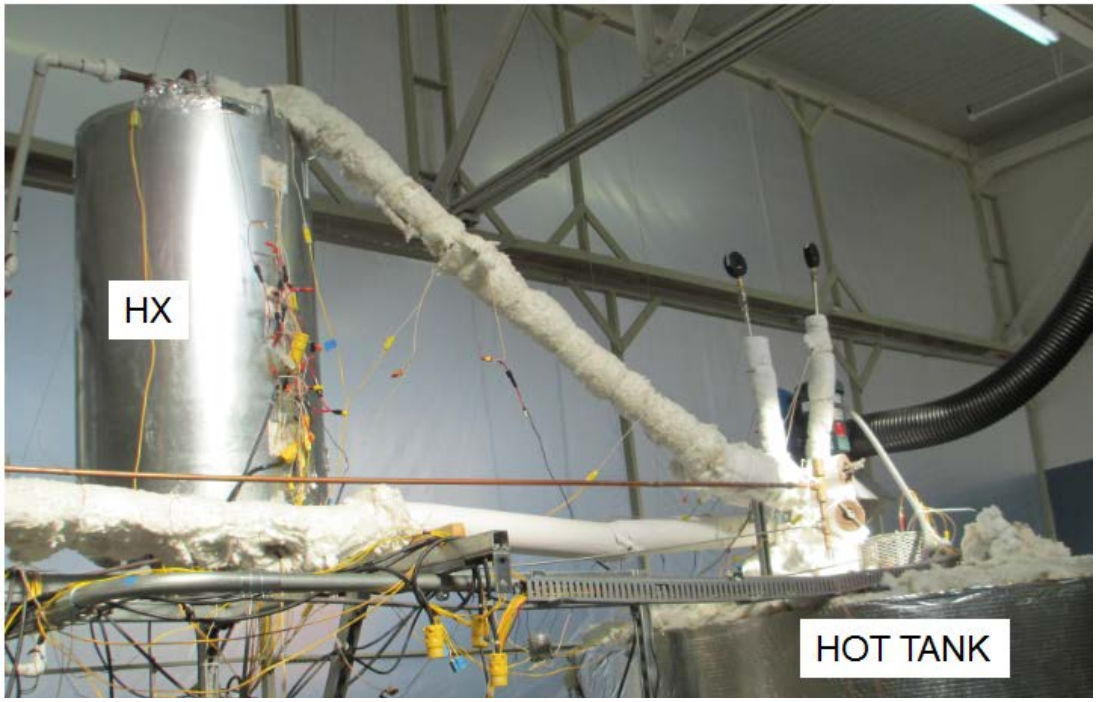

Figure 40. The HX is installed, plumbed, and electrical connections are made to the Hot Tank.

HX Performance

The results demonstrating that 8 kW of heat can be removed from the heat exchanger (HX) are presented.

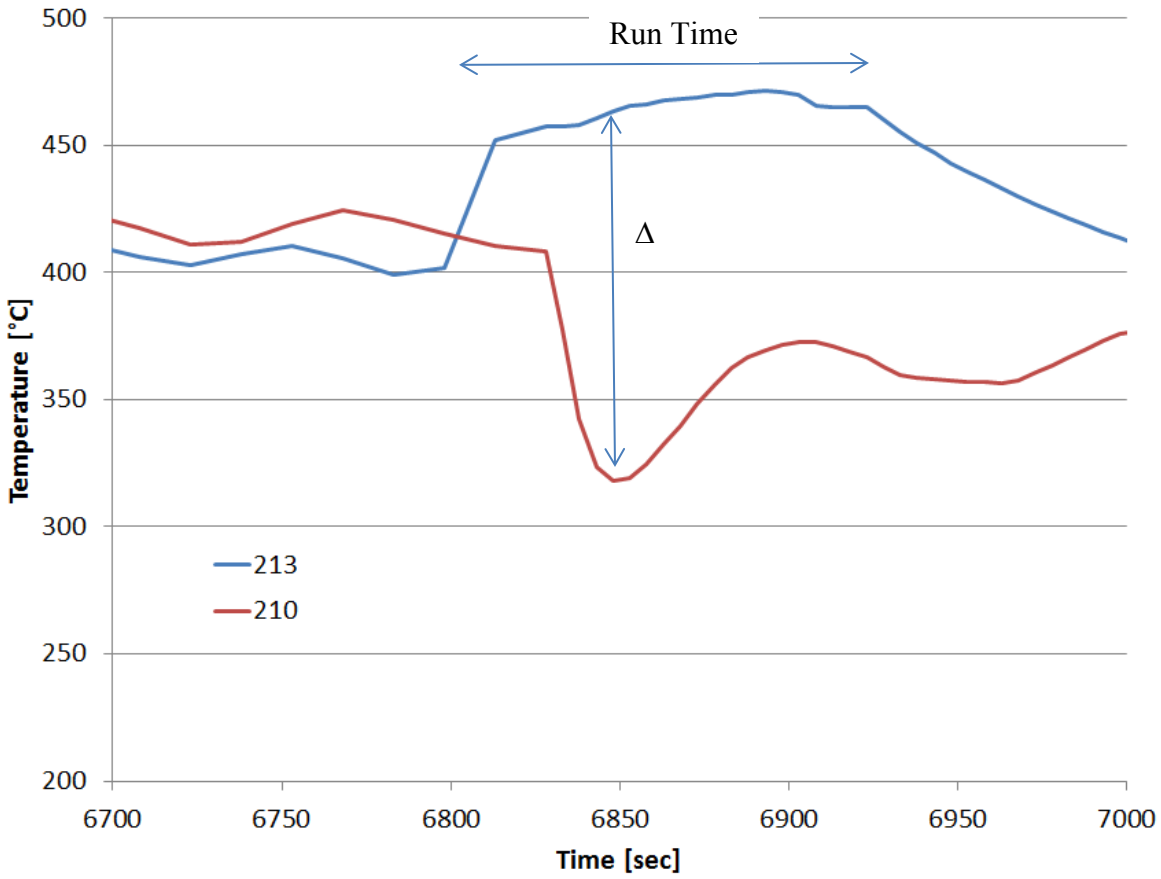

Figure 41. Temp response from thermocouples on the inlet (213) and outlet (210) of the HX.

The test was performed at a higher flow rate than the system spec because the temperature of the hot tank had not yet reached 700°C and the intent was to demonstrate a heat removal of more than 5 kW . Figure 41 shows the thermal response at thermocouples on the inlet and the outlet of the HX at the high flow rate. The salt flow rate is not measured accurately, however we do have an accurate measurement of the cooling water flow rate and so we can provide an accurate heat removal by the cooling water circuit. The cooling water was flowing at a fixed 19 L/min. Using the equation below the performance of the HX can be determined by measuring the temperature of the cooling water on the inlet and outlet of the HX.

$$Q = \dot{m}\, Cp\, \Delta T$$

$$\dot{m} = 19 \frac{kg}{min}$$

$$Cp = 4{,}185 \frac{J}{kg.K}$$

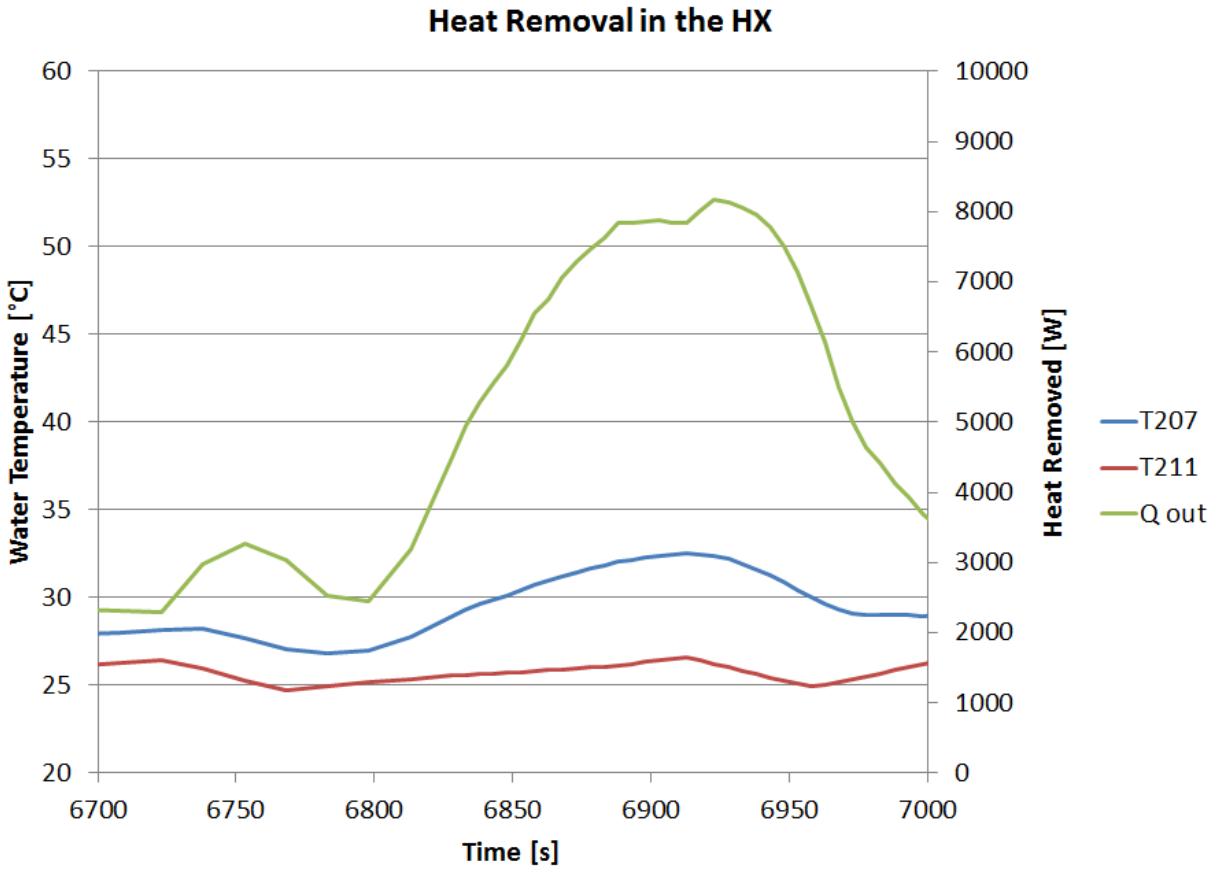

Figure 42. Heat output from the HX cooling water line. T211 is cold water in, T207 is hot water out.

Figure 42 shows the cooling water temperature during the demonstration. T211 is the inlet temperature and T207 is the outlet temperature. From these values the amount of heat; Q is calculated. As seen on Figure 42 a maximum of 8 kW of heat was removed by the heat exchanger under these conditions.

The heat exchanger (HX) was tested by flowing molten salt through it at a high flow rate and demonstrated a capacity to remove 8 kW of heat. As the system heats up to the specified 700°C the heat exchanger should be capable of removing 5kW or more heat out of the molten salt.

System Performance

Charge Cycle

The charging part of the system cycle consists of pumping molten salt from the cold tank at 300C through the 5 kW furnace, thereby heating the salt to 700C, and storing the salt in the hot tank.

The cold tank was full of salt, and the hot tank contained 20” of salt, with 20” of empty space left to store incoming salt.

Thermocouples in both tanks situated at different depths were used to monitor the fill progress. As the salt reaches a thermocouple at a known depth in the tank, the temperature rises and indicates that the salt level has reached that depth. Conversely, in the cold tank, as the tank empties, when a thermocouple is no longer immersed in the salt, the measured temperature drops to that of the head space above the melt, and indicates that the salt level is below the known depth.

Thermocouples located throughout the length of the FX provide insight into the heating of the salt, as shown in Figure 5.

The FX heater zones were set to control the furnace wall temperature to 740°C, which ensures that the bulk salt temperature is 700°C.

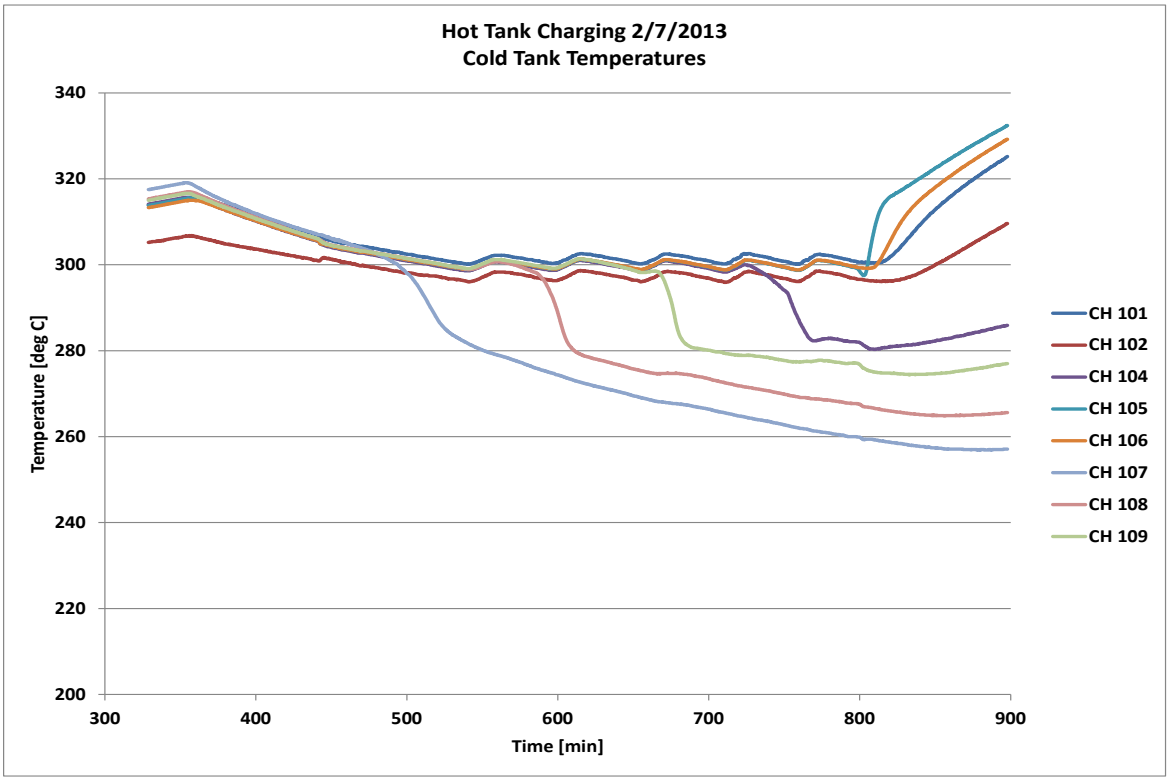

Figure 43. Charging the hot tank (cold tank response). Thermocouple locations described in Figure 5.

Figure 43 shows the cold tank thermocouple response. The thermocouple depths are in increments of 5”, and over the course of the 350 minutes of the charge cycle, 20” of salt were moved through the furnace. This was also confirmed with a pre- and post-measurement of the depth of the salt melt in the cold tank.

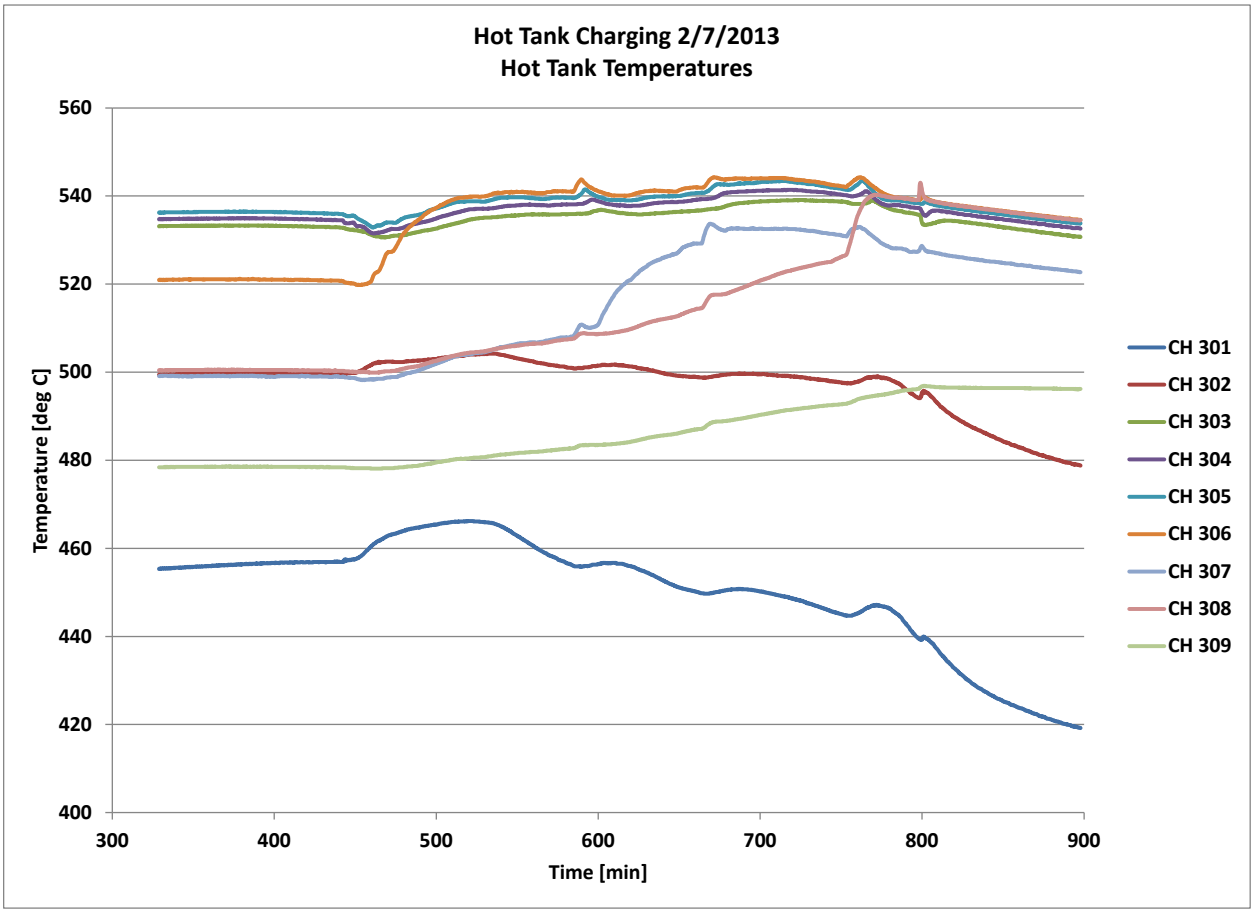

Figure 44. Charging the hot tank (hot tank response). Thermocouple locations described in Figure 5.

Figure 44 shows the hot tank thermocouple response. The thermocouple depths are in increments of 5”, and over the course of the 350 minutes of the charge cycle, the hot tank level increased by 18”. This is attributed to the fact that the ceramic brick lining is porous, and the bricks located near the top of the tank had not been fully saturated yet.

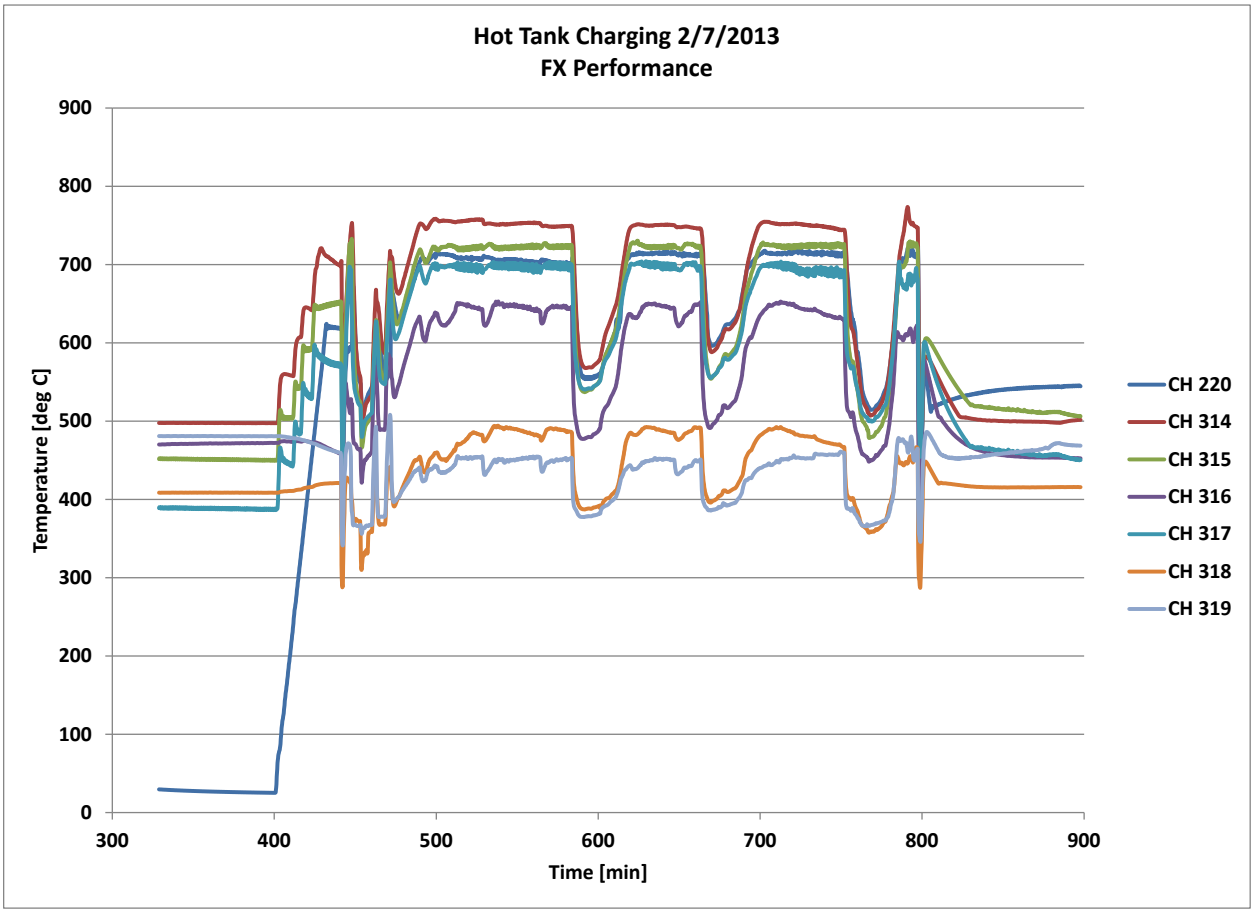

Figure 45. Charging the hot tank (FX response). Thermocouple locations described in Table 2.

Figure 45 shows the FX thermocouple response. CH314 was located at the exit of the FX, and shows that an exit temperature of 740° was reached during the charge cycle. The dips in output temperature at minutes 580 and 650 are due to the required periodic pump RPM increase to maintain a constant flow rate. As the cold tank drains, the head pressure that the pump must generate increases, which was achieved by increasing pump RPM. The RPM increase causes the flow rate to step up, which means the salt does not dwell in the FX long enough to get to 740°C momentarily, until the flow and temperatures stabilize again.

During this charge cycle, 200 kg of SS700 were heated from 300° to 700° over the course of 350 minutes. The heat transferred to the salt was therefore:

$$Qin = mC_p\Delta T = (200\ kg)(800\ J/kg/K)(700\text{-}300°C) = 64\ MJ = 17.8\ kWh$$

Discharge Cycle

The discharging part of the system cycle consists of pumping molten salt from the hot tank at 700°C through the heat exchanger, thereby cooling the salt to 300°C, and storing the salt in the cold tank.

The hot tank was full of salt, and the cold tank contained 20” of salt, with 20” of empty space left to store incoming salt.

Thermocouples located throughout the length of the HX provide insight into the cooling of the salt. The chiller cooling water was also turned on to its nominal 29 L/min at 40°C, which is the primary mechanism for removing heat from the salt. Measuring the temperature difference in the cooling water temperature as it enters and exits the HX provides a good measurement of heat removed from the system.

The HX heater zones were set to control the wall temperature to 300°C, which ensures that the initial salt to enter the HX will not freeze in the lines. As the salt enters the HX, the wall temperatures increase to match that of the salt flowing through the pipes, and the electric heaters turn off as cooling down to 300°C takes place.

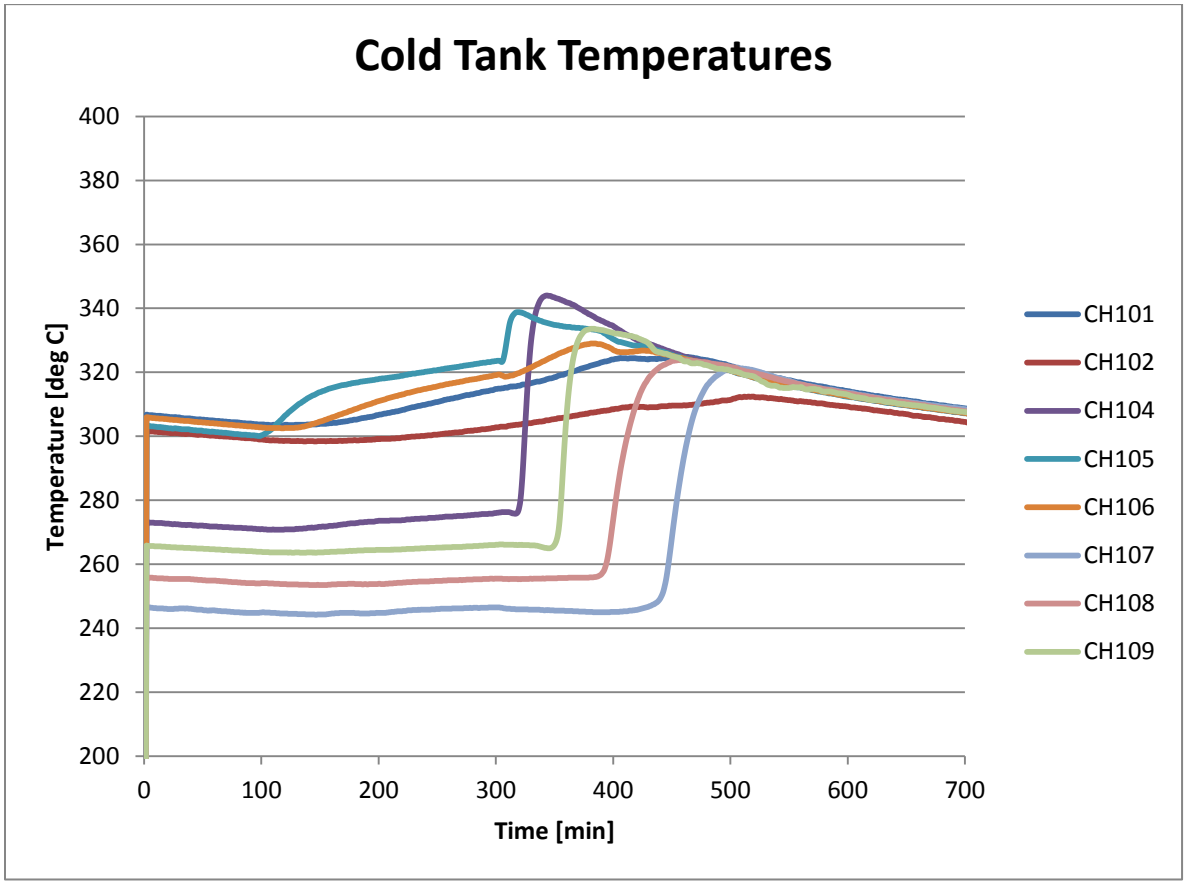

Figure 46. Discharging the hot tank (cold tank response). Thermocouple locations described in Figure 5.

Figure 46 shows the cold tank thermocouple response during the discharge part of the cycle. The thermocouple depths are in increments of 5”, and over the course of the 200 minutes of the discharge cycle, 25” of salt were moved through the furnace. This was also confirmed with a pre- and post-measurement of the depth of the salt melt in the cold tank.

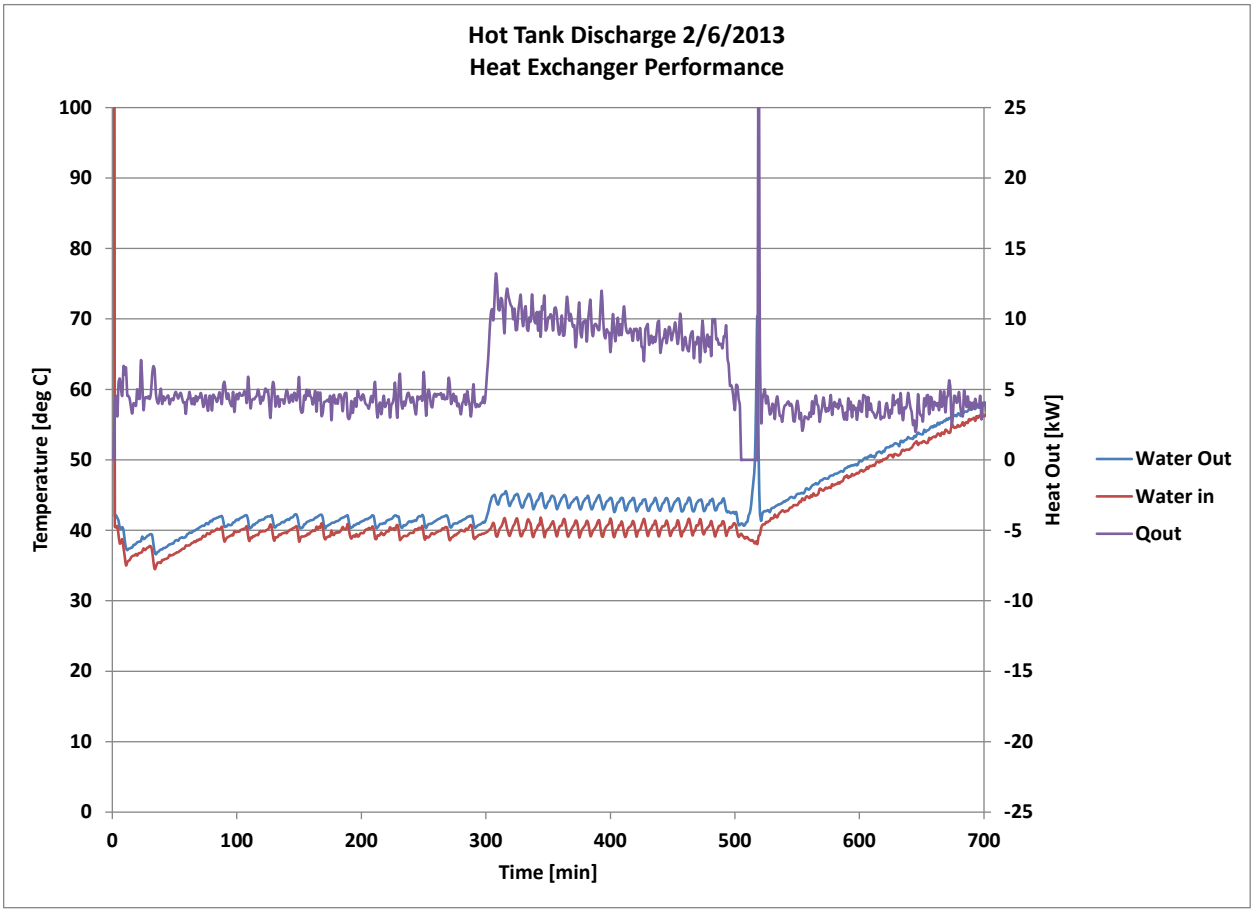

Figure 47. Discharging the hot tank (HX performance).

Figure 47 shows the heat exchanger water inlet and outlet temperatures, as well as a calculation of heat removed based on the measured water flow rate. Salt flow starts at minute 300. During the warm-up period prior to this point, both the electric heaters and the cooling water are on, and the HX wall temperatures were allowed to stabilize at 300°C. The average heat removed during this period is 4.5 kW. During the discharge cycle, the heat removed starts out at 10 kW, and gradually decreases over the course of the test to 7.7 kW, or an average of 8.9 kW. The average heat removed by the cooling water during the test was therefore 8.9 kW, because the electric heaters were not active during the duration of the flow. The test was shut down due to a chiller failure around minute 500.

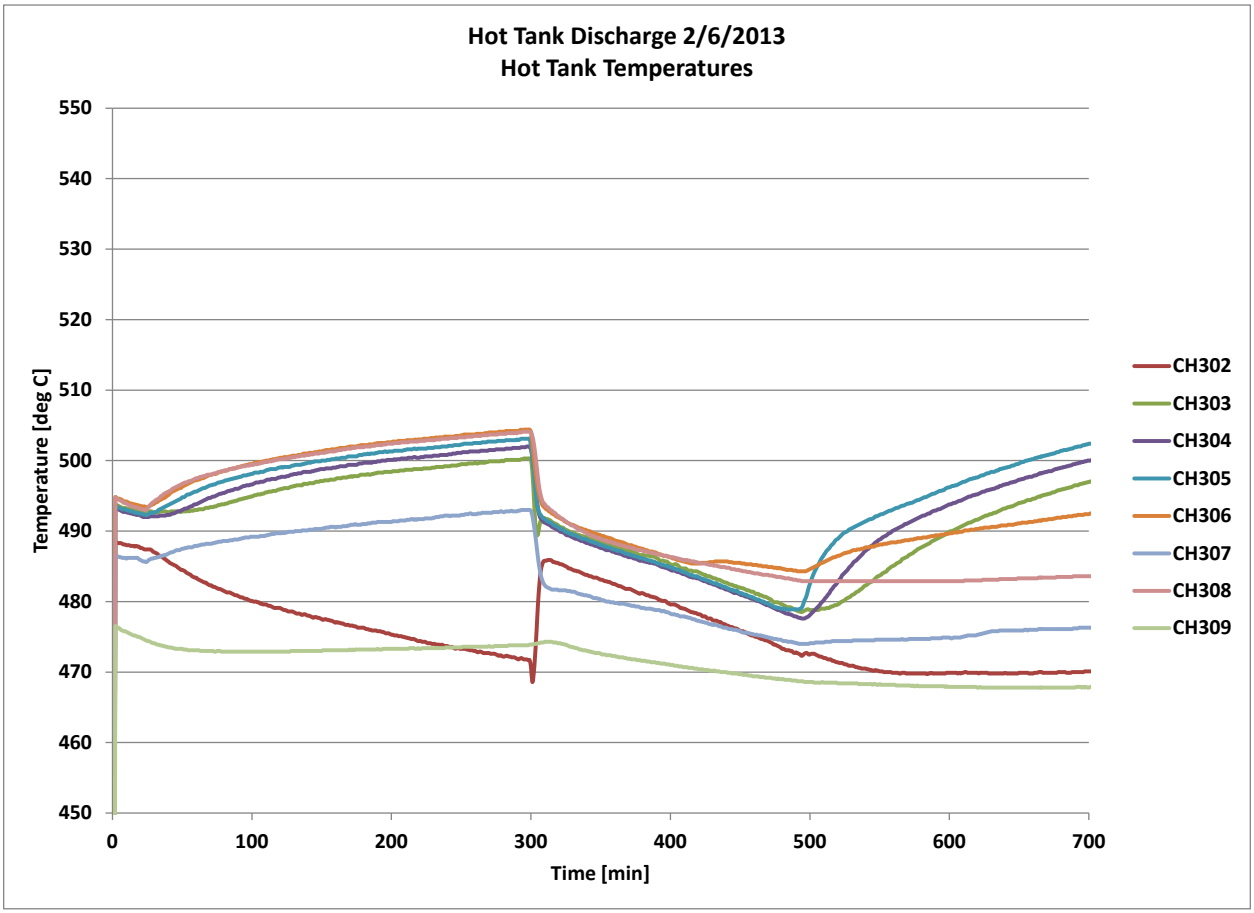

Figure 48. Discharging the hot tank (hot tank response). Thermocouple locations described in Figure 5

Figure 48 shows the hot tank thermocouple response during the discharge cycle. The thermocouple depths are in increments of 5", and over the course of the 200 minutes of the charge cycle, 25" of salt were moved through the HX. This was also confirmed with a pre- and post-measurement of the depth of the salt melt in the cold tank. The moment when the thermocouples are no longer immersed in salt is less apparent from this graph. We relied on the cold tank thermocouple readings to provide us with mass flow indication.

During this discharge cycle, 250 kg of SS700 were cooled from 490° to 300° over the course of 200 minutes. The heat transferred to the salt was therefore:
Qout = mCpΔT = (250 kg)(800 J/kg/K)(490-300°C) = 38 MJ = 10.6 kWh

The hot tank was at a bulk temperature of 490°C when this test took place. Because the salt which penetrated the ceramic lining altered the insulation properties of the hot tank, we had not reached the target temperature of 700°C at this point yet. The team had to add 2,000 kg of salt to fully soak the bricks, and this was the first time that the hot tank was maintaining a constant salt level.

Thermal Performance

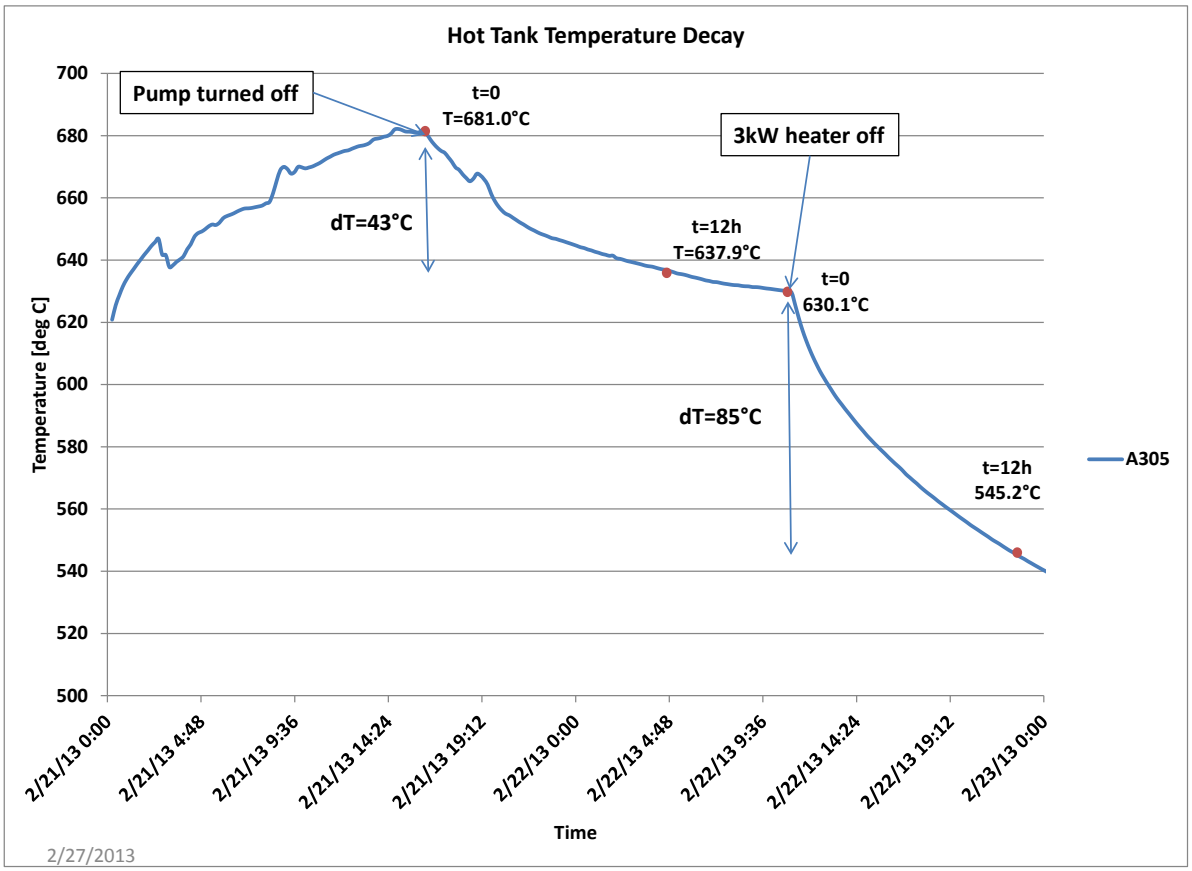

Figure 49. Hot tank temperature decay.

Figure 49 shows the evolution of the salt temperature in the hot tank after a charge cycle. The hot tank level was 20" when the pump was shut down. 12 hours after shutdown, the temperature in the tank dropped 43° from 681°C to 638°C. During this time, the 3 kW immersion heater was left on. After the 12 hours had elapsed, the immersion heater was turned off, and the tank temperature dropped from 630°C to 545°C over the next 12 hours, or 85°.

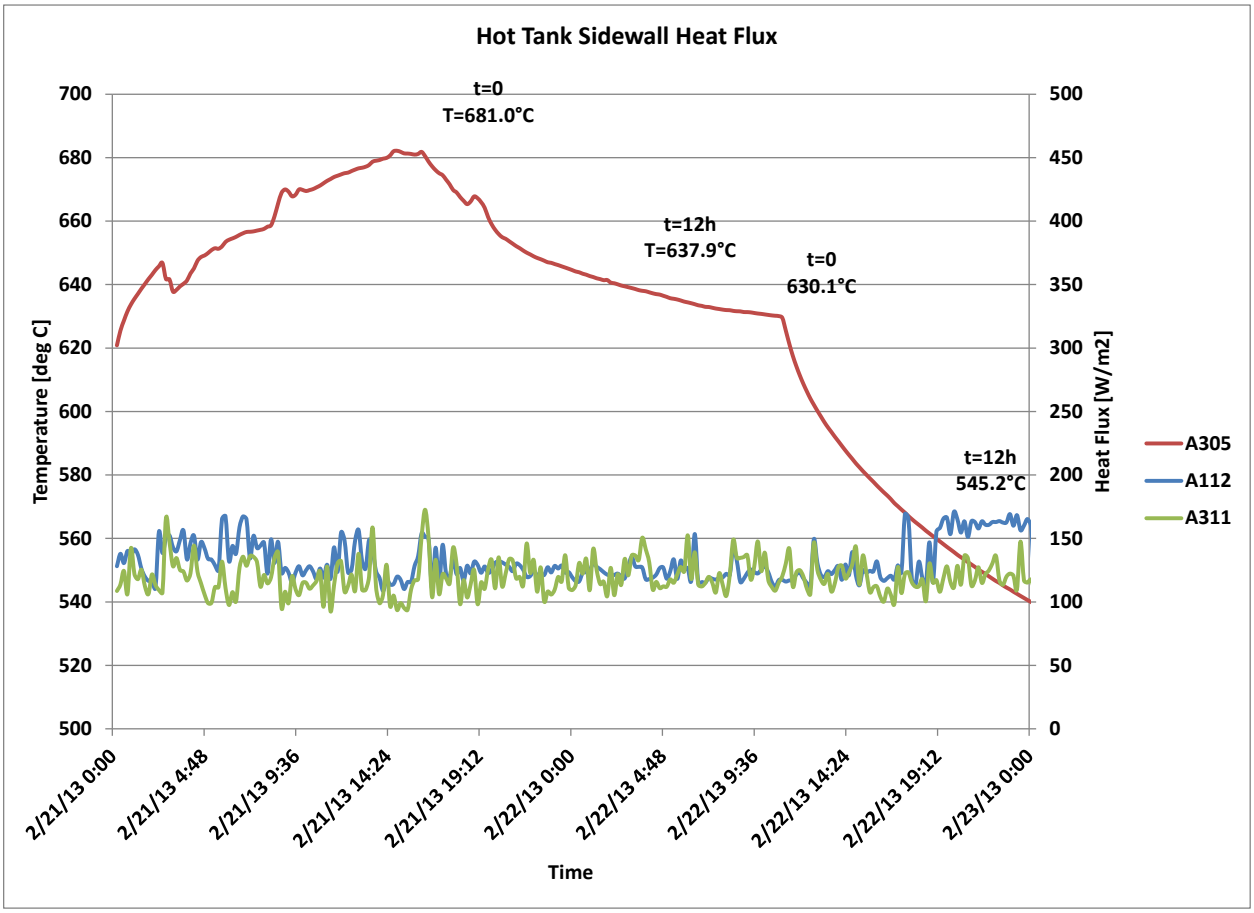

Figure 50. Hot tank heat flux through the tank sidewall during storage. Heat flux sensors located on the exterior sidewall of the hot tank.

Figure 50 shows the evolution of the heat flux measured through the hot tank sidewalls after a charge cycle. The two heat flux sensors are placed in close proximity to one another on the outside of the external tank insulation, 20" from the bottom of the tank. The heat flux recorded in this location never exceeds 170 W/m^2.

Stored Thermal Energy

Material properties relevant to a calculation of thermal storage are:

$\rho = 2100\ kg/m^3$
$Cp = 800\ J/kg\text{-}K$

The salt cavity dimension is:

D= 20" (0.508 m)
L= 45" (1.143 m)

The length is reduced 4" for the plug (see text above). Therefore the actual length U available for salt is:

U = (45-4) = 41" (1.04 m)

The Area is reduced 10% for protrusions (heater and pump) giving a usable volume:

$V = 0.9 \times \pi/4\ D^2 \times U = .190\ m^3$

$\Delta T = 700°C - 300°C = 400°C$

The Energy Storage Capacity is then:

$Es = \rho VCp\Delta T = 2100 \times 0.190 \times 800 \times 400 = 127.6\ e{+}6\ J =$ 35.45 kW-hr.

The amount that can be cycled is about 71% of this:

$0.71 \times 35.45 =$ 25.1 kW-hr.

This is because the pump inlet was located to prevent exposure of the heating element (insertable heater).

Salt Properties

The salt used to demonstrate the viability of the 700°C flow control loop was prepared from common inorganic chlorides.

A summary of the important material properties is given below:

- The weight averaged cost of the raw materials as we purchased them for this program is $1.8/kg. The cost is based off of current quotes of the individual components at ~1 ton quantity. Large quantity purchases of these raw materials would result in a lower price of $1.4/kg. This value was compiled using a quote from large US suppliers for a quantity of 10,000 tons.
- The melting point, heat of fusion, and heat capacity of the salt were determined using differential scanning calorimetry (DSC). The liquidus was measured to be 257°C. The heat of fusion was measured to be 87.2 J/g. The heat capacity at 300°C was measured to be 0.79 J/g-C. The tendency for the salt mixture to creep and evaporate made DSC scale measurements difficult and unreliable at higher temperatures. In general, since the heat capacity of the LiCl-KCl[7] eutectic and the (60%-40% by weight) $NaNO_3$-KNO_3[8] systems do not vary greatly as a function of temperature, the heat capacity of the salt can be taken as 0.8 J/g-C at 700°C.
- The viscosity of the molten salt fluid was measured at 300°C and 500°C to be 16.9 cP and 3.7 cP, respectively. Fitting the measured viscosities from 300°C to 550°C to an exponential curve with a coefficient of determination of 0.9795, the viscosity at 700°C is estimated to be 1.0 cP.
- The density of the salt was measured at 300°C to be 2.31 g/cm^3. Fitting the measured densities from 300°C to 403°C to a linear curve with a coefficient of determination of 0.997, the density of the salt is estimated to be 2.10 g/cm^3 at 700°C.
- The thermal conductivity of the salt was estimated by taking a mole average of the thermal conductivity values of the individual components. The thermal conductivity is estimated to be between 0.35 – 0.40 W/m-K.
- The stability of the salt was evaluated gravimetrically by subjecting a covered, pre-dried 500 g sample of the salt to 700 °C for 92 hours. The mass loss of the sample was 0.20%.

[7] Clark, Robert P., Journal of Chemical and Engineering Data, 18(1), 67, **1973**
[8] Bradshaw, Robert W., Sandia Report, SAND87-8007, **1987**

Corrosion Experiments

Introduction

This section summarizes the results of corrosion testing of alloys that could be used as container materials for Saltstream700 relevant to the NREL SunShot 700 project. Saltstream700 is a molten salt consisting of earth-abundant chlorides and its intended usage range is from 700°C to 300°C. Corrosion testing was conducted to validate materials selections for the components of the NREL Thermal Energy Storage (TES) system project.

Alloys Tested

The alloys selected for corrosion testing at 700°C were 316L Stainless, Inconel 600, Inconel 625, Incoloy 800H/HT, Haynes 230 and Nickel 201. The alloys tested at 300°C were A516 Grade 70 carbon steel, 304L Stainless and Nickel 201. Corrosion specimens were prepared by Metal Samples Co., Munford, AL from sheet stock to produce coupons having nominal dimensions of 1 in. by 2 in. by 0.125 in. thick. Each coupon was stamped with an identification code. Mill certification sheets were obtained for each alloy. The elemental compositions of the alloys tested are given in Table 10 below. Minor elements are not listed, thus the entries do not sum to 100% in all cases.

Table 10. Elemental compositions of alloys tested in Saltstream700; weight%.

Alloy	Fe	Ni	Cr	Mo	C	Other
Inconel 600	9.89	73.07	16.56		0.02	
Inconel 625	4.16	60.65	22.18	8.80	0.02	Nb 3.46
Nickel 201	0.22	99.56			0.02	
Incoloy 800H/HT	46.7	30.36	20.62		0.07	Al 0.51 Ti 0.55
Haynes 230	1.32	Bal.	22.37	1.27	0.11	W 14.16
316L SS	Bal.	10.00	16.90	2.04	0.018	
304L SS	Bal.	10.00	16.90	2.04	0.018	
A516 Grade70	Bal.				0.24	Mn 1.05

Corrosion Testing Conditions

The molten chloride salt was Saltstream700 (SS700). The tests were conducted at 700°C for 500 hours and at 300°C for 1000 hours. The corrosion specimens were removed for inspection and weighing at various intervals during the tests. The time-at-temperature data for the two groups of tests are collected in Table 11 and Table 12 below. Approximately 800 gm of SS700 was prepared for each corrosion test using either industrial grade or reagent grade salts. The molten salts were melted in aluminum oxide crucibles without any purification or deoxidation treatment. The coupons were hung from 304L Stainless hooks attached to the rim of the crucibles. Nitrogen flowed through the headspace to exclude air but was not bubbled through the molten salt.

Table 11. Time-Temperature history of Saltstream700 corrosion tests at 700°C using Industrial grade salts.

Test Hours	Interval 1	Interval 2
Time	281	216
Total	281	497
Temp. (°C)	692	696

Table 12. Time-Temperature history of Saltstream700 corrosion tests at 300°C.

Test Hours	Interval 1	Interval 2	Interval 3	Interval 4	Interval 5
Interval Time (hrs)	289	252	312	188	311
Group 1 (cumulative time)	289	541	853	1041	
Group 2 (cumulative time)		252	564	(Cont)	1062
Salt Grade	**Temperature**				
Industrial	276C	300C	297C	298C	299C
Reagent	322C	300C	300C	297C	302C

Results of 700°C Corrosion Tests

The photos in Figure 51 show the appearance of the six alloy coupons tested at 700°C after 497 hours. The coupons were rinsed with hot water and brushed to remove loosely adherent corrosion products before weighing and photographing. All the alloys appeared to corrode to a relatively minor extent, as the stamped markings were easily identifiable on each coupon. The general mode of corrosion was uniform and no pitting was visually evident. All the alloys, except Nickel 201, were covered with loosely adherent black scales. The surface scales had detached in patches less than 1 mm in diameter upon cooling to room temperature in many locations to reveal the base metal.

The rinse water for the coupons contained some insoluble black flakes, implying that these residues were metallic oxides, rather than metallic chlorides which would have been very soluble. The black flakes were magnetic, further implying that they were primarily composed of magnetite (Fe_3O_4). Samples of the black residue were archived for subsequent analysis, if deemed necessary. Corrosion appeared to occur generally by oxidation, due to oxygen impurities in the molten salt, rather than a direct interaction of the molten chlorides with the metallic alloying elements. Oxygen (present as water in the constituent solid salts) is a common impurity in chloride salts.

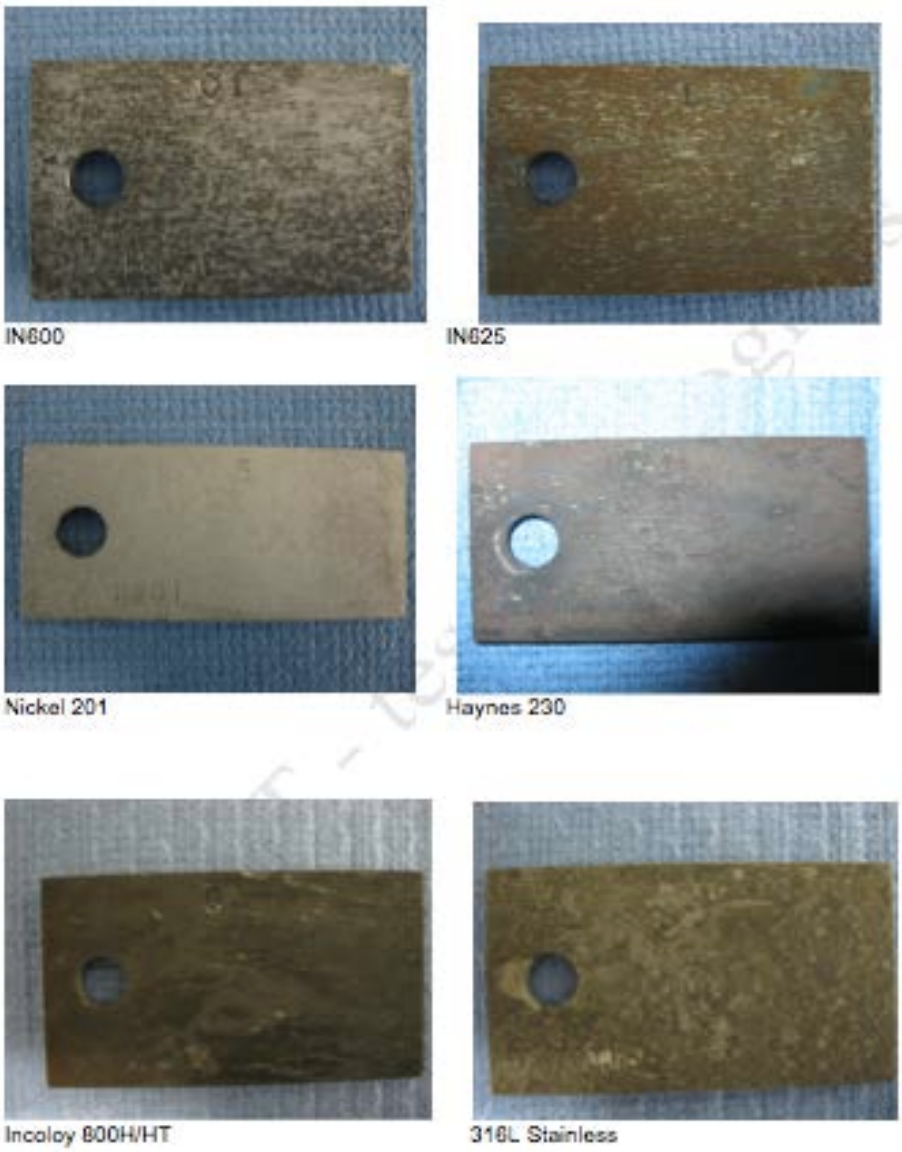

Figure 51. Appearance of corrosion coupons after 497 hours in Industrial grade Saltstream700 at 700°C.

The principal measure of corrosion was descaled weight loss, which avoids ambiguities arising from surface oxides that are not adherent. Net weight changes are due to both oxide scale retention and spalling and, thereby, may underestimate the amount of metal that corroded. Although net weight change is not an absolute measure of metal loss by corrosion, these data are readily obtained during the course of the corrosion tests and provide supporting information regarding the progress of corrosion. The definitions of net weight change per unit area (ΔW_{net}), weight loss due to corrosion per unit area (ΔW_{loss}) and the metal thickness lost by corrosion (L_{corr}) are given by Equations 1–3. M_0, M_t and M_d are the initial mass of a coupon, its mass at any given time (including adherent corrosion products) and its mass after chemical descaling, respectively. A_s is the total surface area of a coupon and r_m is the density of the alloy.

$$\Delta W_{net} = (M_0 - M_t) / A_s \qquad (1)$$

$$\Delta W_{loss} = (M_0 - M_d) / A_s \qquad (2)$$

$$L_{corr} = \Delta W_{loss} / r_m \qquad (3)$$

The metal losses by corrosion after 500 hours were determined by chemically stripping the oxide scales using the APAC method described in ASTM G1-03, Standard Practice for Preparing, Cleaning, and Evaluating Corrosion Test Specimens. The results are shown in Table 13. The annual corrosion losses, in millimeters, were calculated by linearly extrapolating the weight loss data to 8760 hours and applying the density of each alloy, according to Equation 3. The estimated metal losses range from 0.074 mm for the nickel-base alloys, I-600 and I-625, to a maximum of 0.493 mm for the iron-nickel-chromium alloy, IN800H/HT.

Table 13. Metal losses of alloys due to corrosion in Saltstream700 at 700°C after 500 hours and estimates of annual metal losses.

Alloy	Metal Loss (497 hours)	Annual Loss
	mg/cm^2	mm
316L	7.5	0.165
Ni201	13.9	0.276
I625	3.6	0.074
I600	3.6	0.074
Haynes 230	8.1	0.160
I800H/HT	22.2	0.493

A plot of the net weight changes of the alloy coupons vs. test time is shown in Figure 52. Refer to the legend to identify the alloys. The small values of net weight changes imply that these alloys are corroding relatively slowly. The largest estimated metal losses are those of Incoloy 800H/HT at 0.020 mm and Nickel 201 at 0.016 mm during the 500-hour test. These estimates are somewhat less than the true metal losses, which were determined by chemically stripping the oxide scales, as discussed above.

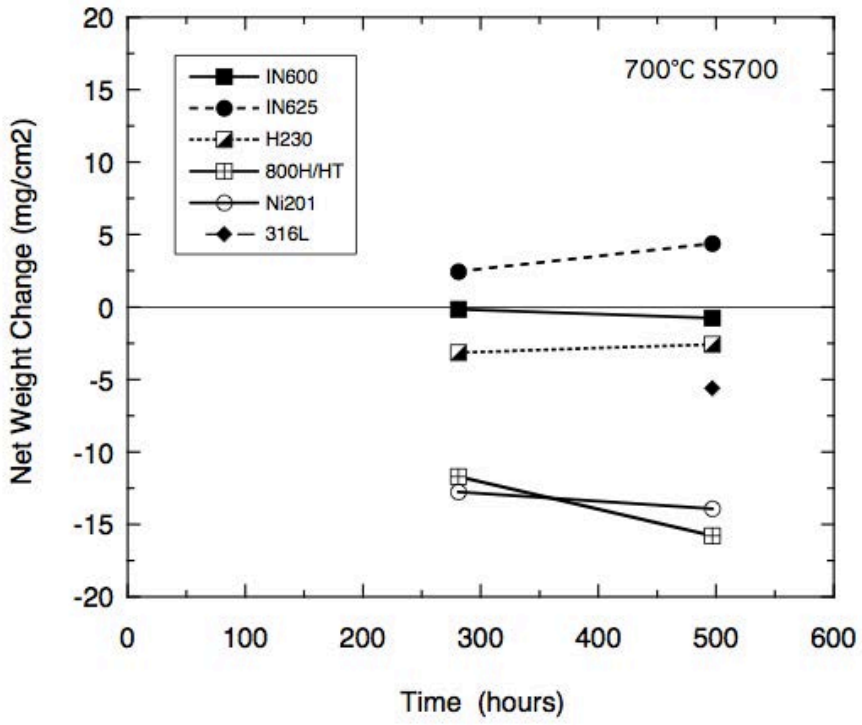

Figure 52. Net weight changes of the six alloys tested in Saltstream700 at 700°C after 500 hours.

Results of 300°C Corrosion Tests

The three alloys tested at 300°C, A516, 304L and Nickel 201, were organized into two groups which were started at separate intervals in the two grades of SS700; see Table 12. The purpose of this procedure was to observe if depletion of oxygen contaminants in the molten salts during the first interval affected corrosion of coupons started later. In addition, the delayed start provided replication of testing results.

The photos in Figure 53 show the appearance of the Group-1 coupons after 1041 hours and the Group-2 coupons after completing 1062 hours. A516 coupons were covered with a loosely adherent black scale. The A516 coupons in both salts had corroded sufficiently after 1040 hours that the stamped markings were not visible. 304L and Nickel 201 corroded only superficially and the markings were easily identifiable. The rinse water for the coupons contained a significant amount of insoluble black flakes, implying that the residue was iron oxide, rather than a chloride corrosion product. The black flakes were magnetic, further implying that they were primarily composed of magnetite (Fe_3O_4). Samples of the black residue were archived for subsequent analysis, if necessary.

Figure 53. Appearance of corrosion coupons after approximately 1000 hours in Industrial grade or Reagent grade Saltstream700 at 300°C. In each photo, the order is A516, 304L, Nickel 201 from left to right.

The metal losses of A516 coupons vs. test time are shown in Figure 54. Metal losses, as thickness in millimeters, were calculated from net weight change data because virtually all of the corrosion products were removed from the coupons during rinsing in water and brushing, effectively descaling them. Net weight changes can be converted to the equivalent thickness of metal consumed if we disregard the minor portion of scale remaining on the coupons. Metal losses were calculated using Equation 3 given that the density of A516 is 7.86 gm/cm^3.

Data for the coupons in reagent grade salt are shown as open symbols and those for industrial grade salt by filled symbols. Although A516 (Group 1) experienced much greater corrosion in the reagent grade salt versus industrial grade, this result is confounded by significant deviations from the intended test temperature during the initial interval. The higher temperature in reagent grade salt, 322°C, vs. 276°C, industrial grade, during the first 289 hours of testing (as shown in Table 12) contributed significantly to this difference. However, Group-1 A516 coupons continued during the second testing period, during which the temperature was 300°C, showed much less additional corrosion than during the first period. Group-2 A516 coupons started during the second testing period also showed somewhat more corrosion in the reagent grade salt versus

industrial salt. During the complete test period, about 0.5 mm of A516 was consumed during 1040 hours in the reagent grade melt.

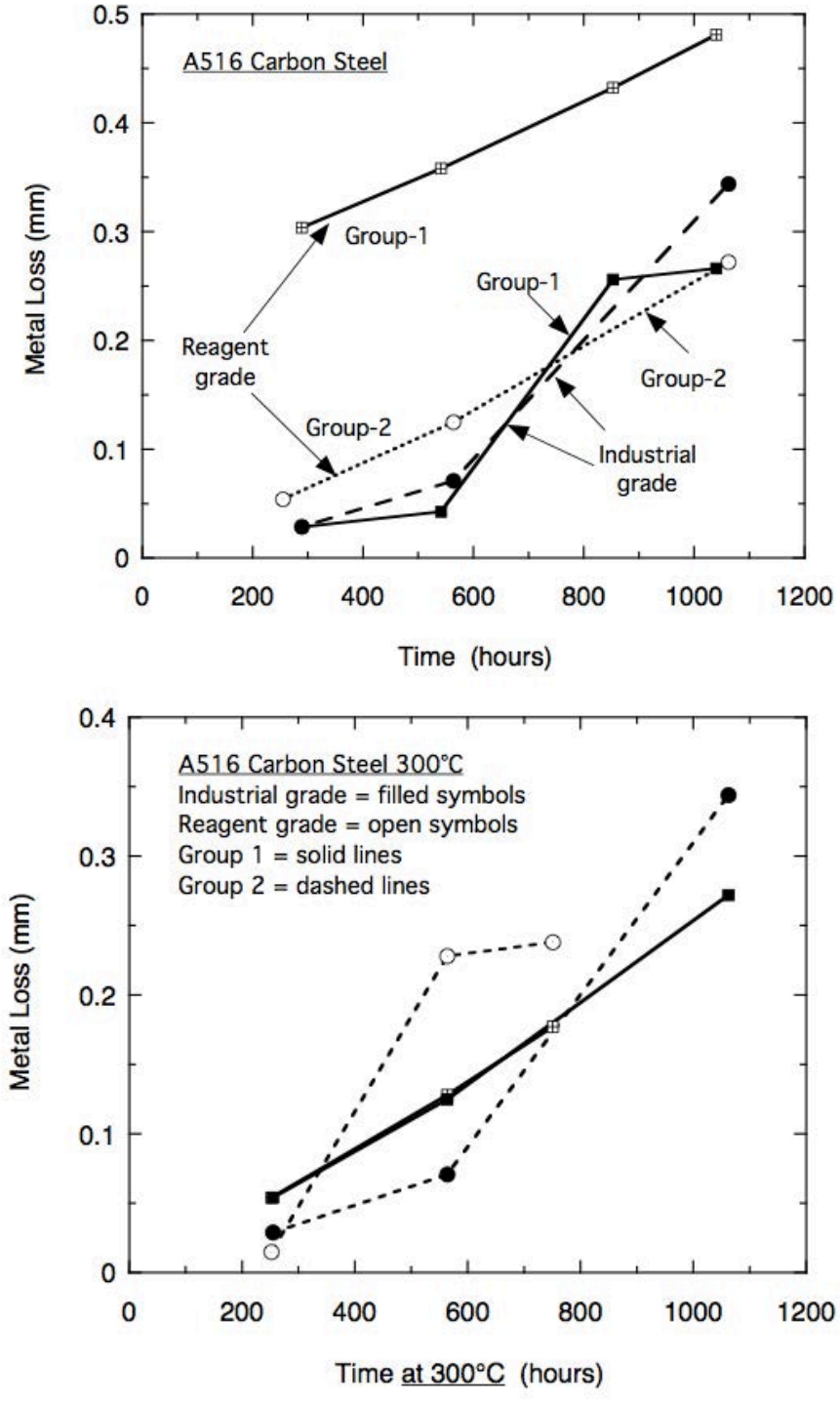

Figure 54. Metal thickness losses of A516 carbon steel after 1000 hours in two grades of Saltstream700 at 300°C. The upper plot shows all the data and the lower only data at 300°C.

and about 0.25 mm in the industrial grade salt. It is possible that more corrosion is occurring in the reagent grade salt because it has a higher level of oxygen contamination than the industrial grade but that is a conjecture because the concentration of oxide in these salts were not determined.

The upper plot in Figure 54 shows metal loss data at all times and temperatures while the lower plot shows only data acquired at 300°C. In the lower graph, the time scale for the Group 1 data was offset by 289 hours (the initial interval) and the metal losses were offset to account for losses after the initial interval at the deviated temperatures. This calculation assumes that the corrosion kinetic equation is linear with time and thus corrosion rates do not depend on the prior state of a coupon. This assumption is consistent with the observed poor adhesion of surface oxide layers, at all test intervals, which thus provided little or no protection against further oxidation.

The lower plot in Figure 54 indicates that the difference in corrosion between the two grades of molten salt is much less than implied by the upper plot. We cannot determine error bars for the data plotted in Figure 54. The data were derived from single coupons because the capacity of the test crucible precluded replicates during the planned-interval test. However, we suspect that the error bars are a relatively large fraction of the individual values because the random detachment of weakly adherent surface scale layers very likely created much variability both in time and over the surface on each coupon.

A plot of the net weight changes of 304L Stainless and Nickel 201 (N201) coupons vs. test time is shown in Figure 55. Refer to the legend to identify each alloy and the test group. These coupons were tested in the same crucibles as the A516 carbon steel. These materials corroded very slowly at 300°C and the markings are clearly visible on all the coupons at the end of the test. The weight changes may be due primarily to some oxide scale that was observed on the minor portion of the coupons that were above the molten salt level, especially for N201, which had a green oxide scale at the very top of the coupons.

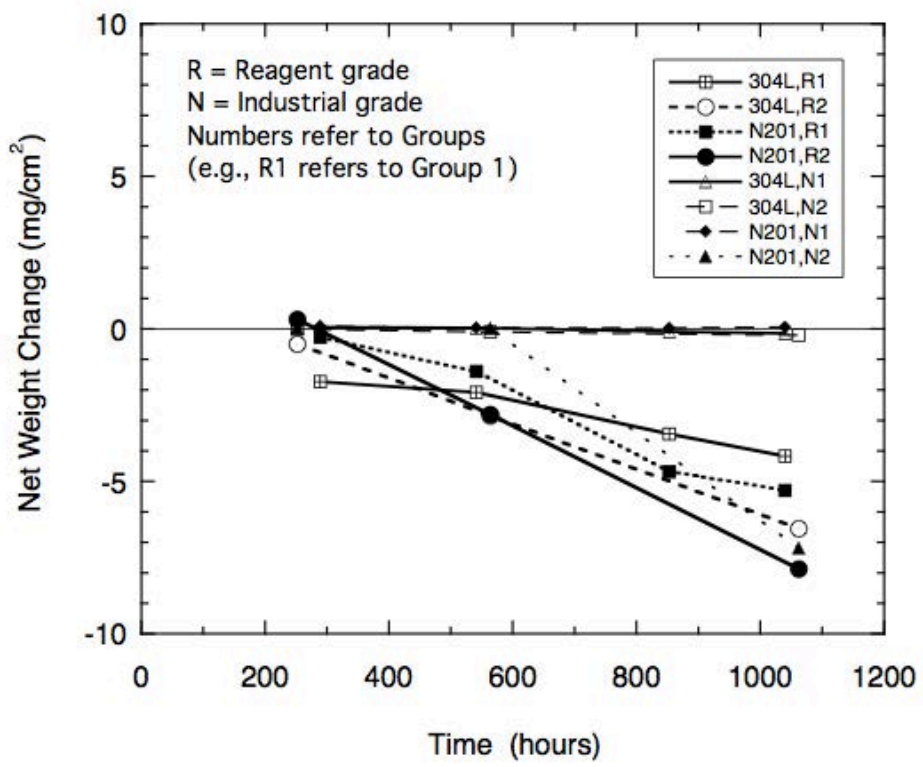

Figure 55. Net weight changes of 304L Stainless and Nickel 201 after approximately 1000 hours in two grades of Saltstream700 at 300°C.

Assessment of Corrosion Results

Metal consumption by corrosion of several nickel-base and iron-base high temperature alloys at 700°C was generally a few hundredths of a millimeter of metal thickness loss during 500 hours of testing. The corrosion products were oxides of the alloying elements, indicating that the molten salt containing an appreciable amount of oxygen impurities in the as-melted condition. At 300°C, the metal losses of A516 carbon steel are much larger than those of 304L Stainless or Nickel 201. A516 also corroded primarily by oxidation, forming an iron oxide which appears to be Fe_3O_4 (magnetite). These observations suggest that corrosion was driven by an impurity mechanism due to oxygen and was likely considerably faster than is expected in a molten chloride salt that is largely free of oxygen contamination. The source of oxygen contamination of the molten salt is water present in the constituent salts in their solid form. If the amount of oxygen contamination can be reduced by treatment of the salts, corrosion will be reduced as well. Similarly, corrosion due to oxygen will decline as soluble oxide is depleted from the starting batch of molten salt.

The primary source of oxygen contamination in Saltstream700 arises from the reaction of absorbed water in the solid salts, generating HCl (gas).

The soluble oxide can be removed from the molten salt by chemical treatment using methods adapted from the heat treating industry. As an example, molten mixtures of molten barium, magnesium, sodium and potassium chlorides are used to heat-treat various types of steel at temperatures up to 900°C. The heat-treating tanks necessarily contact air and develop soluble oxide contamination that is corrosive to work pieces machined to final dimensions. Such melts are periodically deoxidized or 'rectified' by various methods. Three examples of rectifiers are NH_4Cl (soluble solid)[9], HCl (gas)[10] or carbochlorination (combination of carbon and chlorine gas)[11].

Halotechnics has adapted a titration method used in heat-treating practice to determine the oxide concentration of solidified samples of molten Saltstream700. We have performed preliminary tests using NH_4Cl as the rectifier and found that it is effective in significantly reducing oxide concentration of molten Saltstream700 at the low temperature range intended for thermal energy storage systems. These data are preliminary, and outside the scope of the current project, so discussion of the results will not be made here.

[9] Heatbath/Park Metallurgical Co. Product brochure, http://heatbath.com/heat-treating-products-2/salt-bath-rectifiers/

[10] P. J. Gardner and P. Pang, Can. J. Chem., vol. 66, 566 (1988).

[11] D. F. Williams, Assessment of Candidate Molten Salt Coolants for the NGNP/NHI Heat-Transfer Loop, Oak Ridge National Laboratory report, ORNL/TM-2006/69, June 2006.
V. L. Cherginets and T. P. Rebrova, Electrochimica Acta, vol. 45, #3, 469-476 (1999)

Lessons Learned

Salt – Ceramic Interaction

The active volume of the hot tank was sized to contain 400 kg of molten SS700 salt. However, due to the porosity of the ceramic brickwork, the amount of salt that was loaded into the hot tank was close to 2,400 kg, of which 2,000 kg was absorbed by the brick. This amount is consistent with the 57% porosity of the insulating firebrick (IFB), which corresponds to an empty volume of 1,000 liters (2,200 kg of SS700).

The salt-soaked IFB's thermal conductivity is affected by this salt penetration. The nominal specs from the vendor specify a k of 0.35 W/m.K. As measured, the k of the salt-soaked IFB is 0.73 W/m.K at 500°C, and 0.77 W/m.K at 650°C, which is roughly twice the nominal thermal conductivity.

The design of the tank was such that the salt would not completely penetrate the brickwork, but rather would "freeze" in the brick before reaching the stainless steel tank. We know now that this was not the case, but despite this full soaking, the design of an internally-insulated tank with fully soaked brick is viable.

Molten Salt Pumps

Obtaining a pump to match our pressure and flow requirements proved challenging. There exist molten salt pump manufacturers who have experience with the thermal energy storage industry, but these pumps are dramatically oversized for our application. The metal heat treating industry also uses molten salt pumps which can operate at temperatures over 700°C, but they are designed to provide high flow rates at low head pressure, which is not suitable for our application.

We purchased a centrifugal cantilever pump from a molten salt pump vendor that would fit in our storage tank, which generates the right amount of head (15 psi). Due to the nature of centrifugal pumping, the associated flow rate with the 15 psi of head was close to 100 times our target flow rate of 0.5 L/min.

In order to successfully integrate this pump into our thermal energy storage system, we devised a flow control system centered around a recirculation loop, whereby most of the molten salt flow was recirculated back to the tank. The desired flow rate of 0.5 L/min was achieved by diverting a fraction of the recirculation flow using a bleed valve. By adjusting the setting on the bleed valve, on the recirculation valve, as well as the pump RPM, the desired flow rate was achieved after a few calibration runs.

The pump operating curves were developed for both hot and cold pumps for specific valve settings. The tank level also has an influence on the pump operation, because the head pressure required increases as the tank level drops. All these consideration were built into a control schedule, which takes tank fill level as an input.

The hot pump impeller and volute were made of 316 stainless steel, which performed well when immersed in SS700. 304 stainless steel (pump support rods) and 400 series stainless steel (shaft)

did not perform well after being immersed in SS700, as discussed in the corrosion results section of this report.

The welds that were used to manufacture the pump volute were fuse welds, and failed during pump operation. All the welds were upgraded to full penetration welds.

Piping

The joining of pipe and the heat tracing of pipe proved to be significantly larger challenges than anticipated. Great care should be taken in selecting the right plumbing materials and joining techniques.

We needed to find a good balance between plumbing flexibility and reliability. Because of the nature of the project, the plumbing was not well defined, and had to be redone multiple times in order to meet our objectives. For instance, we wanted to demonstrate the functionality of the HX, but did not have a hot tank built at the time – our solution was to plumb the output of the FX directly into the input of the HX to pump salt from the cold tank into the FX taking it to 700°C, then through the HX taking it down to 300°C, and back to the cold tank. Such plumbing changes were regular occurrences throughout the life of the project, and the originally designed flow loop was not implemented until quite late in the project.

The original plumbing design was to use ¾" 316 SS pipe with a high temperature thread sealant. However, we experienced multiple leaks at the pipe joints which prevented us from moving forward. Fixing a leak in one part of the system would cause a leak in a different part of the system. In addition, the numerous thermal cycles imparted on the system plumbing from starts and shutdowns would cause the pipe sealant to fail. This plumbing approach was found to be non-viable.

We then decided to convert all the plumbing to ½" 316 SS tube and use Swagelok type fittings to ensure a good seal. The thin wall tubing was easy to install, bend, and join because of the fittings. However, after multiple thermal cycles, the thin wall tubing started to fail at the seam (the tubing used was welded tubing, not seamless). In addition, the weight of the components (valves, gauges, etc) was imparting a lot of stress on the tubing, and places where the tubing was not perfectly supported and bracketed would develop leaks at the Swagelok fittings.

We then progressively replaced the failing sections with ¾" Inconel 600 pipe with welded fittings. We have not experienced any leaks with welded piping, and the Inconel pipe is known to be fully compatible with the salt chemistry.

The final recommendation for piping is welded Inconel pipe.

Heat Exchanger Design

Halotechnics designed and constructed the simulated steam generator (HX) in house to cool the salt down from 700°C to 300°C. We iterated on the design multiple times after the following learning.

Cold spots were the biggest concern during the operation of the HX. The heat tracing was installed outside of the water tubing and copper taping, with no direct contact to the salt-flowing tube. This would cause some areas of the HX to be cold when the cooling water was running. Because of the small fluid velocity in the piping (0.05 m/s fluid velocity to get 5 kW), these areas would be prone to freezing.

In addition to this, the coils of the HX were likely not installed perfectly uniformly, which resulted in some flat spots. These areas of the piping would not drain after shutdown, and the stagnating salt would freeze after shutting down the heating system. Some of these flat spots would then be impossible to thaw because they lined up with the cold spots described previously.

A flushing procedure was therefore implemented, whereby a purge flow of nitrogen was injected through the HX coil immediately following a shutdown, to prevent any salt from accumulating in the non-draining portions of the HX. In addition, upon startup, a high flow rate of salt was run through the HX to warm up the tubing for a few seconds, in order to reduce the risk of a freeze at the design flow rate.

Large Scale Tank Design and Cost Estimate

Table 14. Cost estimate for a large scale tank. Diameter is 38 m, height is 14 m.

	unit cost	thickness	volume	density	mass	cost[12]
	$/1,000 kg	m	m3	kg/m3	1,000 kg	$
Stainless steel (304L)	$3,000	0.0254	100	8,030	804	$2,410,000
Refractory brick	$2,000	0.37	1,458	2,960	4,315	$8,629,006
Carbon steel	$800	0.0127	50	7,750	388	$310,000
Ceramic insulation	$1,500	0.25	985	128	126	$189,100
SS700	$1,450		15,878	2,100	33,343	$48,347,000
TOTAL		**0.6581**	**18,470**		**38,975**	**$59,900,000**

Table 14 shows the cost breakdown of a larger scale thermal energy storage system using Saltstream700 as storage media using quotes from our current vendors. For a 38 meter diameter, 14 meter high tank, the amount of heat stored is:

$$Q = mC_p\Delta T$$

$$C_p = 800 \text{ J/kg-K}$$

$$m = 33 \text{ e+6 kg}$$

$$\Delta T = 400°C$$

$$Q = 3{,}000 \text{ MWht}$$

The cost of a large thermal energy storage system built around the current formulation of SS700 is high due to the physical properties of the molten salt. As it stands, the heat capacity of SS700 is 800 J/kg/K, which is small compared to 60/40 solar salt (1,500 J/kg/K).

In Table 15 presents a cost comparison between a conventional nitrate and a high temperature chloride hot storage tank. The tanks are both sized for a 3,000 megawatt hour thermal storage requirement. The increased delta T achieved with the SS700 (from 288°C to 700°C, compared to the nitrate salt's 288°C to 565°C) is cancelled by the lower heat capacity. The price per ton of SS700 is roughly 50% higher than solar salt, making the salt inventory over 80% more costly. In addition, the brickwork and extra insulation that lines the chloride tank is roughly two times more expensive than the 347 SS liner in a nitrate tank.

Halotechnics is actively researching new combinations of salts which would bring the heat capacity up to levels closer to that of solar salt in order to make it more competitive. Current research is also focused on increasing the operating temperature difference between the hot and

[12] Cost numbers for each category are rounded to the nearest $1,000 and to the nearest $100,000 in the total

cold salt by looking at compositions closer to the eutectic of the Chloride salt system, as well as introducing other constituents with a favorable impact on melting point and heat capacity.

Table 15. Comparison between a conventional hot tank for nitrate salt (60/40 solar salt) and a high temperature hot tank for SS700 chloride salt.

		60/40	SS700	Chloride % delta
Storage req	MWht	3,053	3,053	0%
Cp	J/kg.K	1,495	800	-46%
delta T	°C	277	412	49%
metric tons[13]	1,000 kg	26,538	33,343	26%
salt cost per ton[14]	$/1,000 kg	$1,000	$1,450	45%
salt cost	M$	$26.54	$48.35	82%
liner cost[15]	M$	$4.02	$0.00	-
insulation cost[16]	M$	$0.19	$8.82	4563%
other tank cost[17]	M$	$2.91	$2.91	0%
Total hot tank cost	M$	$33.65	$59.89	78%
cost delta	**M$**	**$0.00**	**$17.79**	**-**
$/kWht	$/kWht	$11.02	$19.62	78%

[13] Calculated from Q=m.Cp.dT
[14] Figures obtained from Halotechnics supply chain analyst.
[15] Nitrate tank liner is assumed to be made of 347 Stainless at a bulk cost of $5,000/ton of the same dimensions as the chloride salt tank liner described in Table 12.
[16] Both tanks are assumed to have a 10" ceramic blanket insulation, and the chloride tank has an additional ceramic brick internal insulation layer 0.37 meters thick.
[17] These costs are common to both systems and include a carbon steel shell

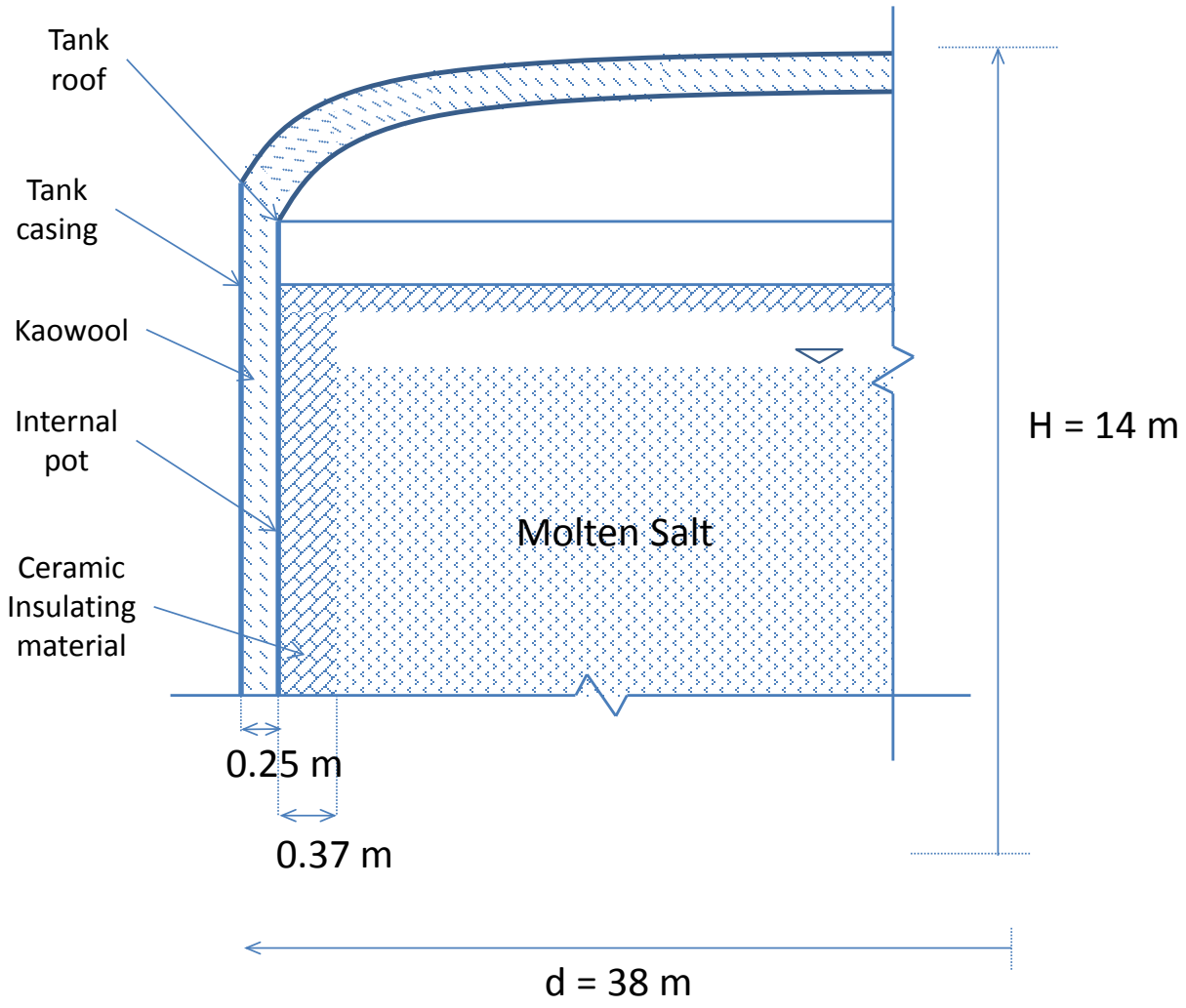

Figure 56. Large Scale Hot Tank Design.

Figure 56 shows a schematic of the proposed full scale tank design[18]. The salt is in direct contact with a 0.37 m thick insulating ceramic brick layer to bring the stainless steel tank case to 550°C. The remaining 0.25 m of insulation brings the outer wall temperature down to 30°C. According to the cost model shown in table 2, the cost of the large scale hot tank would be $60M, $48M of which is the salt inventory cost and $12M is the tank material cost, not including freight or labor.

[18] R. Gabbrielli and C. Zamparelli**,** Optimal Design of a Molten Salt Thermal Storage Tank for Parabolic Trough Solar Power Plants, **2009**

Future Activities

An important piece of learning on this program will be the teardown of the hot tank. There is abnormal behavior in the thermocouple data from the bottom of the melt, which settles at a temperature roughly 100°C lower than the temperature in the center of the molten salt. This may indicate a crack or a leak past the brick, but the cause is currently unknown. A careful teardown needs to take place in order to know with certainty the cause of this temperature drop.

The integrity of the refractory brick in direct contact with the molten salt at 700°C also needs to be characterized. Careful removal of this brickwork should be analyzed for crushing strength and modulus of rupture, as well as other structural properties in order to determine if this is truly a viable solution for building a larger scale tank.

Modifying the composition of Saltstream 700 in order to improve the heat capacity is an important task to compete with the cost of conventional nitrate salt systems operating at 565°C. A thermal energy storage system built around SS700 in its current formulation enables integration with high temperature steam generating cycles, but does not offer an advantage over nitrate salts at conventional operating temperatures.

Conclusions

Thermal Energy Storage at 700°C using Saltstream 700 is both technically and economically achievable. The program has demonstrated that a commercial version of the internally insulated storage tank can be designed and built.

Salt

The salt developed by Halotechnics, Saltstream 700, is stable at temperatures exceeding 740°C. Its current formulation was developed to meet short term objectives, and suffered from a low heat capacity. The company's core competency is development of new fluids for various applications. A new formulation of Saltstream 700 is currently under development, with the intent to raise heat capacity while keeping cost under control.

Hot Tank

An internally insulated hot tank has been demonstrated for molten salt storage at 700°C. The internally insulated tank with salt in direct contact with dense ceramic insulating brick proved to be a good alternative to the use of a costly Nickel alloy liner. The tank can be designed to account for the modified thermal conductivity of the insulating brick, and maintain a stainless steel pot at a temperature where corrosion rates are low.

Cold Tank

A carbon steel cold tank has been demonstrated for molten chloride salt storage at 300°C. Corrosion effects are low if the salt is formed outside of the tank, hence baking out most of the trapped moisture in the individual constituents, and a nitrogen blanket or another inert gas is used to keep oxygen out.

System Hardware

- Cantilevered vertical pumps performed well in transporting molten salt.
- Full penetration welds are essential for all wetted components.
- Piping should be welded in order to avoid leaks.
- Standard insulation materials such as ceramic blankets provided good external thermal insulation at a low cost.

TES System Design

The estimated cost of a 3,000 MWht chloride salt storage tank operating between 300°C and 700°C is 60 million dollars, of which 48 million is the salt inventory alone. This results in an overall cost of $20/kWht. This cost analysis is preliminary, and more factors should be considered for a more accurate assessment. The Saltstream 700 formulation is also preliminary, and there is some margin for cost reduction by altering the composition.

Thermal storage at 700°C was demonstrated during this program, which would enable the integration of this system to supercritical and ultra-supercritical steam cycles.